



THE HONG KONG
POLYTECHNIC UNIVERSITY

香港理工大學

Pao Yue-kong Library

包玉剛圖書館

Copyright Undertaking

This thesis is protected by copyright, with all rights reserved.

By reading and using the thesis, the reader understands and agrees to the following terms:

1. The reader will abide by the rules and legal ordinances governing copyright regarding the use of the thesis.
2. The reader will use the thesis for the purpose of research or private study only and not for distribution or further reproduction or any other purpose.
3. The reader agrees to indemnify and hold the University harmless from and against any loss, damage, cost, liability or expenses arising from copyright infringement or unauthorized usage.

IMPORTANT

If you have reasons to believe that any materials in this thesis are deemed not suitable to be distributed in this form, or a copyright owner having difficulty with the material being included in our database, please contact lbsys@polyu.edu.hk providing details. The Library will look into your claim and consider taking remedial action upon receipt of the written requests.

**CHARACTERIZATION OF BIOGENIC NANOBUBBLE FOR
MOLECULAR ULTRASOUND IMAGING AND THERAPY**

YANG YAOHENG

M.Phil

The Hong Kong Polytechnic University

2016

The Hong Kong Polytechnic University
Interdisciplinary Division of Biomedical Engineering

**Characterization of Biogenic Nanobubble for Molecular Ultrasound
Imaging and Therapy**

Yang Yaoheng

A thesis submitted in partial fulfillment of the requirements for the
degree of Master of Philosophy

Aug 2015

CERTIFICATE OF ORIGINALITY

I hereby declare that this thesis is my own work and that, to the best of my knowledge and belief, it reproduces no material previously published or written, nor material that has been accepted for the award of any other degree or diploma, except where due acknowledgement has been made in the text.

_____ (Signed)

YANG Yaoheng _____ (Name of Student)

ABSTRACT

Microbubble is a widely used ultrasound contrast agent with a spherical shell encapsulating inertial gas. However, due to the micrometer size, microbubble is limited within blood circulation, so it is mainly used for mapping blood vessels and endothelium cells therapy. Reducing size may make it possible to image extravascular region providing the particle can leak out of vessel wall. However, in traditional artificial synthesis method, the bubble in nano-meter size (nanobubble) is unstable and hard to be surface modified. The poor stability results in short circulation time and make it hard accumulate in focused region. Recently, biogenetic nanobubble called nano gas vesicle at the size of ~250nm is reported. It is much more stable than synthesized bubble, and become possible to travel across the endothelial layer to reach cells beyond. To further understand its behaviour in acoustic field and biological environment, this research investigated the acoustic property of the nanobubble, and understand its potential in contrast enhanced ultrasound imaging. In addition, the surface modification ability and the biological effect on cell attachment and endocytosis were also studied

Nanobubble was isolated from *Anabaena flos-aquae* by lysing and centrifuge method.

The basic properties of nanobubble were characterized such as concentration, size distribution, microstructure, zeta-potential and stability. The

morphology characterization result is consistent with previous research. Biogenic nanobubble is demonstrated to be extremely stable in vitro.

To study the acoustic property of nanobubble, attenuation coefficient was measured using pulse echo method by comparing results with and without nanobubble present. Attenuation coefficient is the indicator of resonance frequency, damping and Q-value. The experiments were repeated by three customized high frequency transducers with centre frequencies of 22 MHz, 40 MHz and 48 MHz covering a broad frequency band from 7 MHz to 103 MHz. Resonance frequency is found to be 88 MHz.

Harmonic Property was measured by two transducers, one for transmit and the other for receiver. The center frequency of receiver transducer is twice the transmit one. Different incident ultrasound pressure gradient was tested with transmit ultrasound wave at half of the resonance frequency of nanobubble. Significant second harmonic frequency was observed. The nanobubble stability under sonication is demonstrated to be able to last for over 1 hr. The biogenic nanobubble has both strengthened stability and non-linear property indicating its potential for accumulate in extravascular region and perform molecular imaging.

Biological effect of nanobubble at cellular level was characterized by incubation with HeLa tumor cells. For nanobubble floating effect, two different cell distribution was tested, one attached to the culture dish and one disperse in the culture medium. In addition, the ability of nanobubble for cell attachment and endocytosis was studied. The fluorescence probe PpIX was bond to nanobubble surface and confocal microscope was used to characterize the intracellular distribution of nanobubble. Experiments have demonstrated that biogenic nanobubble can be internalized by tumor cells. Enhanced stability ensures nanobubble enough circulation time to accumulate in extravascular site; non-linear property can improve the contrast in ultrasound imaging; easily surface modified property indicates its ability to be a smart molecular or cellular probe with antibody ligand; endocytosis ability make it possible to deliver drug or gene into cytoplasm. Compared with conventional nanobubble, these four enhanced properties demonstrate the great potential of biogenic nanobubble for molecular imaging and therapy.

ACKNOWLEDGEMENTS

First and foremost, I would like to express my sincere gratitude to Dr. Lei Sun, my supervisor, for being my advisor, mentor and launching my academic career. His profound knowledge and quick thinking give me a deep impression. I always get plentiful suggestions and ideas by discussing with him about my research work. I thank him for patiently guiding me, pointing out the problems with me, providing professional suggestions, and sharing the wisdom in both research and life with me.

I would like to thank Dr. Mo Yang, Prof. Yongping Zheng and Dr. Thomas Lee, in the Department of Interdisciplinary Division of Biomedical Engineering and Dr. Gu Yanjuan from Department of Applied Biology and Chemical Technology in the Hong Kong Polytechnic University for generous support in facility and knowledge.

I am also grateful to many colleagues and students who provide assistant in my experiment and providing knowledge support, most notably Miss. Xiaotong liang, Mr. Zhihai Qiu, Mr. Cheng Liu, Mr. Yongmin Huang, Miss Feifei Guo, Miss Qijin He, Miss Ailin Qing, Miss Weiwei Ye, Blizzard, Miss Jingyu Shi, Miss Jing Lv, Mr Feng Tian.

Finally I want to express my great thanks to my parents and brother for their support and continuous encouragement which have enriched me confidence and strength.

CONTENTS

CERTIFICATE OF ORIGINALITY	i
ABSTRACT	ii
ACKNOWLEDGEMENTS	v
CONTENTS	vii
LIST OF FIGURES	x
LIST OF TABLES	xiv
1 INTRODUCTION	1
1.1 Ultrasound Contrast Agent.....	1
1.1.1. History of Microbubble.....	1
1.1.2. Clinical Applications.....	4
1.2. Nanobubble	7
1.2.1. Approach to Produce Nanobubble	7
1.2.2. Challenge-Stability.....	10
1.2.3. Challenge-Surface Modification	12
1.2.4. Challenge-Nonlinear Property of Nano/Micro-bubble	12
1.3. Gas Vesicle.....	13
1.4. Potential Applications of Biogenic Nanobubble.....	16
1.5. Significance and Objectives.....	17
1.5.1. Significance.....	17
1.5.2. Objectives.....	18
2 NANOBUDDLE PRODUCTION	20
2.1 Introduction.....	20
2.2 Methods.....	21
2.2.1. Cell Culture	21
2.2.2. Intracellular Gas Vesicle Characterization.....	24
2.2.3. Concentrating Cell Solution.....	25
2.2.4. Lysing Cells and Isolation of Gas Vesicle	26
2.2.5. Characterization of Gas Vesicle.....	29

2.2.6.	Stability Test	29
2.3.	Results	30
2.3.1.	Two Cyanobacteria Cell Comparison	30
2.3.2.	Intracellular Gas Vesicle Characterization.....	32
2.3.3.	Isolated Gas Vesicle	34
2.3.4.	Stability Test	39
2.4.	Discussion	40
3	ACOUSTIC CHARACTERIZATION	42
3.1	Introduction	42
3.1.1	Bubble Oscillation and Resonance Frequency.....	42
3.1.2	Non-linear Property.....	45
3.2	Methods.....	47
3.2.1	Attenuation and Resonance Frequency	47
3.2.2	Harmonic Property	52
3.2.3	B-mode Ultrasound Characterization.....	57
3.3	Results	58
3.3.1	Transducer Characterization	58
3.3.2	Attenuation Signal.....	60
3.3.3	Attenuation Coefficient	61
3.3.4	System Error Verification	66
3.3.5	Harmonic Property	70
3.3.6	B-mode Image Characterization	76
3.3.7	Ultrasonic Stability Test.....	78
3.4	Discussion	80
4	BIOEFFECT CHARACTERIZATION.....	82
4.1	Introduction	82
4.2	Methods.....	83
4.2.1	Cell Culture	83
4.2.2	PpIX Coating.....	83
4.2.3	PpIX-nanobubble Characterization.....	84
4.2.4	Cell Attachment Experiment.....	85

4.2.5	Image Analysis.....	87
4.3	Results.....	88
4.3.1	Nanobubble Endocytosis.....	88
4.3.2	PpIX Coating.....	89
4.3.3	PpIX-nanobubble Endocytosis Property.....	91
4.3.4	Incubation Way Influence on Cell Attachment.....	95
4.4	Discussion.....	97
5	CONCLUSION AND FUTURE STUDY.....	99
5.1	Conclusion.....	99
5.2	Future Study.....	101
	REFERENCE.....	103

LIST OF FIGURES

Figure 1-1 Schematic structure of ‘Sonovue’	3
Figure 1-2 Biophysical effects of stably and inertial cavitating microbubbles. (A), (B) and (C) refer to biophysical effects caused by stable cavitation. (A) Pushing (left) and pulling (right) effects during the expansion and compression phase, respectively, of a stably oscillating microbubble, thereby disturbing the membrane integrity. (B) Acoustic radiation force causes microbubble displacement and compresses the microbubble against the cell membrane resulting in membrane disruption. The microbubble may even be pushed through the lipid bilayer to enter the cell. (C) Stable oscillation of a microbubble creates microstreamings in the surrounding fluid, which exert mechanical stress on the cell membrane, causing pore formation.19	6
Figure 1-3 A, Transverse section of a dividing cell of the cyanobacterium <i>Microcystis</i> sp. showing hexagonal stacking of the cylindrical gas vesicles. Magnification, x 31,500.58 B, Possible arrangement of GvpA molecules in the rib of the gas vesicle, based on X-ray crystallographic data of Blaurock and Walsby.59	14
Figure 1-4 Geometry of the <i>Anabaena</i> gas vesicle drawn to scale, with all measurements in nanometers; (a) intact gas vesicle longitudinal half, with double lines representing the wall thickness in the plain of the section; (b) cross-section of panel a; (c) collapsed gas vesicle, face view; (d) cross-section of panel c. The gas vesicle may be formed from two identical halves joined back-to-back at the center line. 63	15
Figure 2-1 Ana culture solution in luminance incubator (up) and customized air filter (lower).	23
Figure 2-2 High pressure providing and monitoring system	25
Figure 2-3 Left, Ana cell in 0.7M sucrose solution (arrow) covered by PBS (arrowhead). Right, microscope image of Ana cell during lysis, arrows point to isolated gas vacuole.....	27
Figure 2-4 <i>Anabaena</i> FACHB-245 (left) and <i>Anabaena</i> FACHB-1255 (right). Arrows point to cyanobacteria.	30
Figure 2-5 Phase contrast imaging of FACHB-245 (left) and FACHB-1255 (right). The bright dot (arrow head) represents the gas vesicle cluster in the cell.	31
Figure 2-6 The turbidity difference before and after gas vesicle collapse; data from FACHB-245 (left) and FACHB-1255 (right). (n=3, error bar is 1 standard deviation).....	32
Figure 2-7 Cell distribution change before (left) and after (right) gas vesicle collapse by 0.4MPa hydrodynamic pressure. Arrows point to cyanobacteria.	33

Figure 2-8 Phase contrast imaging of a single FACHB-1255 cell before (left) and after (right) applied with 0.4MPa pressure. Arrowhead point to a gas vesicle cluster before (left) and after broken (right).	33
Figure 2-9 Gas vesicle reserve percentage in relation with hydrostatic pressure (n=5, error bar= 1SD).	34
Figure 2-10 Upper, isolated gas vesicle with gradient concentration from low density to high density (left to right). Bottom, absorbance index in 500nm wavelength of gas vesicle vs normalized concentration. Y axial is concentration of gas vesicle represented by optical density at 500nm wavelength.	35
Figure 2-11 TEM image of a single gas vesicle from FACHB-1255	36
Figure 2-12 Hydrodynamic particle size measured by Particle Size Analyzer (PDI=0.09)	37
Figure 2-13 Size distribution in longitudinal direction (A) and transverse direction (B) calculated from TEM image. (n=38).	37
Figure 2-14 Mean and error bar (SD) size of transverse diameter, longitudinal diameter and hydrodynamic size.....	38
Figure 2-15 Mean value of hydrodynamic size from different batches (n=12), (error bar=1 SD).	39
Figure 2-16 Nanobubble concentration as the function of time. (n=3, error bar =1 SD)	39
Figure 2-17 Average size as the function of time. (n=3, error bar=1 SD)	40
Figure 3-1 Schematic diagram for attenuation measurement. Dark dots are nanobubbles.	47
Figure 3-2 A, photo of the attenuation characterization system. B, focused transducer. C, sample cell with acoustic membrane. D, quartz plane.....	49
Figure 3-3 Attenuation coefficient calculation flow chart	52
Figure 3-4 Setup to measure harmonic property	54
Figure 3-5 sample cell scheme and photo. Black dots represent nanobubble. Transmitter transducer covers 40 MHz and receiver transducer covers 80 MHz.	54
Figure 3-6 sampling cell for system harmonic noise testing.....	56
Figure 3-7 transducer characterization signal. Left column, signal in time domain; right column, power spectrum after Fourier transformation. From up to bottom plotted transducer #1, transducer #2 and transducer #3.....	58
Figure 3-8 backscatter signal with (B) and without (A) nanobubble; C, the power spectrum from A (solid line) and B (dotted line). Transducer #3, Concentration=0.27nM, OD500=0.7.	60
Figure 3-9 Backscatter signal of (A) transducer #1 and (B) transducer #2. Concentration=0.27nM, OD500=0.7. Solid line, signal from nanobubble; dotted line, signal from reference.....	61

Figure 3-10 Attenuation coefficient calculated from measurement of 3 transducers. From lower frequency to higher frequency is transducer #1, transducer #2 and transducer #3. Concentration=0.27nM, OD500=0.7.....	62
Figure 3-11 Attenuation coefficient from multiple measurement. Average of measurement (solid line) and each measurement (dotted line). Transducer #3, n=4, oncentration=0.27nM, OD500=0.7.....	63
Figure 3-12 Attenuation coefficient of NGV (0.125nM) got from narrow bandwidth pulse test. N=3.....	64
Figure 3-13 Backscatter signal intensity of nanobubble concentration gradient normalized to reference. N=4, error bar=1 SD.	65
Figure 3-14 Signal from function generator. Upper part, signal in time domain; lower part, frequency components. Vp-p=200 mV, frequency=40 MHz, cycle=30, PRF=100 Hz.....	67
Figure 3-15 Verification signal from power amplifier. Gain=54dB, input: Vp-p=200mV, frequency=40MHz, cycle number=30, PRF=100Hz.	68
Figure 3-16 System verification signal in time domain (upper) and frequency domain (bottom). Frequency=40 MHz, cycle bumber=30, PRF=100 Hz.	69
Figure 3-17 Backscatter signal from sample cell with (B) and without (A) nanobubble. Input voltage (p-p) =30 V, frequency=40 MHz, cycle number=30, PRF=100 Hz, OD500=3.0 time<1 min. *:80 MHz.....	70
Figure 3-18 Frequency components from reference (up) and nanobubble (bottom) after 200 average. Input voltage (p-p) =30 V, frequency=40 MHz, cycle number=30, PRF=100 Hz, OD500=3.0, time<1 min. *:80 MHz.	72
Figure 3-19 Peak negative acoustic pressure as the relation with input voltage (r2=0.995). Transducer #1, frequency=20 MHz, sine wave, cycle number=30, PRF=100 Hz.....	73
Figure 3-20 Nanobubble backscatter signal in frequency domain from up to bottom is related to normalized pressure 0.5, 0.6, 0.7, 0.8 and 0.9. Transmit signal: transducer #2, frequency=40 MHz, sine burst, cycle number=30, PRF=100 Hz, OD500=3.0, t<1 min.	74
Figure 3-21 Amplitude 2nd harmonic frequency as the function of acoustic pressure. Transmit signal: transducer #2, frequency=40MHz, sine burst, cycle number=30, PRF=100Hz, OD500=3.0, t<1min.....	75
Figure 3-22 fundamental and second harmonic frequency amplitude in relation with time. Transmit signal: transducer #2, frequency=40MHz, sine burst, cycle number=30, PRF=100Hz, OD500=3.0.	76
Figure 3-23 Ultrasound image of nanobubble as the function of concentration. (Frequency=40 MHz, n=3, number represent the optical density OD500).	77
Figure 3-24 Ultrasound image of nanobubble before (A) and after (B) broken by high intensity ultrasound. (OD500=1.0). Arrows point to marker which is not influenced by high intensity ultrasound. White frames represent nanobubble region terms from gray to dark after bubble broken.	77

Figure 3-25 Ultrasound image intensity compared to PBS in different time point. (n=3).....	78
Figure 3-26 Signal intensity of ultrasound image from the sample stimulated by ultrasound pulse continuously for 60 mins. (n=3, frame rate=5Hz)	79
Figure 4-1 Molecule formula and fluorescence property of PpIX. (Information from Sigma Aldrich).....	84
Figure 4-2 Image of purified nanobubble solution in PBS by phase contrast microscope. Concentration=0.5nM.....	88
Figure 4-3 Control group without nanobubble (left) and HeLa cell incubated with nanobubble (right). Arrows and arrowheads point to suspicious nanobubbles. 89	
Figure 4-4 Comparison with pure nanobubble and nanobubble coated with PpIX. A, photo of nanobubble before (left) and after PpIX coating kept steady for 2 hrs. B, zeta potential of nanobubble before (red) and after (green) PpIX coating....	90
Figure 4-5 PpIX-nanobubble stability test by size distribution.	91
Figure 4-6 Microscope image of PpIX-nanobubble from phase contrast, bright field and fluorescence. Excitation light wavelength is 405 nm.....	91
Figure 4-7 HeLa cell incubated with (A and B) and without (C and D) PpIX- nanobubble. A and C, bright field; B and D fluorescence microscope (Incubation overnight, nanobubble concentration= 0.5 nM, cell density= 3×10^4 cells/dish, excitation wavelength= 405 nm.).....	92
Figure 4-8 HeLa cell incubated with PpIX-nanobubble overnight. Left, phase contrast image; right, fluorescence image. Excitation light wavelength = 405 nm, nanobubble concentration = 0.5 nM, cell density = 3×10^4 cells/dish.	93
Figure 4-9 Optical density/pixel of PpIX incubation cells and control group. (n=8)	94
Figure 4-10 HeLa cells incubated with (A, B) and without (C, D) PpIX-nanobubble overnight imaged by confocal microscopy. A and C, bright field; B and D, bright field image merged with fluorescence image. Arrowheads point to PpIX- nanobubble. Excitation light wavelength = 488nm, nanobubble concentration = 0.5nM, cell density= 3×10^4 cells/dish.	95
Figure 4-11 Cell endocytosis with different incubation way, suspension cell incubation (A and B) and dish-adherent cell (C and D). A and C, phase contrast microscope image; B and D, fluorescence microscope image. Excitation light wavelength = 488 nm, nanobubble concentration = 0.5 nM, cell density = 3×10^4 cells/dish.	96
Figure 4-12 Optical density/pixel analysis based on fluorescence image between two incubation way. (n=4)	97

LIST OF TABLES

Table 1.1-1 List of first generation microbubble	2
Table 1.1-2 List of second generation microbubble.....	4
Table 1.2-1 Recent representative nanobubble with size and stability information	8
Table 1.2-2 Ostwald coefficient and disappearance time for 3 um diameter bubbles containing different gases. ²⁵	11
Table 2.1-1 BG11 Medium for cyanobacteria	23
Table 3.1-1 Scatter cross-section between different martial scatterer (r=5 um, f=5 MHz)	43
Table 3.2-1 Transducer characterization information regarding focal depth, center frequency, bandwidth and -20dB region.	59

1 INTRODUCTION

1.1 Ultrasound Contrast Agent

Ultrasound contrast agent is an echogenic particle to enhance the contrast of interested lesion in ultrasound imaging. The common type of UCA is microbubble whose acoustic impedance is significant different from soft tissue resulting in high intensity ultrasound contrast. Besides the enhanced ultrasound imaging contrast, the microbubble also can generate the harmonic frequency ultrasound wave. The transmit ultrasound frequency is named as fundamental frequency (f_0), then the harmonic frequency wave is double or triple the fundamental frequency ($2f_0$, $3f_0$). This harmonic property is not obviously in biological tissue and can be separated from ultrasound signal of tissue to help to allocated contrast agent. Microbubble, in addition to imaging function, is also widely used in controllable drug and gene delivery.

1.1.1. History of Microbubble

Gramiak *et al.* was the first group to use free bubble to enhance ultrasound echocardiography and used the term ‘ultrasonic contrast injections’ in 1968. They injected saline into the supra-avalvular position during continuous echocardiographic recording and found ‘a cloud of echoes limited by the parallel signals of the aortic root.’¹ However, this kind of free bubble without shell is very unstable and collapses dramatically in a short time when produced. Because of the stability problem, it was

not widely used in the following 15 years until laboratory production was realized. In 1984, Feinstein *et al.* invented sonication method to produce microbubble with relatively uniform and small size (< 10 μm). The prolonged and small size property facilitate it with the capability to pass through capillary beds especially the pulmonary vessels to reach left ventricle and imaging the left heart myocardium.² It is the milestone in the history of ultrasound contrast agent. After that, some commercial products came to market known as the first generation microbubble. The most famous commercial microbubble is *Echovist*³ by Scheing Company, *Albunex*⁴ by Molecular Biosystems Company and *Levovist*⁵ by Schering Company (Table 1.1-1). However, because the gas core used in first generation microbubble is air, it is easy to diffuse to the surrounding fluid and make it easy to break. Therefore the clinical application still was limited.

Table 1.1-1 List of first generation microbubble

Name	Filling Gas	Shell	Approval
Albunex	Air	Albumin	FDA
Echovist	Air	Galactose	European Medicines Agency
Levovist	Air	Galactose	European Medicines Agency

It is in 1993, researchers started to focus on the gas core molecules. Perfluoropentane as the gas core to replace air was proved to be more stable and have longer life time.⁶

⁷ Fluorocarbon gas with large molecular weight is hard to dissolve in water can enhance the stability of microbubble in biological environment. In 1997, the second generation microbubble ‘*Optison*’ was approved by American Food and Drug Administration (FDA). The gas core of *Optison* is C₃F₁₂ (Perfluoropentane) and encapsulated in albumin shell. ‘*Sonovue*’ is another second generation microbubble is composed of different shell composition from ‘*Optison*’. It used natural bilayer phospholipid as the shell encapsulating SF₆ (sulfur hexafluoride) gas. The structure is shown in (Figure 1.1-1). The common used commercial second generation microbubble is listed in (Table 1.1-2). The phospholipid shell is relative softer than polymer and protein shells.

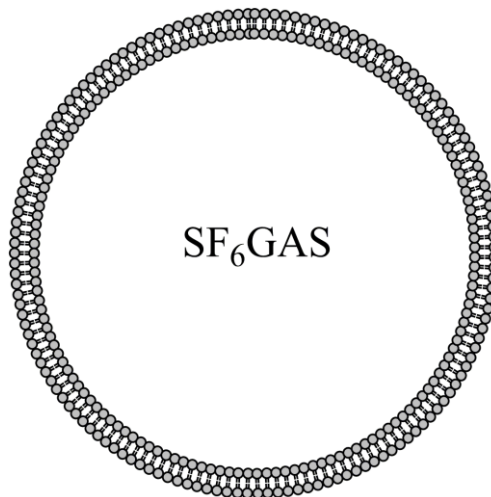


Figure 1.1-1 Schematic structure of ‘*Sonovue*’

Table 1.1-2 List of second generation microbubble

Name	Filling Gas	Shell	Approval
Echogen⁹	Perfluorocarbon	Sucrose	EMA
Definity¹⁰	Perfluorocarbon	Phospholipid	FDA, EMA
Optison¹¹	Perfluorocarbon	Albumin	FDA, EMA
SonoVue	Sulfur hexafluoride	Phospholipid	EMA, Switzerland, China,

1.1.2. Clinical Applications

Diagnostic Applications

Microbubble has been widely used in clinical ultrasound contrast imaging. It has good performance in artery stenosis evaluation in the lesions where conventional Doppler cannot tackle with. Clinical researches have demonstrated that it can increase the efficiency to detect renal artery stenosis.¹² Similar disease related to artery is carotid artery stenosis where the residual blood flow is too weak to be detected by Doppler. However the weak blood flow is an indicator to make surgery strategy and no blood flow is a risk sign. In this circumstance, intravascular microbubble can enhance the specificity of blood flow evaluation compared to conventional Doppler.

In addition to applications in artery stenosis evaluation, microbubble is also widely used in Echocardiography. One important and straightforward application is to delineate endocardial border to assess myocardial contractility.¹³ The poor visualized

endocardial border in B-mode ultrasound image can be detected clearly after intravenous injection of microbubble. It can also help to evaluate micro-vasculature such as myocardial vessels which cannot be detected without microbubble. Compared to angiograph and nuclear method it is non-invasive and free of radiation.

Microbubble also used in liver disease diagnosis such as focal nodular hyperplasia (FNH), regenerating nodules and haemangiomas¹⁴ because liver contains approximate 30% blood and very large vascular volume of the sinusoids.

Therapeutic Applications

Microbubble is also used in therapy purpose or assistant therapy. It has been widely used in drug and gene delivery. The mechanism is based on ‘sonoporation’ effect. Microbubble attached to cell surface can open cell membrane like drilling a hole when stimulated by ultrasound wave. Cell membranes can close and repair provided the damage is limited. During ‘sonoporation’ effect, even large molecules like pharmaceutical agents (chemotherapeutic drug) and DNA/RNA can enter cytoplasm (and possible also the nucleus).^{15, 16, 17, 18} There is several mechanism can explain sonoporation effect (Figure 1.1-2). Though the microbubble has been demonstrates good performance in drug delivery and gene therapy, the application is still limited in endothelial cell because it is too large to penetrate through vessel wall.

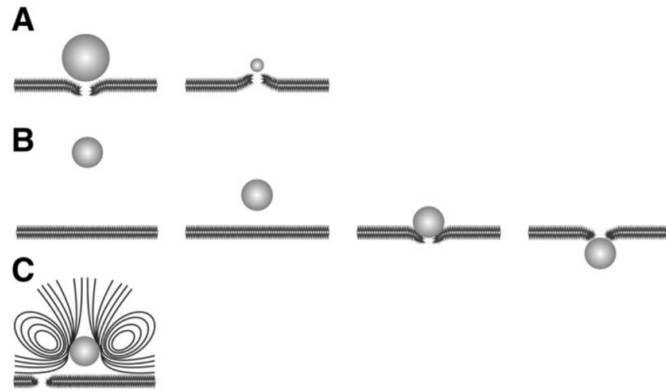


Figure 1.1-2 Biophysical effects of stably and inertial cavitating microbubbles. (A), (B) and (C) refer to biophysical effects caused by stable cavitation. (A) Pushing (left) and pulling (right) effects during the expansion and compression phase, respectively, of a stably oscillating microbubble, thereby disturbing the membrane integrity. (B) Acoustic radiation force causes microbubble displacement and compresses the microbubble against the cell membrane resulting in membrane disruption. The microbubble may even be pushed through the lipid bilayer to enter the cell. (C) Stable oscillation of a microbubble creates microstreamings in the surrounding fluid, which exert mechanical stress on the cell membrane, causing pore formation.¹⁹

Currently all of the clinical application of microbubble is limited within vasculature such as endocardial border, renal and carotid artery and liver sinusoids. Though it can be used to evaluate tumor, the scope is still restricted to tumor neovasculature detection. The critical factor attribute to the limitation is the size of microbubble. The large diameter of microbubble in micrometer scale makes it impossible to penetrate through endothelial cells even in the region with enhanced permeability and retention effect (EPR) where the maximum gap is around 400nm.

1.2. Nanobubble

Though microbubble is widely used in clinical application and cancer diagnosis, their relatively large size (1 – 8 μm) limits its application within vasculature. To precisely image the extravascular region and perform efficient therapy, the size of bubble needs to be reduced to nanometer scale to penetrate through leaky vessel wall in tumor region. The neovasculature in tumor region is malfunction with leaky gaps between endothelial cells and lack of lymphatic drainage. Therefore the nanoparticle, smaller than 400~700nm can penetrate out of the vessel wall and accumulate in tumor extravascular matrix, the phenomenon known as EPR effect (enhanced permeability and retention).²⁰ However reducing bubble size is not an easy task by using traditional microbubble synthesis method. Many research teams are trying to synthesize nanometer size bubble using novel techniques.

1.2.1. Approach to Produce Nanobubble

Several approaches was tried to produce nanobubble in laboratory way. The most common way is through post-generation separation. The bubble synthesized in conventional way is polydispersed from hundred nanometer to several micrometer.²⁹ Nanometer size bubble can be separated from the original polydispersed bubble by centrifuge method with the help of the buoyance difference.^{30, 31, 32, 33, 34} Hengli *et al.* (2015) used this method to produce nanobubble (average size $478 \pm 29.7\text{nm}$) with C_3F_8 gas core encapsulated by liposome film.³⁵ The stability was tested by measuring

the concentration change with time. In the 20th min, the residual concentration is only 30% of the original one and the bubble almost disappears in 25th min. The stability test result, though comparative with the commercial microbubble, is not strong enough to perform tumor molecular imaging which needs at least 1 h half-life time. The recent progress made by researchers is collected and listed in (Table 1.2-1). Many groups have succeeded to synthesize nanobubble, but the stability still remains a problem.

Table 1.2-1 Recent representative nanobubble with size and stability information

Name	Year	Shell	Gas	Size (nm)	Stability test
Nanobubble ³³	2012	DPPC, DPPA, PEG- DSPE	C ₃ F ₈	436.8±5.7	Half-time: 21 mins
Cationic-nanobubble ³²	2013	DSPC, DPPG, PEG	C ₃ F ₈	521.2±37.57	Duration of contrast enhancement: 23.2±1.4 mins
Affibody-nanobubble ³⁵	2015	DPPC, PEG- DSPE	C ₃ F ₈	478 ±29.7	In vitro concentration test: disappear over 25 mins

Changing the gas core to large molecular weight gas, though extensively enhances the stability of bubble, seems not to solve the problem intrinsically. Some researches started to change the shell mechanical property. Liyi *et al.* (2013) succeeded to replace the lipid shell by chitosan layer and significantly increased shell strength and bubble

stability. The average size is 359nm (PDI=0.46) measured by dynamic light scatter method. The strongest ultrasound signal was found over 2hr injection representing the significant increased life time compared with lipid nanobubble.³⁶ However, the researcher also found the sacrifice of ultrasound harmonic signal, which is fundamental property for ultrasound contrast imaging. Without the harmonic property, the bubble signal is hard to be differentiated from surrounding tissue. To conquer the stability problem, alternative ultrasound contrast agent like silica nanoparticles (MSNs) are developed for ultrasound imaging and therapy with tumor-specific targeting ligand.^{37, 38, 39, 40, 41} However, these nanoparticle all loss the microbubble harmonic and controllable broking property as well. A. Exner *et al.* (2015) developed a new nanobubble with enhanced stability by adding pluronic and N-N-Diethyacrylamide as stabilizing agent.⁴² However, whether the strengthened crosslink structure of stabilizer has negative influence on its harmonic oscillation property is not mentioned in her report.

Challenges still exist in developing nanometer size bubble. Three major issues should be taken into consideration: stability (steady state and under sonicating), surface modification and harmonic property

1.2.2. Challenge-Stability

Stability and circulation half-life is a significant issue for nanoparticle molecular imaging or therapy. Circulation half-time ($t_{1/2}$) describes blood pool residence and is the period over which the concentration of circulating nanoparticles (NPs) remains above 50% of the injected dose, analogous to a drug's half-life.²¹ The ideal $t_{1/2}$ is dependent on application. In imaging, 2-6 hrs is optimal for injection, accumulation at targeted site.²² For nanobubble, the major factor determines $t_{1/2}$ is bubble stability.

The most significant problem comes with the bubble size reduction is stability. Bubble stability is related to the counteractive forces of the partial pressures of dissolved gasses in the surrounding fluid and the total pressure inside bubble.²³ According to Eq.1.2-1, the Laplace pressure is inversely proportional to bubble radius. Therefore the smaller the bubble size, the larger the Laplace pressure and total pressure inside bubble. The increased pressure inside bubble makes the gas dissolve more quickly to the surrounding environment.

$$P_b = \Delta P + P_a = \frac{2\sigma}{R} + P_a \quad (1.2-1)$$

Equation 1.2-1: P_b : total pressure inside bubble, ΔP : Laplace pressure, P_a : ambient pressure outside of bubble (constant in steady state), σ : surface tension at gas bubble interface, R : bubble radius.

The Ostwald coefficient (L) is the milliliters of gas dissolved per milliliter of liquid and per atmosphere (760 mm Hg) partial pressure of the gas at any given temperature. It is an important parameter describing dissolution of bubbles and is defined as the dimensionless ratio of the solubility of the gas in the liquid to the gas density. Gases with lower Ostwald coefficients dissolve more slowly compared to gases with higher Ostwald coefficients.²⁴ The disappearance time of different gas as bubble (3 μm) core is listed in the (Table 1.2-2)²⁵. Though the Perfluoropropane increase the disappearance time about 50 times compared with air core, it is still only 1.1s for 3 μm free bubble. The time will even be shorter than 1.1 s if bubble size reduced.

Table 1.2-2 Ostwald coefficient and disappearance time for 3 μm diameter bubbles containing different gases.²⁵

Gas	Ostwald coefficient (x10⁶)	Disappearance time (s)
Air	23168	0.02
Sulfur hexafluoride	5950	0.1
Perfluoropropane	583	1.1
Perfluorohexane	24	2

Adding shell to free bubble like surfactant and lipid can help to increase the disappearance time to stabilize the bubble in nanometer scale size. However the real stability and disappearance time varies and almost less than 30 mins.

1.2.3. Challenge-Surface Modification

Nanoparticle can attached to specific cell and targeted site with increased specificity by appropriate targeting ligand on bubble shell like HER2 and EGFR.²⁶ There are two basic methods of attaching ligand to the microbubble surface: direct covalent bond or biotin-avidin linking.²⁷ Biotin-avidin attachment, though useful in preclinical experiment and test, is hard for clinical transport because of the potential immunological effect.²⁷ Covalent ligand binding can be performed prior or subsequent to creation of the microbubble shell; the ligand including carbodiimide or thiol group.²⁸ For lipid-coated agents, the advantage of using a preformed ligand-lipopolymer is that fewer steps are required in the clinical setting between microbubble production and administration into the patient. However the covalent binding strategy is never used in bubble in nanometer size. One possible reason may be the unstable structure of nanobubble which makes the ligand attachment process more complex and the final structure unpredictable and unstable.

1.2.4. Challenge-Nonlinear Property of Nano/Micro-bubble

Non-linear property of nano/micro bubble is both the physical property and ultrasound contrast imaging technique. When bubble excited by ultrasound of fundamental frequency, it can generate and scatter ultrasound wave with additional higher frequency component other than fundamental frequency. Therefore the non-linear effect of nanobubble are used in ultrasound contrast mode, because bubble typically

response more non-linearly than tissue. However, with the increased strength of bubble shell, the non-linear property will be reduced. Thus to enhance the stability of nanobubble without sacrificing the harmonic response is still a scientific challenge.

1.3. Gas Vesicle

Gas vesicle is a biogenic air nanobubble with extremely high stability and found to shown high ultrasound contrast ability and harmonic property by the research of Shapiro *et al.*⁴³ Because the nanostructure of gas vesicle intact with gases through a mechanism that is fundamentally different from that in microbubbles. Whereas artificial microbubbles trap pre-loaded gas, gas vesicles exclude water but permit gas from the surrounding media to freely diffuse in and out of through 4.6nm interval on 2 nm thick protein wall. The property excluding water and permitting gas flow is attributed to its special wall structure. The wall of gas vesicle is a bilayer structure. The outer layer is hydrophilic to reduce surface tension and the inner layer is hydrophobic to exclude water out of the 4.6 nm intervals. And the gas can still flow in and out through the interval freely. As a result, no pressure gradient exists between the inside and outside of gas vesicles, permitting them to be inherently stable despite their nanometer size.

Gas vesicles are the components of gas vacuoles, which were discovered in cells of waterbloom-forming cyanobacteria by German microbiologists nearly a century ago

(Figure 1.3-1).^{55, 56, 57} The function of gas vesicle and gas vacuole is to provide buoyance to the cyanobacteria.

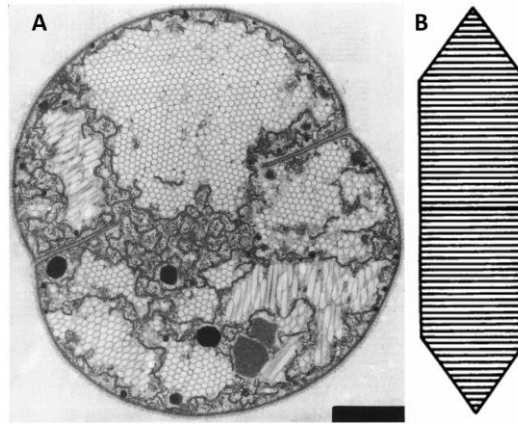


Figure 1.3-1 A, Transverse section of a dividing cell of the cyanobacterium *Microcystis* sp. showing hexagonal stacking of the cylindrical gas vesicles. Magnification, x 31,500.⁵⁸ B, Possible arrangement of GvpA molecules in the rib of the gas vesicle, based on X-ray crystallographic data of Blaurock and Walsby.⁵⁹

Gas vesicle with a wide range of size and shapes are found in different cyanobacteria species. In the kind of freshwater cyanobacteria like *Anabaena flos-aquae*, the common shape is long and narrow like cylinder.⁶⁰ The average width and length is about 84 nm and 500 nm for *Anabaena flos-aquae* (Figure 1.3-2).^{61, 62} Within each species of cyan bacterium the cylinder diameter is fairly uniform, with a standard deviation of about $\pm 4\%$.

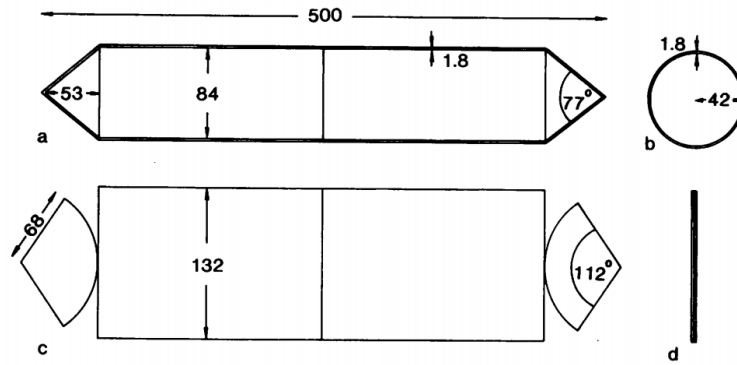


Figure 1.3-2 Geometry of the *Anabaena* gas vesicle drawn to scale, with all measurements in nanometers; (a) intact gas vesicle longitudinal half, with double lines representing the wall thickness in the plain of the section; (b) cross-section of panel a; (c) collapsed gas vesicle, face view; (d) cross-section of panel c. The gas vesicle may be formed from two identical halves joined back-to-back at the center line.⁶³

The structure of gas vesicle shell is like ribs. The thickness of the rib is about 1.95 nm in *Anabaena flos-aquae* by X-ray crystallography.⁵⁹ This value is smaller compared to Electron-microscopic measurement 2.8nm.⁶⁴ The X-ray crystallography is more reliable than electron-microscopy result because the metal layer produced in measurement process is calculated in electron-microscopic result. The ribs are periodically aligned and the periodicity of the ribs indicated by the various methods was between 4 and 5 nm.⁶⁵ Gas vesicle shows both compressibility and strength in Walsby's experiment.⁶⁶

1.4. Potential Applications of Biogenic Nanobubble

If biogenic nanobubble is proven to be a stable, oscillating non-linearly and easily surfaced modified contrast agent, it may equip ultrasound technology with the ability to perform extravascular molecular imaging and therapy.

Firstly, it is an intrinsic theranostic nanoparticle. It can leakage outside of vessels in tumor region to accumulate more efficiently and help to detect tumor with increased specificity and sensitivity making tumor diagnosis possible in early stage with ultrasound modality. Combined with targeting ligand, it can attach to tumor cell specifically. At the time tumor is detected, drug or gene can be controlled to deliver by modifying ultrasound intensity and focal depth by breaking nanobubble or sonoporation effect.

Secondly, nanobubble can help to increase diagnosis and therapy efficiency by ultrasound radiation force provided it carrying other contrast agent or drug. The reason why it can increase sensitivity is because nanobubble can be pushed out of vessel wall when stimulated by ultrasound wave. This phenomenon is known as acoustic radiation force. Vitro experiment has demonstrated that it can increase accumulation rate to as high as 20% about 20 times the passive accumulation. The intensively increased accumulation rate can increase the sensitivity of diagnosis and efficiency of therapy. The potential application is far beyond these 2 points if combined with other nano technology and imaging technology like ultrasonic super resolution.

1.5. Significance and Objectives

1.5.1. Significance

Microbubble, as an ultrasound contrast agent, has been widely used to detect and cure diseases related to vasculature. However the application of microbubble is restricted within blood pool because of its micrometer size. To explore the application of ultrasound contrast agent beyond vasculature, a new generation contrast agent is extremely needed. The size should be smaller than 400 nm to penetrate through vessel wall by EPR effect. Some group have made great effort to synthesize nanometer size bubble. The results are encouraging, but challenges are still faced by researchers. The most significant challenge is the balance of stability and ultrasound harmonic signal. To retain bubble-nonlinear effect (harmonic signal), the bubble shell should be soft and easy to be deformed. However, this structure will make nanobubble unstable lasting less than 25 mins even in PBS solution. 25 mins existent time is not enough for its accumulation in focus region. A rigid shell can solve the stability problem, but it sacrifices the non-linear property resulting in low contrast ability. Surface coating is another problem of nanobubble because of its unstable feature.

A biogenic nanobubble called gas vesicle, generated by cyanobacteria, has the nature structure to provide both great stability and non-linear property without compromising strategy. Because the nanostructure of gas vesicle intact with gases through a

mechanism that is fundamentally different from that in microbubbles. Whereas microbubbles trap pre-loaded gas, gas vesicles exclude water but permit gas from the surrounding media to freely diffuse in and out.

The in vitro and in vivo performance of gas vesicle have been studied by Shapiro *et al.* using commercial ultrasound machine. However, previous researches did no further investigation in the physical property (resonance frequency and non-linear effect at proper stimulation) and its bioeffect to tumor cell like endocytosis rate. In my research, gas vesicles are characterized in these properties: stability, resonance frequency, non-linear oscillation, surface modification and cellular endocytosis.

1.5.2. Objectives

The specific objectives in my research including:

- To produce biogenic nanobubble from cyanobacteria including production rate evaluation between different cell species and isolation method.
- To characterize the morphology, concentration, surface charge of isolated nanobubble.
- To characterize the steady state and stability under sonication by measuring concentration, size distribution and ultrasound signal intensity.

- To find resonance frequency by attenuation method using pulse echo testing system.
- To characterize the non-linear property as the function of acoustic pressure and time.
- To test the surface modification ability by fluorescence dye (PpIX)
- To test the tumor cell (HeLa) endocytosis ability using different imaging modality for verification including: fluorescence microscopy, phase contrast microscopy and confocal microscopy.

2 NANOBUBBLE PRODUCTION

2.1 Introduction

Gas vesicles are the components of gas vacuoles, which were discovered in cells of waterbloom-forming cyanobacteria. The function of gas vesicle and gas vacuole is to provide buoyance to the cyanobacteria. Gas vesicle with a wide range of size and shapes are found in different cyanobacteria species. In the kind of freshwater cyanobacteria like *Anabaena flos-aquae*, the common shape is long and narrow like cylinder.⁶⁰ The structure of gas vesicle shell is like ribs. The thickness of the rib is about 1.95 nm in *Anabaena flos-aquae*. Gas vesicle shell shows both compressibility and strength.

Some researches find that gas vesicle production varies between different cyanobacteria species even within the same species.⁷¹ *Anabaena flos-aquae* was reported commonly to produce gas vesicle with relative high chance. However whether the cyanobacteria contains gas vesicle should be tested case by case before isolation procedure. In my research, two categories under same species (*Anabaena flos-aquae*) were tested on gas vesicle concentration.

Isolating gas vesicle from cell body including four steps: concentrating, lysing cells, isolation and purification. Concentrating can be achieved by cell floating for overnight. After that, lysing cyanobacteria like *Anabaena* can be done by Osmotic shrinkage.

When the cell placed in strongly hypertonic sucrose solutions, cell lose water and shrink. The cell plasmolemma is firmly attached to the cell wall, and the shrinkage plasmolemma pull the cell wall and finally destroy it. After gas vesicle separated from cell, it can be collected by centrifuge and gas vesicle can floating on the fluid surface because of buoyance. Purification is performed by the same centrifuge procedure as isolation for three times.

The Isolated gas vesicle characterization including morphology, size distribution, surface charge, concentration and stability rest. Stability test includes two aspects: one regarding concentration and other regarding size distribution.

2.2 Methods

2.2.1. Cell Culture

Two cyanobacteria were selected to produce gas vesicle which are *Anabaena flos-aquae* (FACHB-1255) and *Anabaena flos-aquae* (FACHB-245). The algae seeds were acquired from Freshwater Algae Culture Collection at the Institute of Hydrobiology. The initial concentration and volume is 10^6 cells/L, 15ml. The seeds were transferred to 30ml BG-11 (Table 2.2-1) culture medium (QingDao Hopebio-Technology Co., Ltd., QingDao, Shandong, China) in sterilized Erlenmeyer flask. Erlenmeyer flask containing cells were sealed by tinfoil and kept in illumination incubator (PGX-180A, LNB Instrument Co. Ltd., Shanghai, China) (Figure 2.2-1). The temperature, luminance intensity and day-night cycle were set to be 25 ± 1 °C, 1000Lux, 14Hr day/

10Hr night. The cell solution were required to be shaken gently by 3 times per day to artificially diffuse carbon dioxide to cell solution. After 20 – 30 days, if the concentration of cells recovered to the initial concentration, it can be retransferred to new medium with the volume 5 times the cell solution and cultured in the same condition. When the cell volume was larger than 500 ml, it need air pump to deliver air constantly instead of shaking. The air pumped to cell solution was sterilized and purified by customized purification system (Figure 2.2-1) consisting of activated carbon tube and physical air filter with 0.22 μ m pore size. The concentration of cyanobacteria can be characterized by the light absorbance index of cell solution using spectrophotometer (Ultrospec 2100 pro, GE Healthcare Life Sciences, Piscataway, NJ, USA). For *Anabaena*, the characteristic light wavelength is 650nm. To verify the optical density concentration characteristic method, 7 known concentration gradient was prepared to test the absorbance index as the function of concentration. Growth rate can be calculated by absorbance index in 650nm for *Anabaena* $\mu (d-1) = (\ln(x1)-\ln(x2))/t$. x1 and x2 are the starting point of cultivation and measurement point; t is the time interval between two measurement.

Table 2.2-1 BG11 Medium for cyanobacteria

Component		Concentration (/L)
NaNO ₃		1.5 g
K ₂ HPO ₄		0.04 g
MgSO ₄ ·7H ₂ O		0.075 g
CaCl ₂ ·2H ₂ O		0.036 g
Citric acid		0.006 g
Ferric ammonium citrate		0.006 g
EDTA (disodium salt)		0.001 g
NaCO ₃		0.02 g
Trace metal mix A5	Stock Concentration (/L)	1.0 ml
H ₃ BO ₃	2.86 g	
MnCl ₂ ·4H ₂ O	1.81 g	
ZnSO ₄ ·7H ₂ O	0.222 g	
NaMoO ₄ ·2H ₂ O	0.39 g	
CuSO ₄ ·5H ₂ O	0.079 g	
Co(NO ₃) ₂ ·6H ₂ O	49.4 mg	
Distilled water		1.0 L



Figure 2.2-1 *Ana* culture solution in luminance incubator (up) and customized air filter (lower).

2.2.2. Intracellular Gas Vesicle Characterization

Phase contrast microscopy (Eclipse TS100, Nikon Corporation, Chiyoda, Tokyo, Japan) was used to observe the existence of gas vesicle. The strong contrast between the gas vesicle and cytochylema is from the refraction index difference between gas and cytochylema and phase contrast microscope can visualize this difference. Moreover, the intracellular gas vesicles exist in cluster way forming gas vacuole at the size of micrometer which is easier to observe under microscope.

The quantitative way to characterizing the intracellular gas vesicle is to measure the light scattering by using turbidity meter⁵⁸ (SGZ-200A, Shanghai Yuefeng Co., Ltd., Shanghai, China). The principle is that cyanobacteria with gas vesicle can scatter more light than the one without gas vesicle and this correlation is linear. To measure the relative gas vesicle concentration and characterize the critical pressure of intracellular gas vesicle, a simple customized high pressure system (Figure 2.2-2) was made to provide and monitor high pressure environment to the cell solution. The maximum pressure can reach 3MPa (30atm) and the sensitivity is 0.1 atm. Firstly, the turbidity of two kind *Ana* cells were measured and recorded. Then, a max 1 MPa was given to the cyanobacteria cell to ensure all the gas vesicle inside was broken. The turbidity of *Ana* solution after gas vesicle broken was measured again. The difference between first and second measurement was used to characterizing the relative intracellular gas vesicle concentration. The results from these two species cyanobacteria was compared to select a high throughput one. The relation between gas vesicle broken proportion

and pressure is studied to determine the critical pressure of intracellular gas vesicle which will be useful in gas vesicle isolation process.

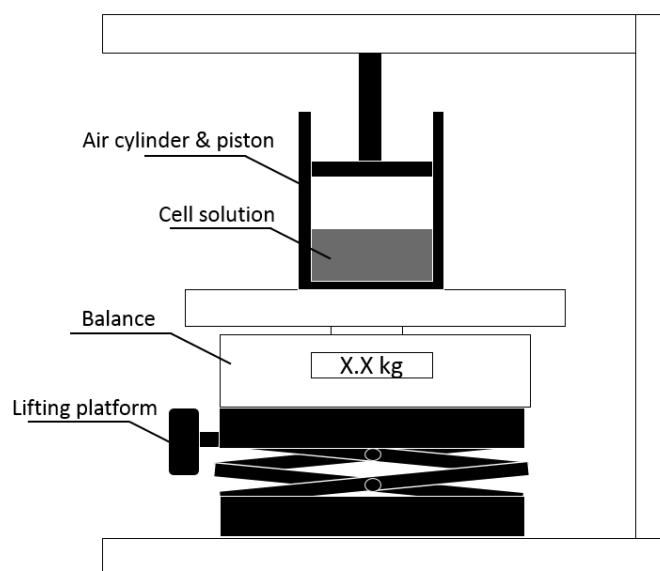


Figure 2.2-2 High pressure providing and monitoring system

2.2.3. Concentrating Cell Solution

To ensure high throughput of gas vesicle isolation, it is an efficient way to concentrating cell solution before isolation. Two methods were used: flotation and filtration.⁶⁷

Flotation is a way to concentrating cell by keeping the solution steady without shaking or air pumping overnight. The *Ana* cell containing great volume of gas vesicle can flow to the surface of the solution and form a green cream-shape layer on top of the solution. The top layer can be collected by drowning off using a syringe needle. This method is high throughput and can reach as high as 10 concentrating rate.

Filtration is the next step after flotation concentrating to get cell solution with even higher concentrating rate using glass fiber filter with 50mm diameter and 1 μ m pore size and a vacuum pump.

2.2.4. Lysing Cells and Isolation of Gas Vesicle

Osmotic shrinkage is a common way to lyse specific cyanobacteria like *Anabaena*. The cell solution was mixed with sucrose rapidly to reach the final concentration of 0.7M.⁶⁷ To control this process under a limited time as short as possible. A sucrose solution of 1.4M concentration was prepared before lysing cell. Then an equal volume of sucrose solution was added to cell solution. The cell with sucrose solution was kept shaking for 1.5 hours to ensure cell fully lysis. When the cell placed in strongly hypertonic sucrose solutions, cell lose water and shrink. The cell plasmolemma is firmly attached to the cell wall, and the shrinkage plasmolemma pull the cell wall and finally destroy it (Figure 2.2-3).

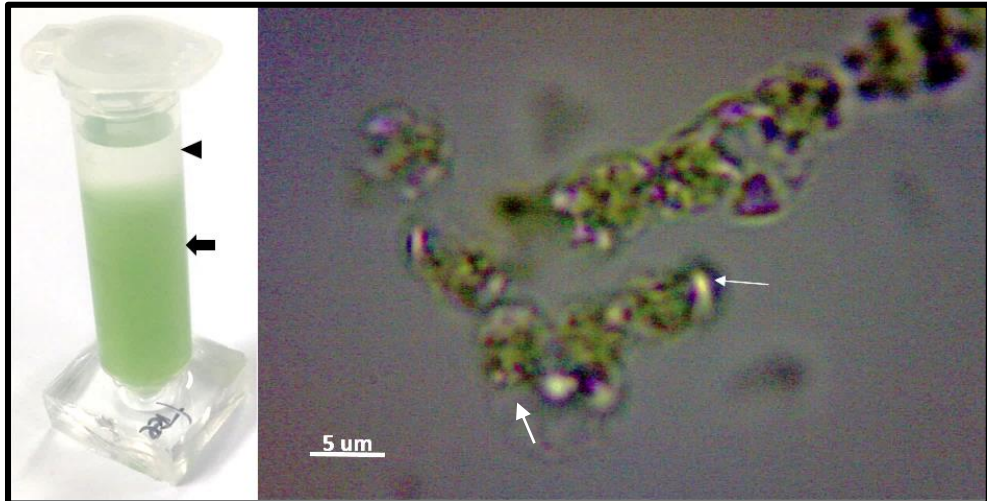


Figure 2.2-3 Left, *Ana* cell in 0.7M sucrose solution (arrow) covered by PBS (arrowhead). Right, microscope image of *Ana* cell during lysis, arrows point to isolated gas vacuole.

After gas vesicle was released from cell, it can be collected by centrifuge. The density of intact gas vesicle is about 100 kg/m^2 lower than other cell components and let it floating more rapidly. This process can be accelerated by centrifuge.⁶⁷

During the centrifuge process, the most important issue to be considered is the pressure under the bottom of sucrose solution. The pressure p is equal to ρah , where ρ is the density of sucrose solution, a the relative centrifuge acceleration and h the fluid depth. The pressure under the bottom of centrifuge tube should not exceed the critical pressure to avoid broken. The centrifuge tube and volume was 2ml corresponding to the depth of 26 mm. If the maximum acceptable pressure is 1.5 atm at the bottom, below which, as much as 90% nanobubble can be reserved according to the bubble

critical pressure measurement. By using the equation, the maximum permissible a can be calculated:

$$a = \frac{p}{h\rho} = \frac{150 \times 10^3 \text{ Nm}^{-2}}{26 \times 10^{-3} \text{ m} \times 1090 \text{ kgm}^{-3}} = 5292 \text{ msec}^{-2} (529 \text{ rcf}) \quad (2.1-1)$$

Therefore the centrifuge speed is selected to be 400 rcf lower than 529 rcf. Just before the centrifuge process, phosphate buffer (PBS) was added on the top of sucrose solution with height of 5mm to purify the isolated gas vesicle and keep the pH within the stable region between 6 and 9.5.⁶⁷ The rate of rise depends on the viscosity of the medium which is 0.5×10^{-3} and $1.2 \times 10^{-3} \text{ mm min}^{-1} \text{ G}^{-1}$ for 0.7M sucrose and water respectively. The centrifuge time was calculated to be 2 hrs26mins for 26 mm height and 400g rcf. The centrifuge time should not exceed the time required to bring all gas vesicles to the surface because the extra time allows the other cell components to float to surface and make the purification process more complicated. Besides some enzyme released during cell lysis may weaker the stability of gas vesicle if gas vesicle left unpurified too long.

After the centrifuge, the isolated gas vesicle flowing on the surface of the sucrose solution formed a white cream layer. A fine oblique needle was used to draw off the white layer in contact with the meniscus. The centrifugation procedure was repeated at least three times by diluting the gas vesicle solution to 5x volume of PBS.

2.2.5. Characterization of Gas Vesicle

Gas vesicle concentration was measured by optical density method which is the light absorbance index of gas vesicle solution at 500nm wavelength using spectrophotometer. According to the study by other researchers, the relation of concentration and optical density is 450pM/OD500.⁴³ A known concentration gradient was used to verify the linearity of the optical density method. Size distribution and zeta potential was test by using Zeta Potential Analyzer (ZetaPlus, Brookhaven Instruments Corp., USA) at the concentration under 100pM. The fine shape and size was got using transmission electron microscopy (TEM) equipped with an Oxford Instrument EDS system, with the operating voltage of 200 kV. A droplet of nanobubble solution (0.5nM, 10 uL) was dripped on holey 400 mesh copper grids coated with carbon for TEM characterization.

2.2.6. Stability Test

Steady state stability is to test the stability of nanobubble without ultrasound stimulation in PBS solution with the similar osmotic pressure to blood at room temperature. This result is important to evaluate the bubble circulation time. Steady state stability was tested from 2 aspects (concentration and size distribution). Concentration as the function of time is measured using optical density method with spectrophotometer. The characterization wavelength was 500nm. Size distribution was measured using dynamic light scattering method with zetasizer.

2.3. Results

2.3.1. Two Cyanobacteria Cell Comparison

Two *Anabaena* cell lines (FACHB-1255 and FACHB-245) are cultured at the same time. These two species are different in the color and distribution in the solution (Figure 2.3-1). FACHB-245 express dark green color and concentrated on the bottom of the bottle, whereas, the FACHB-1255 express white green color and floats on the surface of the solution. This is because the gas vesicle can provide buoyance and make the cell floating upward, and the gas vesicle also can scatter light and make the cell looks like a white green cream. Therefore the color and distribution can provide an easy way to roughly identify whether the cells containing gas vesicle.

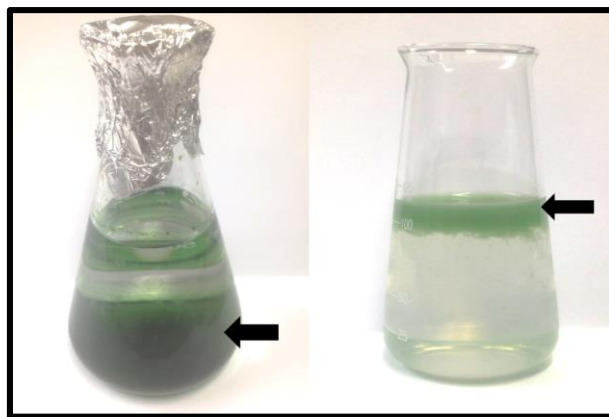


Figure 2.3-1 *Anabaena* FACHB-245 (left) and *Anabaena* FACHB-1255 (right).

Arrows point to cyanobacteria.

The color and distribution, though is an easy way to identify the existence of gas vesicle, is not a solid evidence to get the conclusion. The more scientific way is to use phase contrast microscope (Figure 2.3-2). The cells both FACHB-1255 and FACHB-245 are chaplet shape. However the cell length of FACHB 245 is longer than FACHB

1255 and each single cell is smaller. The most important structure should be notice is the bright dot within the cell which represents the gas vesicle cluster. The more gas vesicles are contained in the cell, the greater number of bright dots are in side cell. From the figure, it can be concluded that the FACHB-1255 contains significantly more gas vesicles than in FACHB-245 which contains even no gas vesicle. This conclusion is consistent with the light scattering result (Figure 2.3-3). The turbidity result is got from the turbidity difference before and after gas vesicle was collapsed by high hydrostatic pressure. The turbidity difference represents the gas vesicle concentration inside the cell. From the result, the turbidity difference of FACHB-1255 (94.3 ± 0.5 NTU) is much larger than FACHB-245 (0.36 ± 0.52 NTU) almost 100 times.

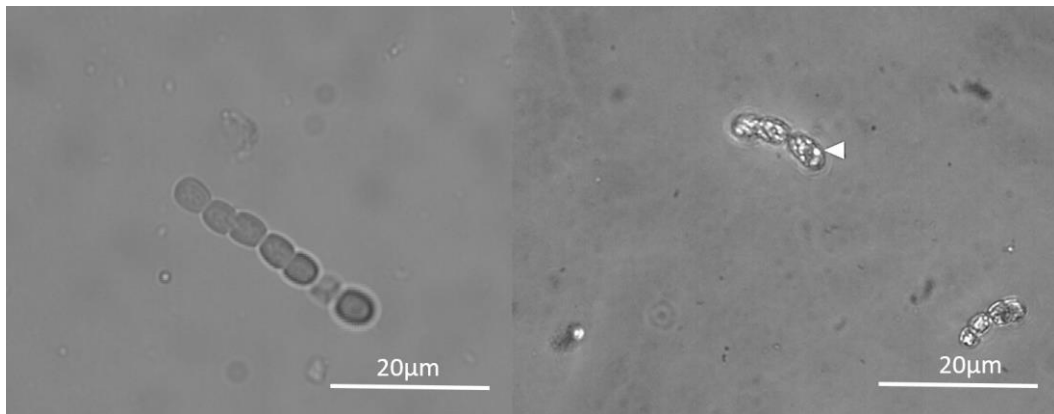


Figure 2.3-2 Phase contrast imaging of FACHB-245 (left) and FACHB-1255 (right).

The bright dot (arrow head) represents the gas vesicle cluster in the cell.

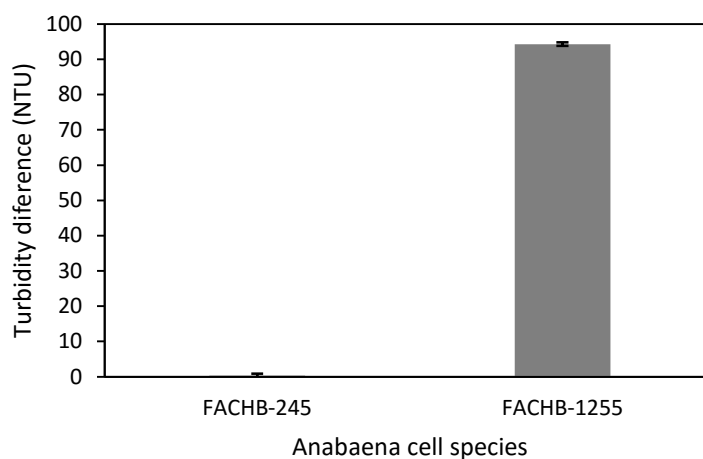


Figure 2.3-3 The turbidity difference before and after gas vesicle collapse; data from FACHB-245 (left) and FACHB-1255 (right). (n=3, error bar is 1 standard deviation)

2.3.2. Intracellular Gas Vesicle Characterization

From the experimental results, conclusion can be drawn that the FACHB-1255 has a higher gas vesicle throughput than FACHB-245. Thus FACHB-1255 was selected as the further experimental subject to produce gas vesicle. Before the isolation procedure, more solid characterization of gas vesicle in intracellular way was done by comparing the difference before and after gas vesicle collapsing by high pressure. The first simple characterization is to observe the distribution change of the *Anabaena* cell (Figure 2.3-4). The cells float on the surface of the solution before it is applied with high hydrostatic pressure, whereas they sink to the bottom after the intracellular gas vesicle broken by 0.4 MPa pressure.

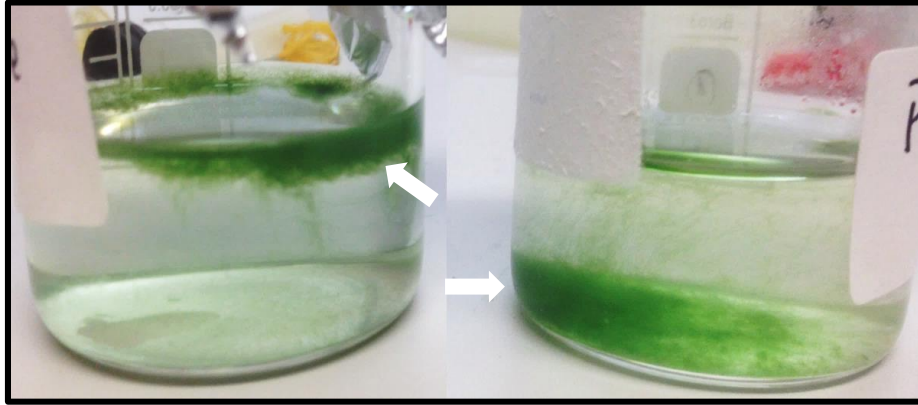


Figure 2.3-4 Cell distribution change before (left) and after (right) gas vesicle collapse by 0.4MPa hydrodynamic pressure. Arrows point to cyanobacteria.

Not only the macro-distribution changes after gas vesicle collapsing, the micro-structure under phase contrast microscope also differs (Figure 2.3-5). The bright dot feature of the *Anabaena* cell which represent the existence of gas vesicle cluster disappears when 0.4MPa pressure applied to the cell solution. The original bright region become dark and give less contrast to the surrounding cytochylema.

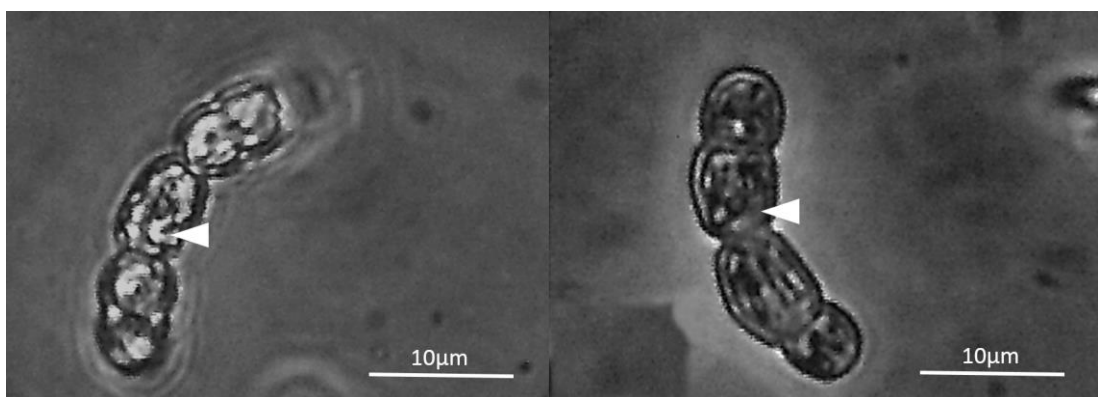


Figure 2.3-5 Phase contrast imaging of a single FACHB-1255 cell before (left) and after (right) applied with 0.4MPa pressure. Arrowhead point to a gas vesicle cluster before (left) and after broken (right).

The intracellular gas vesicles' turbidity change corresponding to the hydrostatic pressure gradient was recorded by 0.2 atm (0.02MPa) steps to get the critical pressure (Figure 2.3-6). From the chart, when the additional pressure below 1 atm, almost all intracellular gas vesicles are intact. 2 atm pressure is the minimum acceptable level for the gas vesicle can reserve 70% under this pressure. 3.5 atm pressure can break almost all intracellular gas vesicle. Therefore, in the following centrifuge procedure, the pressure under the bottom of the centrifuge tube should not exceed 2 atm and the optimal value should be lower than 1 atm.

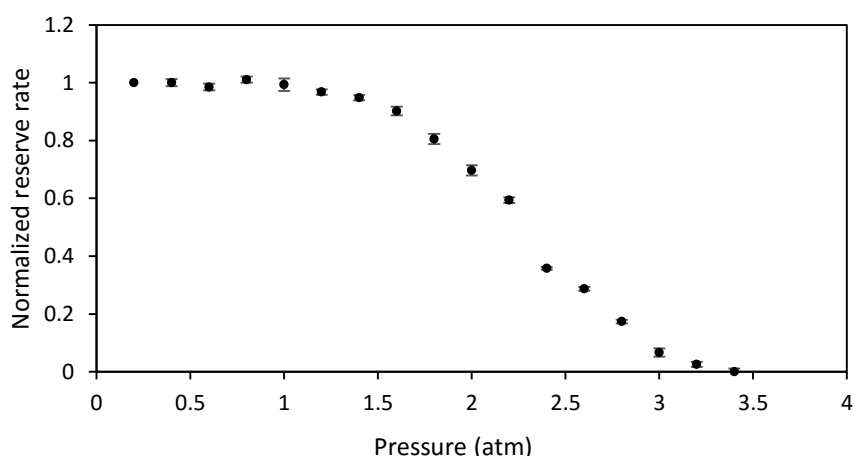


Figure 2.3-6 Gas vesicle reserve percentage in relation with hydrostatic pressure (n=5, error bar= 1SD).

2.3.3. Isolated Gas Vesicle

The isolated gas vesicle is pure white color (Figure 2.3-7) and it forms a white cream on the surface of the solution when it left steady because of the buoyance. With the concentration increasing, the white color become more opaque. This is because when

the concentration is higher, the ability to scatter light is stronger and make it exhibit opaque white color in high concentration.

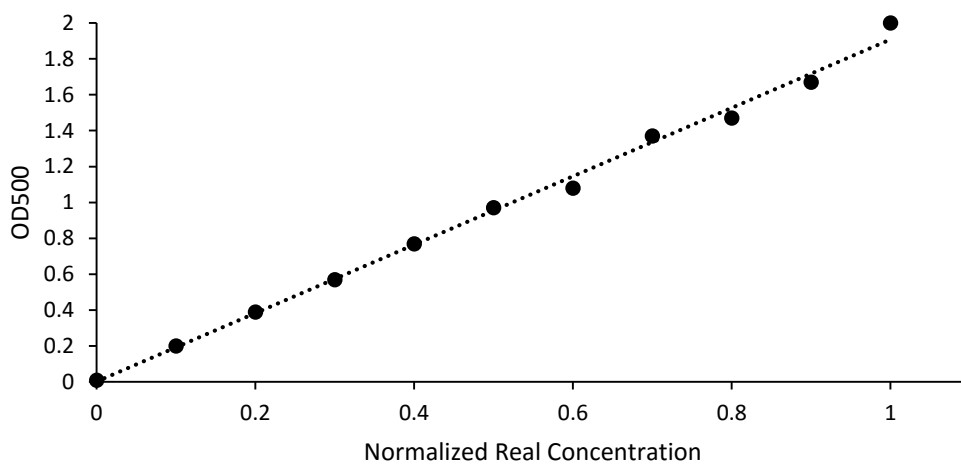


Figure 2.3-7 Upper, isolated gas vesicle with gradient concentration from low density to high density (left to right). Bottom, absorbance index in 500nm wavelength of gas vesicle vs normalized concentration. Y axial is concentration of gas vesicle represented by optical density at 500nm wavelength.

The quantitative way to characterize the specific concentration is by optical density method. The calibration was done to verify the linearity of the method (Figure 2.3-7).

The relation of absorbance index is quite linear to the real concentration when the

excitation light is 500nm wave length with $r^2=0.995$. According to other researchers' study, the real concentration to OD500 ratio is 450 pM to 1 OD500. The typical amount of gas vesicle per isolation procedure is 20ml with 1nM concentration.

The TEM image of gas vesicle shows the cylindrical shape (Figure 2.3-8). The diameter in longitudinal direction is about 400 nm and the transverse diameter is 100 nm. The aspect ratio is around 4:1.

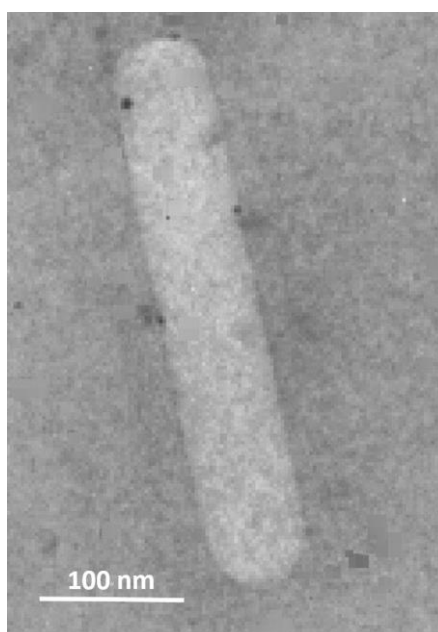


Figure 2.3-8 TEM image of a single gas vesicle from FACHB-1255

The size distribution is got from two way. The hydrodynamic size is calculated from zatasizer (Figure 2.3-9) and physical size is from the statistical calculation of TEM images (Figure 2.3-10). The distribution measured by Particle Size Analyzer is closed to the result of transverse diameter size distribution from TEM statistical calculation.

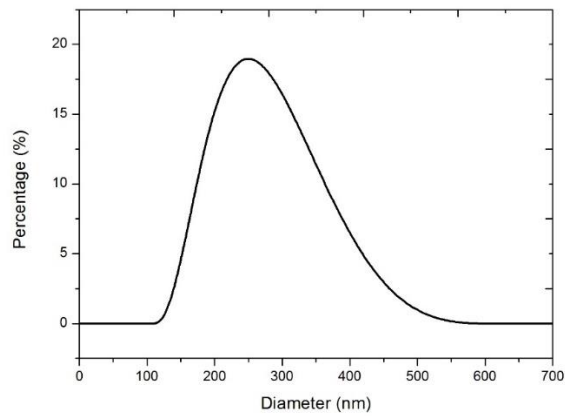


Figure 2.3-9 Hydrodynamic particle size measured by Particle Size Analyzer (PDI=0.09)

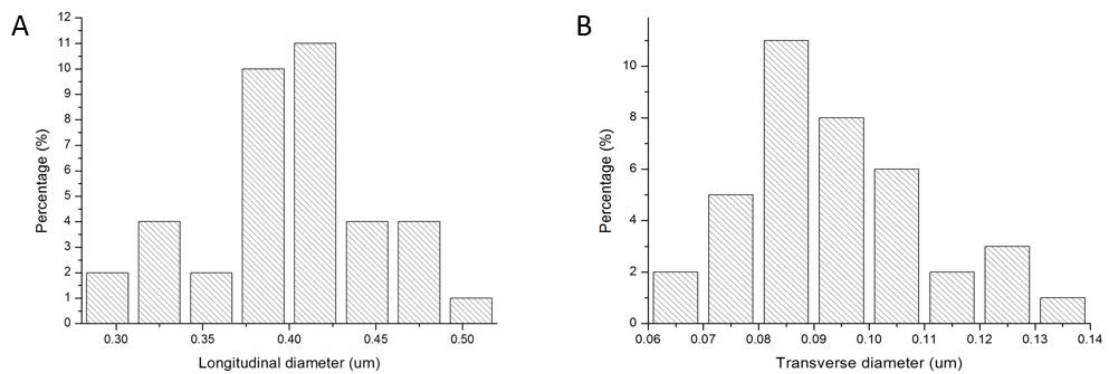


Figure 2.3-10 Size distribution in longitudinal direction (A) and transverse direction (B) calculated from TEM image. (n=38).

Mean size and standard deviation (SD) are plotted as (Figure 2.3-11). The mean size (242.1 ±85.01 nm) measured by Particle Size Analyzer is between the value of physical longitudinal (395.40±43.53 nm) and transverse size (97.53 ±17.29 nm) calculated from TEM results. The SD of hydrodynamic size is much larger than that of transverse size (4 times) and longitudinal size (double). The hydrodynamic size

(242.1 nm) is found to almost equal to the average value of transverse and longitudinal size (246.47 nm).

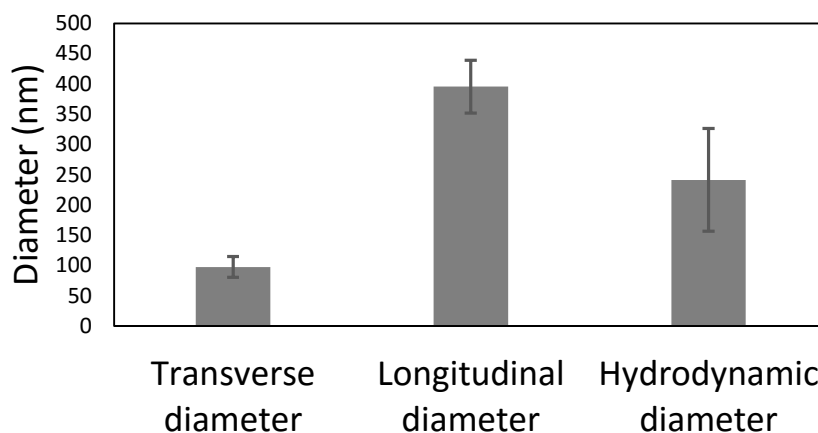


Figure 2.3-11 Mean and error bar (SD) size of transverse diameter, longitudinal diameter and hydrodynamic size.

The consistency was measured by comparing mean value and SD of hydrodynamic size from different batches for 12 times (Figure 2.3-12). Gas vesicle size is almost constant independent of batches.

The zeta potential is -42.77 ± 1.54 mV. Which is beyond the region that will cause aggregation.

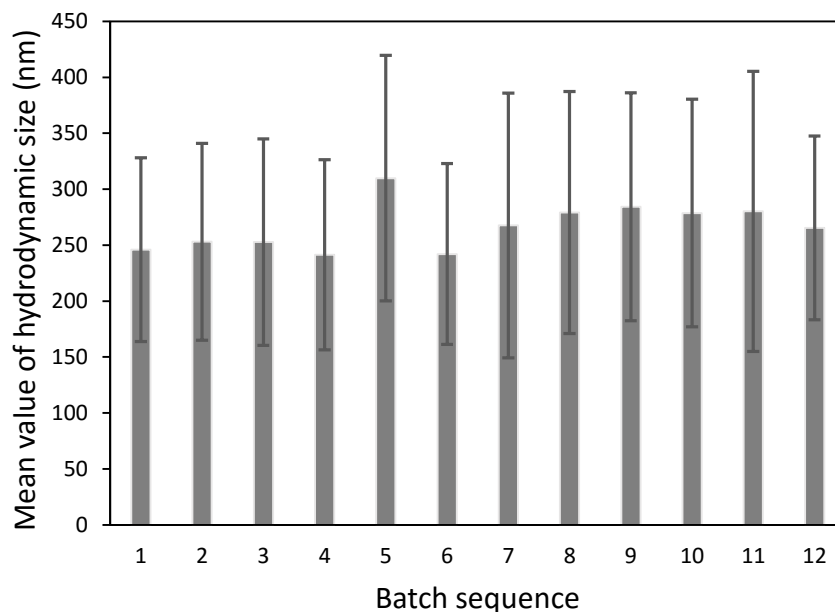


Figure 2.3-12 Mean value of hydrodynamic size from different batches (n=12), (error bar=1 SD).

2.3.4. Stability Test

The steady state stability test result is plotted in (Figure 2.3-13). Concentration was measured in t=0 hr, t=1hr, t=3hr and t=6hr. Though the concentration at 6hr was decreased to 94% (average value) of the original one, the difference is not significant.

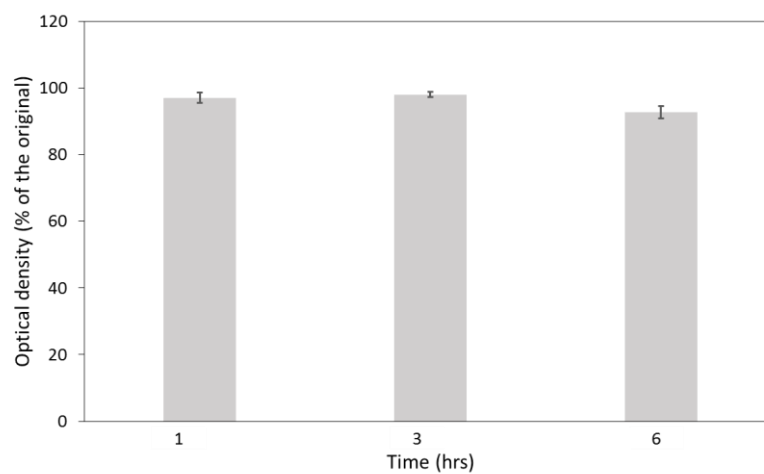


Figure 2.3-13 Nanobubble concentration as the function of time. (n=3, error bar =1 SD)

Zetasizer result is plotted in (Figure 2.3-14). There is no significant change of average size of nanobubbles within the duration of 6 hrs.

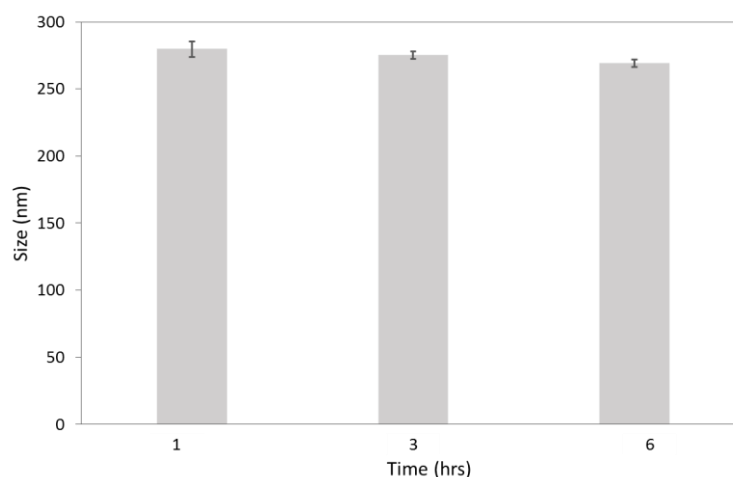


Figure 2.3-14 Average size as the function of time. (n=3, error bar=1 SD)

2.4. Discussion

Gas vesicle is a biogenic nano particle and choosing a proper species is important to increase output. From the experimental result, it is known that even the same species can performs totally differently in the gas vesicle production. The fast way to justify whether the certain cyanobacteria cells contains gas vesicle is to observe the color and cell distribution in the solution. When gas vesicle exists, it will produce buoyance to the cell and make it float on the surface of the fluid.

The intracellular gas vesicle is vulnerable to the high pressure, easy to collapse even in relatively low pressure. This is because gas vesicles inside cell sustain high turgor

pressure originally which can be as high as several atmosphere pressure. Its vulnerability calls for more carefulness in the isolation procedure.

The rod shape and nano-scale size may benefit the permeability of the nano particle to pass through the loose vessel wall by enhanced permeability and retention effect (EPR) in tumor region and other neovascularization condition like atherosclerosis. The size is mono-disperse with relatively low standard deviation and PDI index. This make the acoustic response more predictable. Besides, size distribution is consistence in different batch. This property can bring potential for its future large-scale production.

The steady state stability result is significantly enhanced compared to previous laboratory synthesized nanobubble which disappears in 25 mins and the size increases to 150% of the original one in 20 mins. In our result, the concentration almost has no change for over 6 hrs and size does not increase, as well. The extremely stable property of the biogenic nanobubble may make it circulate long enough to accumulate in extravascular tumor region.

3 ACOUSTIC CHARACTERIZATION

3.1 Introduction

3.1.1 Bubble Oscillation and Resonance Frequency

Scatter

The major purpose to induce nanobubble to ultrasound image is to enhance the contrast of image with the help of strong backscatter ability of bubble. The ultrasound backscatter ability is evaluated by scatter cross-section.⁴⁵ Providing that the physical size of scatterer should far smaller than transmit wavelength ($r \ll \lambda / (2\pi)$), r : physical radius of scatterer, the backscatter ultrasound intensity (I_s) can be calculated by Rayleigh's model with transmit ultrasound intensity (I_0) and scatter cross-section of scatterer σ as shown in (Eq. 3.1-1). The ultrasound backscatter intensity is proportional to scatter cross-section.

$$I_s = \frac{I_0 \sigma}{4\pi z^2} \quad (3.1-1)$$

Equation 3.1-1. z : the distance between scatter and transducer.

The scatter cross-section is determined by the density and compressibility difference between scatterer and the surrounding medium (Eq. 3.1-2)

$$\sigma = \frac{4}{9} \pi k^4 r^6 \left[\left(\frac{\kappa_s - \kappa}{\kappa} \right)^2 + \frac{1}{3} \left(\frac{3\rho_s - 3\rho}{2\rho_s + \rho} \right)^2 \right] \quad (3.1-2)$$

Equation 3.1-2: κ : adiabatic compressibility coefficient, ρ : density, s: represent scatterer

To the whole volume (V) containing cluster of scatterer, backscatter ultrasound intensity I_s can be calculated from (Eq. 3.1-3).

$$\frac{I_s}{I_0} = \frac{1}{9} nV \frac{k^4 r^6}{z^2} \left[\left(\frac{\kappa_s - \kappa}{\kappa} \right)^2 + \frac{1}{3} \left(\frac{3\rho_s - 3\rho}{2\rho_s + \rho} \right)^2 \right] \quad (3.1-3)$$

Equation 3.1-3: n : unit density of scatterer. $K=2\pi/\lambda$.

Ophir and Parker⁴⁶ compared different material of scatterer such as gas, fluid and solid (Table 3.1-1). From the table, scatterer made of gas has extremely larger (10^{14}) scatter cross-section when compared to solid scatterer providing the physical diameter is the same because both the compressibility and density is far different from water. This is the reason why micro/nano bubble can be used as ultrasound contrast agent.

Table 3.1-1 Scatter cross-section between different martial scatterer ($r=5 \mu\text{m}$, $f=5 \text{ MHz}$)

Material	Compressibility relation	Density relation	σ (m^2)
Gas	$\kappa_s \gg \kappa$	$\rho_s \ll \rho$	0.38
Solid	$\kappa_s \ll \kappa$	$\rho_s \gg \rho$	6.65×10^{-15}
Fluid	$\kappa_s = \kappa$	$\rho_s =$	0

Resonance

Rayleigh-Plesset (RP) equation (Eq.3.1-4) describe the basic oscillation model of free bubble without shell.

$$\ddot{R}R + \frac{3}{2}\dot{R} + \frac{p_0 + p_i(t) - p_L + \frac{2\sigma}{R} + \frac{4\mu}{R}\dot{R}}{\rho} = 0 \quad (3.1-4)$$

Equation 3.1-4: R : bubble radius in stable condition, ρ : density of surrounding medium, p_0 : outside pressure at steady condition usually atmosphere pressure, $p_i(t)$: stimulation ultrasound pressure, σ : the surface tension of the bubble in steady condition, μ : the viscosity of surrounding fluid.

After Fourier-transformation, the angular resonance frequency can be found to be:

$$\omega^2 = \frac{3\kappa p_0}{R^2 \rho} \quad (3.1-5)$$

The resonance frequency f_0 is:

$$f_0 = \frac{1}{2\pi R} \sqrt{\frac{3\kappa p_0}{\rho}} \quad (3.1-6)$$

Equation 3.1-6: $\kappa=\gamma$; to air γ is a constant 1.4, f_0 also called Minnaert frequency.⁴⁴

Resonance frequency is highly related to the scatter cross-section and backscatter ultrasound signal intensity. According to the solution of the equation, the scatter cross-section and bubble radius reach maximum when the transmit ultrasound frequency

equal to the resonance frequency of bubble. Therefore, measuring the scatter intensity function is a common method to calculate bubble resonance frequency and attenuation coefficient measurement is an alternative way.^{45, 47}

$$\sigma_s(a, \omega) = 4\pi a^2 \frac{\Omega^4}{(1-\Omega^2)^2 + (\Omega\delta)^2}, \quad \Omega = \frac{\omega}{\omega_0} \quad (3.1-7)$$

Equation 3.1-7: ω : transmit ultrasound frequency.

3.1.2 Non-linear Property

The non-linearity of nanobubble is induced by asymmetric oscillation behavior especially in high acoustic pressure. When bubble stimulated by relatively low acoustic pressure, symmetrical oscillations occurs and backscatter the ultrasound signal at the same frequency as transmit one. Whereas, when the stimulation ultrasound pressure increases, the oscillation behavior becomes asymmetric. The Asymmetric oscillation is caused by the bubble oscillating with different extent between positive ultrasound pressure phase and negative ultrasound pressure phase.⁴⁸ When nanobubble under the stage of positive ultrasound pressure, it will shrinkage caused by the increased outside pressure and bubble will expand under negative ultrasound pressure. However the expansion extent is larger than shrinkage extent because bubble resistant to compression more strongly than expansion. The asymmetric response produces non-linear effect of bubble and backscatter the ultrasound signal with more frequency component double or triple than transmit

fundamental frequency.⁴⁹ These higher frequency components are known as harmonic frequency.

Among the higher frequency components induced by non-linear response, second harmonic frequency twice the fundamental one is widely used for ultrasound contrast imaging. Second harmonic frequency component is filtered at twice the transmit frequency and to form the contrast image. This contrast technique needs a broadband transducer covering both transmit frequency and receiving second harmonic frequency. A compromising method is to transmit the ultrasound in lower frequency range of transducer and receive at higher frequency range, though the sensitivity is reduced.

The first experiment using 2nd harmonic frequency was done by Tucker and Welsby in 1968 to detect blood pool microbubble.⁵⁰ Miller (1981) tested the method in an experimental way without theoretical explanation.⁵¹ He used a long tube to mimic the blood vessel and induced 1.64MHz ultrasound to stimulate bubble at 500 μm diameter. He claimed that the second harmonic frequency was resulted from cavitation effect. The phenomenon was not well explained, until a theoretical principle was developed by Vacher and Gimnez in 1984.⁵² And later second harmonic effect is studied by many researchers from different aspects.^{53, Error! Reference source not found., 54} In this chapter, three acoustic properties of biogenic nanobubble was characterized: resonance frequency, non-linear property and stability under sonicating.

3.2 Methods

3.2.1 Attenuation and Resonance Frequency

System

The attenuation measurement system is mostly based on a method described by de Jong *et al.*⁵³ The system is illustrated by schematic diagram (Figure 3.2-1) and photos (Figure 3.2-2). The equipment consists of a combined pulser and receiver (Panametrics 5900PR, Panametrics Inc., Waltham, Mass, USA), 3 high frequency transducers (made by Shung *et al.*)⁶⁹ and digital oscilloscope (LeCroy 715Zi, LeCroy Corporation, Chestnut Ridge, New York, USA). The computer with Matlab (The Math Works Inc., Natick, Mass., USA) was used to process the data. The cables connecting each component are coaxial cable with length of 1 m smaller than 1/4 wavelength of the radiofrequency signal. External electric coupling circuit was not needed since the transducers have been electrical coupled.

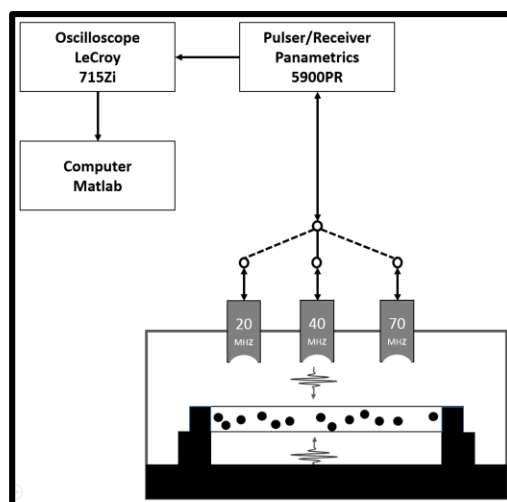


Figure 3.2-1 Schematic diagram for attenuation measurement. Dark dots are nanobubbles.

Ultrasound broadband pulse was transmitted by transducer which were immersed into the degased and deionized water and pass through the sample cell containing the nanobubble. The pulse then reached and reflected by the reflection plane made of quartz (Hefei Kejing Materials Technology Co., LTD , Hefei, Anhui, China). Transducers were placed vertically to the sample cell plane and reflection plane. The thickness of the sample cell was 1.89mm and the distance from bottom membrane of sample cell and the front surface of quartz plane was 1mm.

Sample Cell

The sample cell was composed of two part, the scaffold and acoustic membrane (Figure 3.2-2). Scaffold was made of by EPO-TEK 301 (EPOTEK 301, Epoxy Tech., Billerica, MA, USA). The scaffold thickness was uniform (mean=1.89mm and SD=9 μ m) to eliminate the dislocation intervention of each measurement. The acoustic membrane is made of by Scotch tape 2.5 mils thick (3M 373, 3M Company, Saint Paul, Minnesota, USA). The acoustic impedance of membrane is 2.08 MRayls very close to the value of water (1.5 MRayls) to minimize the attenuation and reserve the ultrasound signal. Nanobubble diluted in PBS was inserted into sample cell.

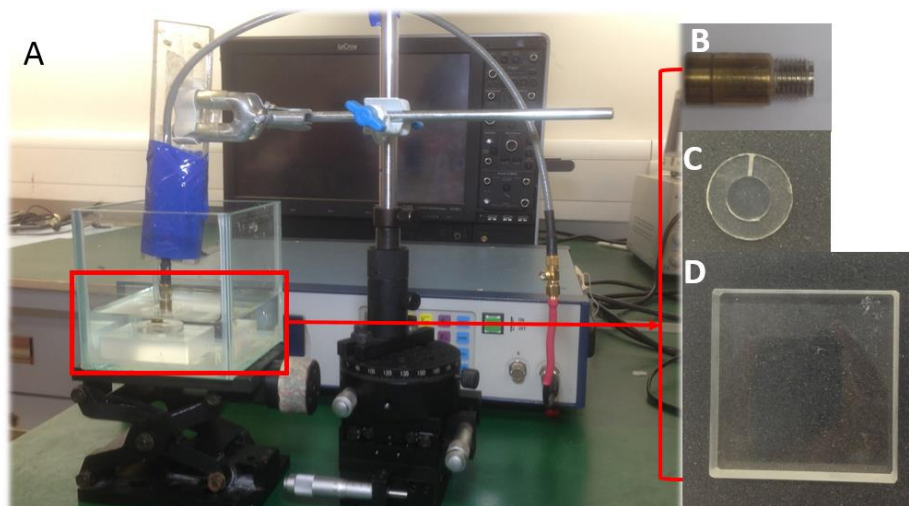


Figure 3.2-2 A, photo of the attenuation characterization system. B, focused transducer. C, sample cell with acoustic membrane. D, quartz plane.

Transducer Characterization

Three focused transducers made by LiNbO_3 piezoelectric material are induced in the experiment. The outer diameters of transducers are 9 mm, 7 mm and 7 mm.

Focal depth of each transducer was characterized by pulse-echo system. In the measurement system, the back scatter sample was quartz plane (a strong acoustic wave reflector with smooth surface). The quartz plane was set initially 1mm at a distance from transducer. Then, the plane was moved continuously with $100\mu\text{m}$ away from transducer, meanwhile, backscattered signal was recorded in oscilloscope after each step. The position corresponding to the maximum amplitude of backscattered during reflection plane movement was marked as focal depth.

The center frequency and bandwidth of the transducer was measured with analysis of the power spectrum of backscattered signal in focal depth. In the power spectrum, the frequency signal was normalized based on the highest point and then was transformed to dB format. Corresponding frequencies at -6 dB were recorded. These two points were marked as F_{low} and F_{high} representing the lower frequency and higher frequency respectively. The center frequency and bandwidth was calculated according to the formula:

$$F_{center} = (F_{low} + F_{high})/2; \quad (3.1-8)$$

$$\text{Bandwidth} = 2 \cdot (F_{high} - F_{low}) / (F_{low} + F_{high}) \quad (3.1-9)$$

Bandwidth within -20 dB was calculated within which region, attenuation coefficient is valid.⁴⁵

Acquisition of Pulse

An electric RF signal was transmitted by the pulse function of pulse and receiver to excite the transducer. It was a short period and broadband (1 MHz to 200 MHz) pulse and repeated 100 per second. Lower energy (1 μ J) was used to avoid transducer saturation. Then the acoustic pulse from transducer pass the sample cell (1.89 mm) through impedance-coupled acoustic membrane and nanobubble-containing medium towards the reflection plane. The backscatter signal from reflection plane passed

nanobubble medium twice. Therefore the total distance of the nanobubble medium that the ultrasound signal pass through should double the sample cell thickness equal to 3.78 mm.

The backscattered signal was received by pulse/receiver and amplified by 10 dB. Oscilloscope was to sample and record the signal from pulse/receiver. The sampling frequency was 10Gsa/s. The sampling window was 2 μ s at the center of receiving signal from reflection plane. Results were averaged over 100 successive pulses, in which way the signal to noise ratio could increase 10 times. The digital data was saved in oscilloscope in *matlab* format and transferred to computer for offline analysis.

Signal Processing

The raw RF data was transferred from oscilloscope to personal computer. Power spectrum corresponding to each RF measurement was calculated and analyzed using Matlab (The Math Works Unc., Natick Mass., USA). Data processing procedure was illustrated in (Figure 3.2-3).⁴⁵

In each calculation, two measurement RF data were induced, one from the nanobubble signal and the other from PBS signal as the reference. The attenuation coefficient was calculate from the normalized data of nanobubble signal by reference. The valid analysis region on transducer power spectrum was chosen within the -20 dB region

according to transducer characterization data. The overlapping region between two transducers are used as the validate testing to the attenuation coefficient measurement. Within the overlapping region the results from different transducer should be the same to eliminate the transducer influence.

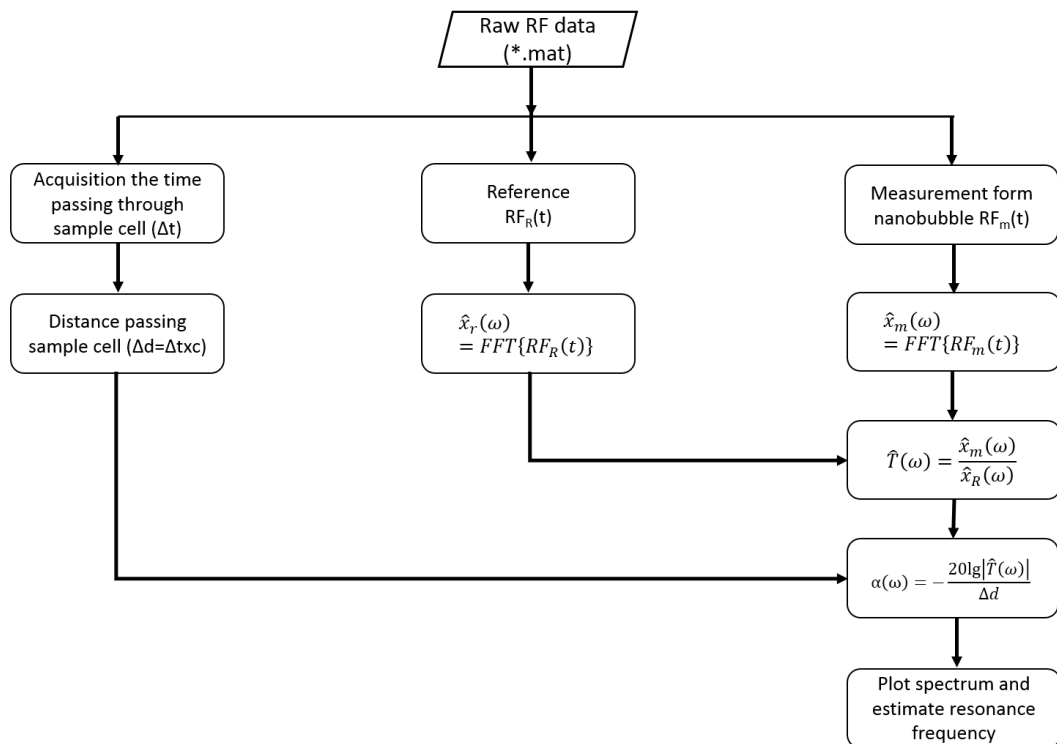


Figure 3.2-3 Attenuation coefficient calculation flow chart

3.2.2 Harmonic Property

System

System to measure the harmonic property of nanobubble is different from the attenuation measurement system. The system was illustrated in Figure 3.2-4. The whole system was composed of Function Generator (AFG 3251, Tektronix Company,

Oregon, USA), Power Amplifier (Model 500A250C, AR Inc., Souderton, PA, USA), Signal Amplifier (AU1467, Miteq Inc., Hauppauge, N.Y., USA) which was supplied by 15V DC voltage (6603D, Topward Company, Hsin Chu, Taiwan) and digital oscilloscope (LeCroy 715Zi, LeCroy Corporation, Chestnut Ridge, New York, USA). Function generator was used to define RF signal to the transducer which is a burst sine wave with 30 cycles. The RF signal was amplified by the power amplifier (valid frequency range 10 kHz to 250 MHz) to the voltage predefined. Two transducers were responsible for transmitting and receiving signal. To detect higher harmonic signal, broad bandwidth transducer was selected as receiver one. Nanobubble within sample cell was stimulated and scattered ultrasound signal to receiver transducer. The received signal then was pre-amplified by signal amplifier with high signal to noise ratio. The amplified signal was received and digitalized by oscilloscope for further analysis in computer by *Matlab*. Before the experiment, system noise from each electronic component which may influence the testing result was characterized.

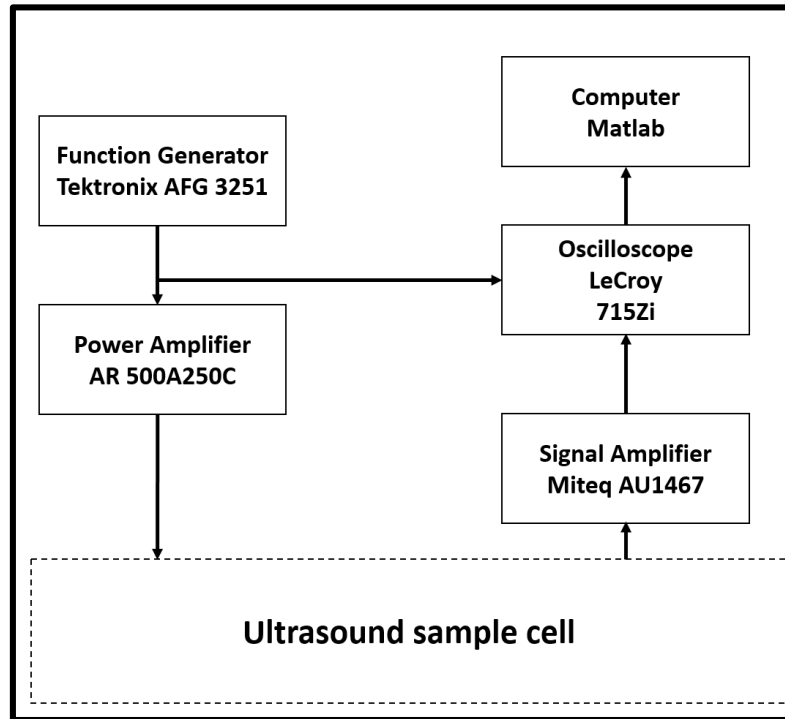


Figure 3.2-4 Setup to measure harmonic property

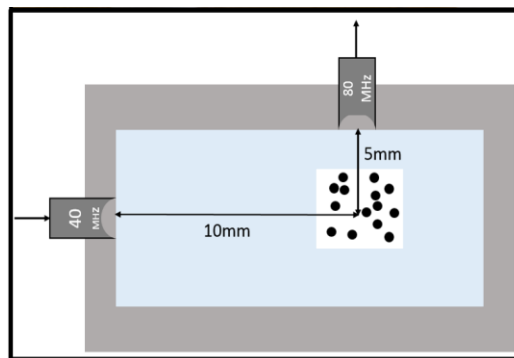


Figure 3.2-5 sample cell scheme and photo. Black dots represent nanobubble. Transmitter transducer covers 40 MHz and receiver transducer covers 80 MHz.

Ultrasound Sample Cell

The ultrasound sample cell was specially designed for high frequency ultrasound scattering measurement (Figure 3.2-5). Two transducers were mounted in the PDMS model with right angle. The sample region containing nanobubble was located in the overlapping region at focal depth of two transducers. Transducer with center frequency at 40 MHz was selected as transmitter and receiver transducer can cover broad

frequency region from 30 MHz to 103 MHz. the focal depth of these two transducers are 10mm and 5mm respectively. Because nanobubble can attenuate ultrasound signal, to maximize the excitation ultrasound intensity and minimize the ultrasound attenuation in the receiving pathway, the regions except for sample chamber was replaced by agar gel.

System Error Test

Two-transducer scattering system was designed to measure the harmonic response of the nanobubble. However, the system itself may induce intrinsic harmonic wave which may induce false positive result to nanobubble non-linear property test. To control such system noise under the acceptable level, it is necessary to test the harmonic noise from the system prior to nanobubble experiment. The same instruments setup (Figure 3.2-4) was used except the sampling cell. In the sampling cell used to measure system noise, the transducer angle was changed to be 180° instead of right angle (Figure 3.2-6). The center of the sampling cell was replaced by deionized and degassed water. 40MHz sine wave burst was transmitted to sampling cell. The received signal was analyzed in power spectrum to make sure the frequency components other than 40MHz are low enough that will not influence nanobubble non-linear property test.

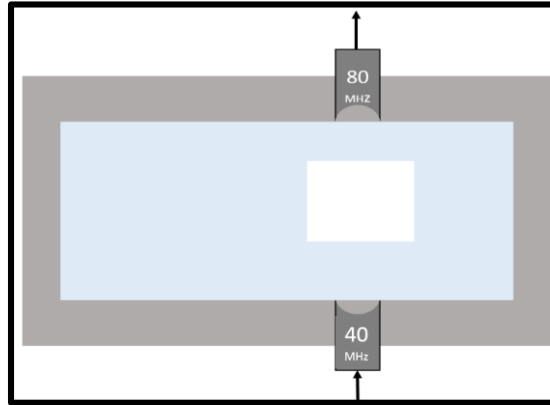


Figure 3.2-6 sampling cell for system harmonic noise testing

Data Acquisition

The signal programmed in function generator was set to be sine burst wave (frequency=40 MHz, Amplitude=200 mV, cycle=30, PRF=100 Hz). The nanobubble diluted in the PBS in sampling cell was excited by the ultrasound stimulation inducing non-linear oscillation. The non-linear oscillation behavior not only scattered ultrasound signal at the stimulation frequency but also generated frequency component double or triple the fundamental frequency known as second and third harmonic signal. Because the signal from nanobubble was scattered in all direction, it can be received by the transducer in right angle (transducer covering 80 MHz frequency). Locating the nanobubble at the focal depth of the focused transmitter transducer can maximize the ultrasound excitation intensity.

When the oscilloscope being triggered by synchronizing signal from function generator, it started to sampling receiving data. By setting the delay and time gating, the oscilloscope only sampled the signal within the region of sampling cell with the

window width of 2us. The sampling data from each pulse was recorded and further processed by frequency analysis. The received data was first transferred to frequency domain and then over 200 FFT signal was averaged.

3.2.3 B-mode Ultrasound Characterization

Ultrasound B-mode image of nanobubble was characterized using Vevo 2100 system (Vevo2100, VisualSonics Inc. Toronto, Ontario, Canada). The transducer used is MS550D (VisualSonics Inc. Toronto, Ontario, Canada) with frequency range of 22-55MHz and penetration depth of 14mm. Nanobubble was diluted in PBS with concentration gradient (OD500=0.125~5.0). The center frequency and energy was set to be 40MHz and 1%. The concentration was measured by spectrophotometer and recorded in OD500 format. Sample was filled within sample cell made of agar gel.

Stability was tested in two way: stead state stability and stability under sonicating. In steady state stability test, nanobubble was diluted in PBS and imaged by ultrasound in four time points (t=0 hr, t=1 hr, t=3 hr and t=6 hr). Three groups were involed and four images were taken at each time point per sample. Stability under sonicating was tested by continuously ultrasound stimulation and images was recorded every 1 min. 3groups was involved in the experiment. Nanobubble was immobilized in agar gel. The frame rate was set to be 5 Hz. All of the recorded image was analyzed in imageJ.

3.3 Results

3.3.1 Transducer Characterization

Totally 3 transducers was characterized using pulse-echo method. The result was plotted in Figure 3.3-1. These three transducers are named by their frequency ranking from lower one to higher one. From the power distribution figure, the transducer #3 have the most broad frequency bandwidth among the three transducers.

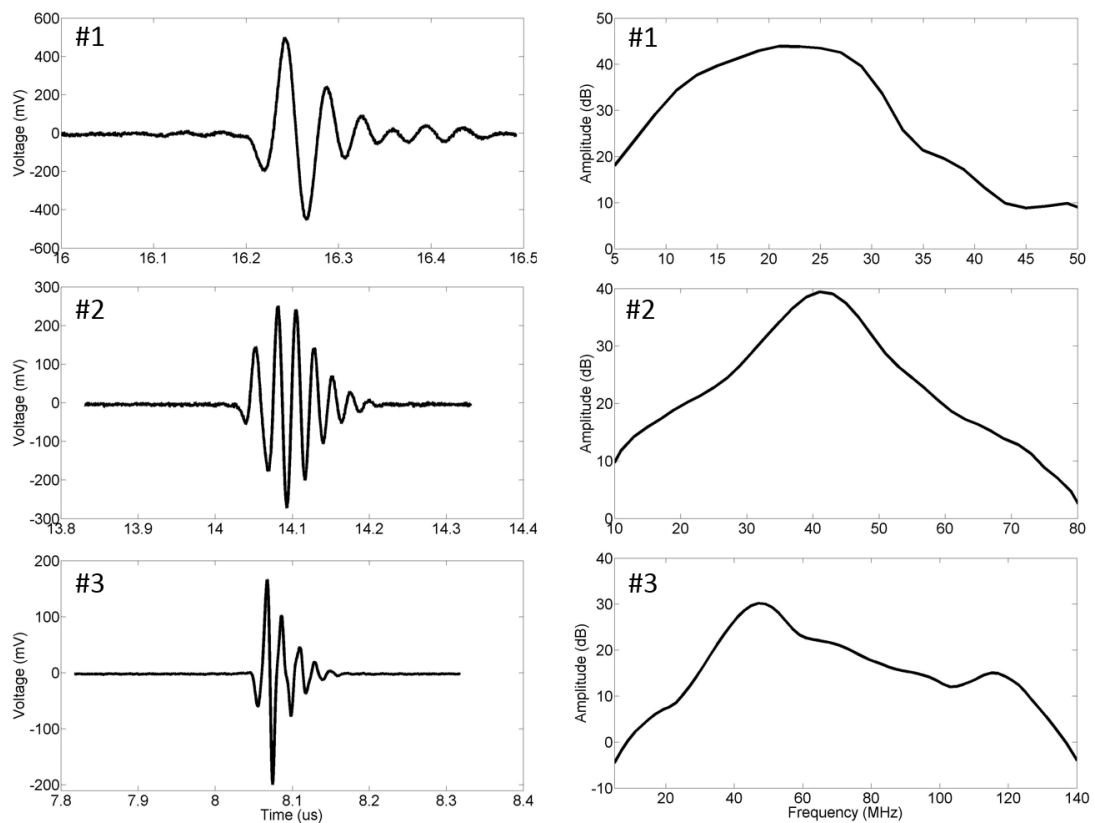


Figure 3.3-1 transducer characterization signal. Left column, signal in time domain; right column, power spectrum after Fourier transformation. From up to bottom plotted transducer #1, transducer #2 and transducer #3.

Quantitative results regarding the center frequency, -6dB bandwidth can be got from power spectrum. Besides these information, -20dB bandwidth is also important in

attenuation measurement, in which region attenuation coefficient is valid. Focal depth is another important information in both attenuation measurement and harmonic property measurement, because focal region is the most sensitive region of a focused transducer to provide better signal to noise ratio. These information are listed in (Table 3.3-1).

From Table 3.3-1, the transducer #1 have the most broadband frequency bandwidth. However, when evaluate the absolute value of -20dB region covered by transducer, #3 transducer performs best. -20 dB frequency range is the fundamental consideration in the attenuation measurement. Therefore, #3 transducer is the most powerful transducer among these three transducers to measure attenuation coefficient. With combination of the three transducers, the whole validate frequency range can cover from 7MHz to 103MHz continuously. The fact that focal depth varies from each transducers indicates that the measurement distance from transducer and reflective plane should be rearranged in each measurement according to focal depth. Two overlapping frequency regions can be used to test the validity, 21MHz to 35MHz and 30MHz to 59MHz.

Table 3.3-1 Transducer characterization information regarding focal depth, center frequency, bandwidth and -20dB region.

Transducer Number	Focal depth (mm)	Center frequency (MHz)	-6dB bandwidth (%)	-20dB region(MHz)
1	11.4	22	81.82	7-35
2	9.8	40	39.02	21-59
3	5	48	45.83	30-103

3.3.2 Attenuation Signal

Typical backscatter signal from reflective plane with and without nanobubble was plotted in (Figure 3.3-2). From signal in time domain, the amplitude of the signal passing through nanobubble is much smaller the reference one. In the power spectrum figure, the nanobubble signal is also smaller than the reference and the amplitude difference increases in high frequency region than lower frequency.

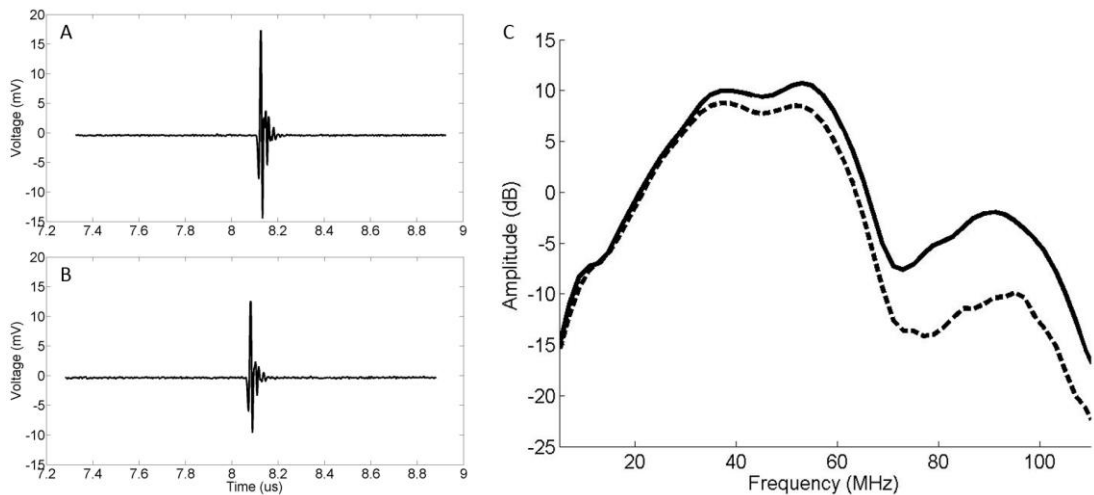


Figure 3.3-2 backscatter signal with (B) and without (A) nanobubble; C, the power spectrum from A (solid line) and B (dotted line). Transducer #3,

Concentration=0.27nM, OD500=0.7.

The backscatter signal of lower frequency region was plotted in (Figure 3.3-3) measured by transducer #1 and transducer #2 respectively. In both measurement, the signal intensity from nanobubble is normally smaller than reference (signal passing water medium). Such difference is greater in transducers with higher center frequency

(40MHz) than the lower one (22MHz). The same result can be observed from the power spectrum.

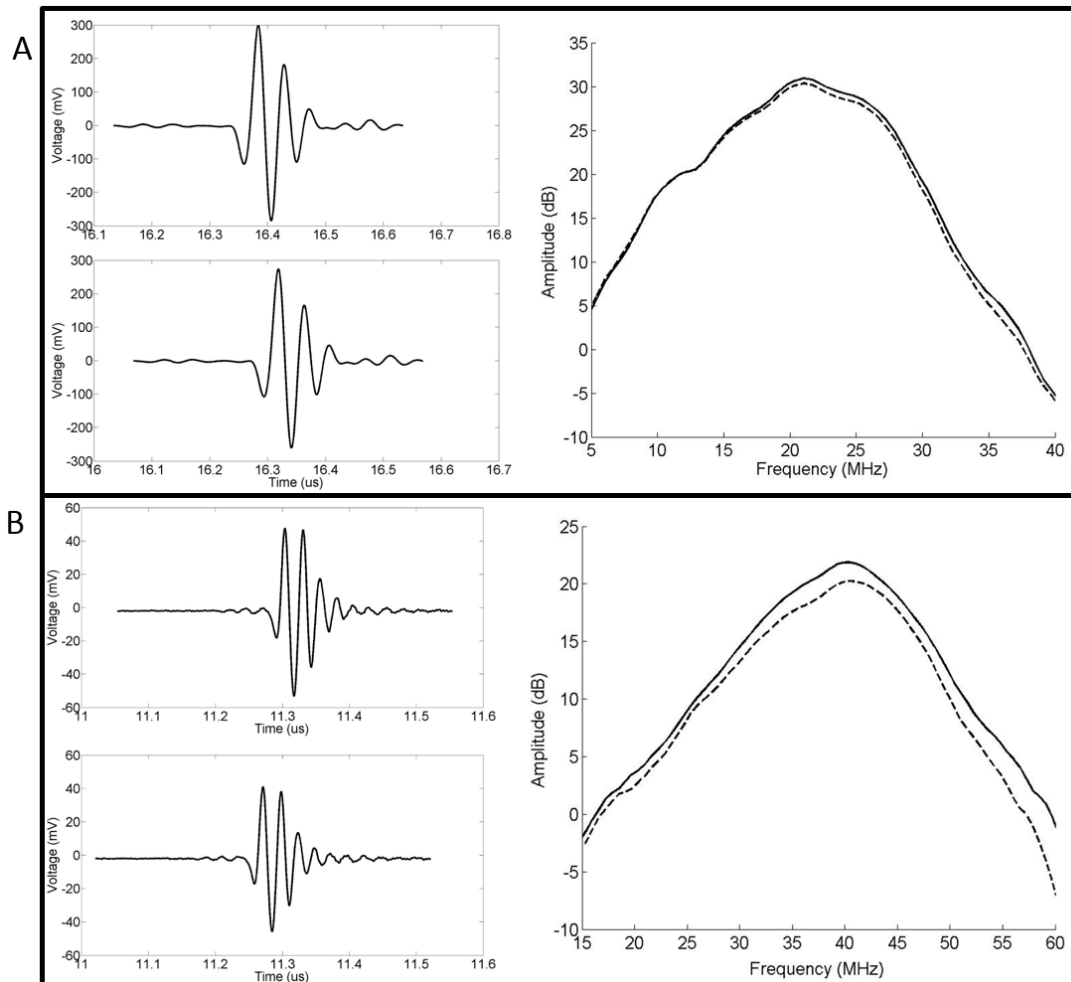


Figure 3.3-3 Backscatter signal of (A) transducer #1 and (B) transducer #2.

Concentration=0.27nM, OD500=0.7. Solid line, signal from nanobubble; dotted line, signal from reference

3.3.3 Attenuation Coefficient

Attenuation coefficient can be calculated from the normalized backscatter signal after Fourier transformation. Attenuation is plotted in (Figure 3.3-4) with measurement

from 3 transducers covering the frequency from 7 MHz to 103 MHz. The peak is on 88 MHz. However because of the measurement error, the real attenuation peak should be between 80 MHz to 90 MHz. This result indicates that the resonance frequency of the nanobubble should be in the region of 80 MHz to 90 MHz. There is no significant difference between different transducers in the overlapping region. The slight difference may be caused by experiment error. Because in each measurement of different transducers, the ultrasound pulse pass the different location of the sampling cell. This error cannot be eliminate by reference calibration.

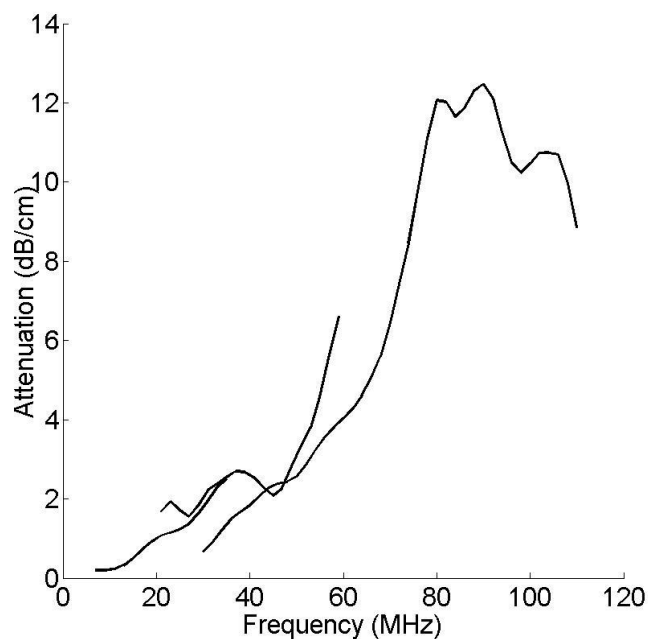


Figure 3.3-4 Attenuation coefficient calculated from measurement of 3 transducers.

From lower frequency to higher frequency is transducer #1, transducer #2 and transducer #3. Concentration=0.27nM, OD500=0.7.

To verify the attenuation result, multiple measurement was conducted using the same transducer #3 because its broad frequency can cover the resonance frequency region.

Each measurement using the nanobubble from the same batch and the concentration was adjusted to OD500=0.7 (0.27nM). The result is plotted in Figure 3.3-5. Though each measurement is not exactly the same value, the distribution and shape of the function is similar. The peak attenuation can be found between 80MHz to 90MHz. In the frequency region lower than peak frequency, the growing speed is very similar between each measurement. The numerical difference in whole frequency region may be caused by the concentration difference between each measurement and the location variance. However these difference does not influence the resonance frequency and the attenuation growth rate.

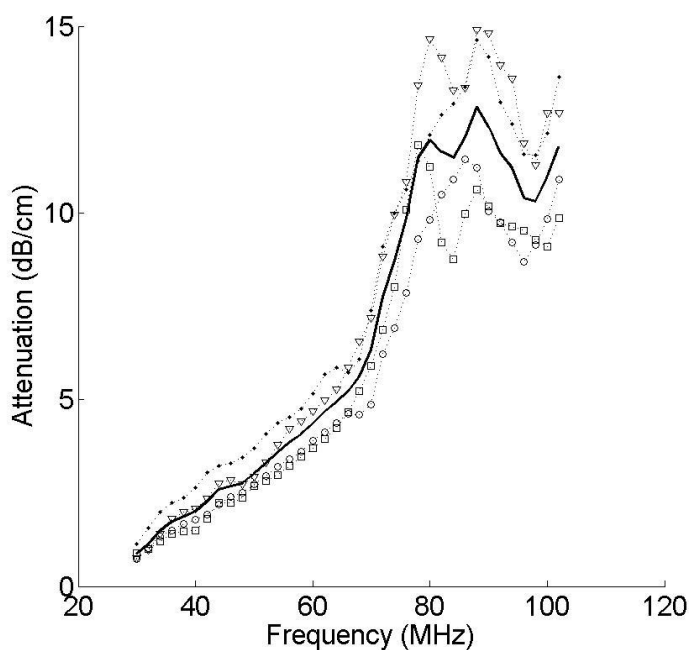


Figure 3.3-5 Attenuation coefficient from multiple measurement. Average of measurement (solid line) and each measurement (dotted line). Transducer #3, n=4, concentration=0.27nM, OD500=0.7.

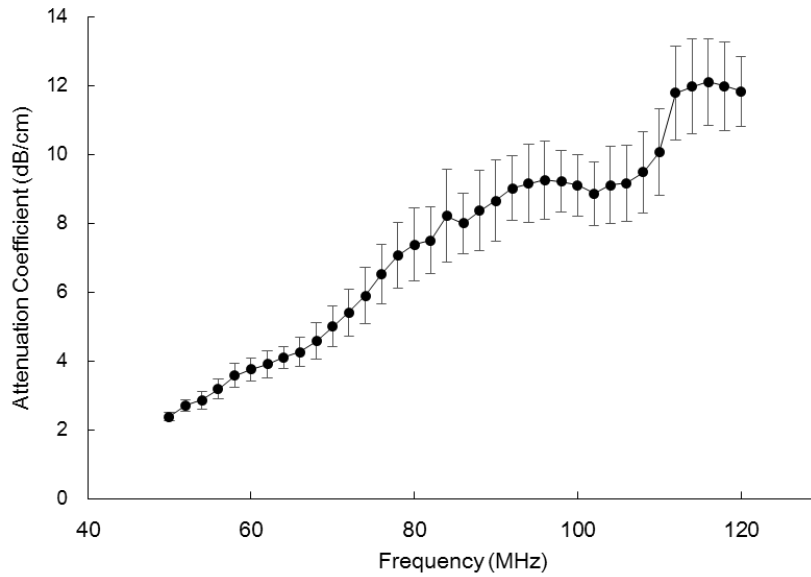


Figure 3.3-6 Attenuation coefficient of NGV (0.125nM) got from narrow bandwidth pulse test. N=3

To broadening the valid testing region, narrow bandwidth measurement was used instead of broad bandwidth one. The attenuation coefficient result is plotted in Figure 3.3-6. The extra frequency components (103MHz to 120 MHz) reveal a new property apart from previous testing. A new observation was happened on the attenuation coefficient plot that there is two resonance peaks one at around 90MHz and the other around 115MHz. This property has never been observed on conventional micron size bubble. One possible reason may be because NGVs is rod shape structure unlike spherical-shaped microbubble. Oscillation mode in diameter direction and in longitudinal direction contribute to 115MHz and 90MHz respectively. The similar phenomenon also can be observed in the optical property of gold nanorod, the attenuation spectrum of which shows two resonances. The additional resonance is

caused by surface plasma resonance in longitudinal direction. Because of these two oscillation modes, the band of resonance is wider than conventional microbubble.

Linearity of the attenuation as the function to nanobubble concentration was plotted in (Figure 3.3-7). The attenuation is linear to the concentration under 0.45nM for $r^2 > 0.99$. The figure indicates that within this concentration region, there is no obvious rescattering between gas vesicles on signal passway. This information is useful to the application of nanobubble in ultrasound imaging to avoid significant attenuation caused by high concentration.

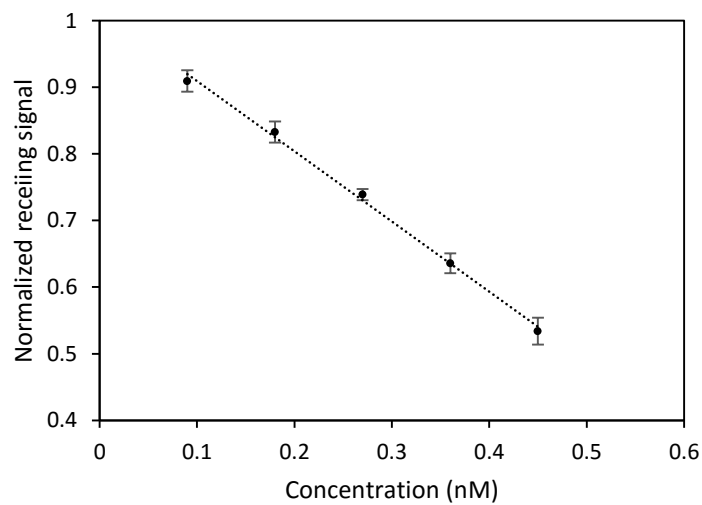


Figure 3.3-7 Backscatter signal intensity of nanobubble concentration gradient normalized to reference. N=4, error bar=1 SD.

3.3.4 System Error Verification

The signal from function generator was measured by oscilloscope with coupling impedance =50 Ω (Figure 3.3-8). In time domain signal, the amplitude, cycle number is almost the same as set in function generator, though there is 2 trailing pulse with acceptable low amplitude. In the frequency components, the main frequency component is 40 MHz the same as preset value. Evaluating the second harmonic frequency 80 MHz, the amplitude is 15 dB 43 dB lower than peak value and almost the same as the background frequency. The noise from function generator will not influence the nanobubble experiment results.

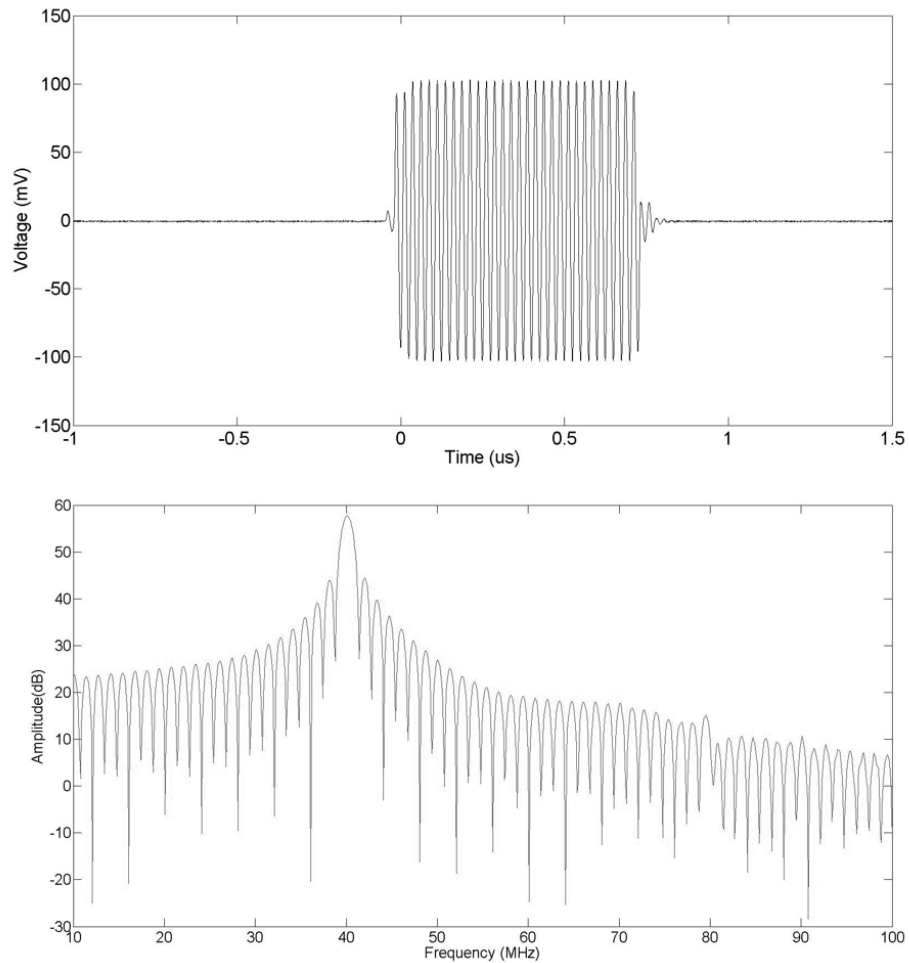


Figure 3.3-8 Signal from function generator. Upper part, signal in time domain; lower part, frequency components. $V_{p-p}=200$ mV, frequency=40 MHz, cycle=30, PRF=100 Hz.

The verification of Power Amplifier was tested with the input from function generator of same parameter in previous validate test. The output of power amplifier is connected to 40MHz transducer. The gain of power amplifier is set to 54dB which is the maximum value in nanobubble experiment. The testing result is plotted in (Figure 3.3-9). In temporal signal, the peak to peak voltage in the main part of the signal is 30V. However there are two extra peaks in the start and end of the signal sequence which is -31 V and 20 V respectively. The extra peaks result may influence the

experiment in the way that nanobubble can be broken in relative lower acoustic pressure and reduce the valid acoustic pressure testing region. In frequency domain, the major frequency component is 40 MHz the same as preset. The second harmonic amplitude is inhibited to a relative low level equal to background frequency components.

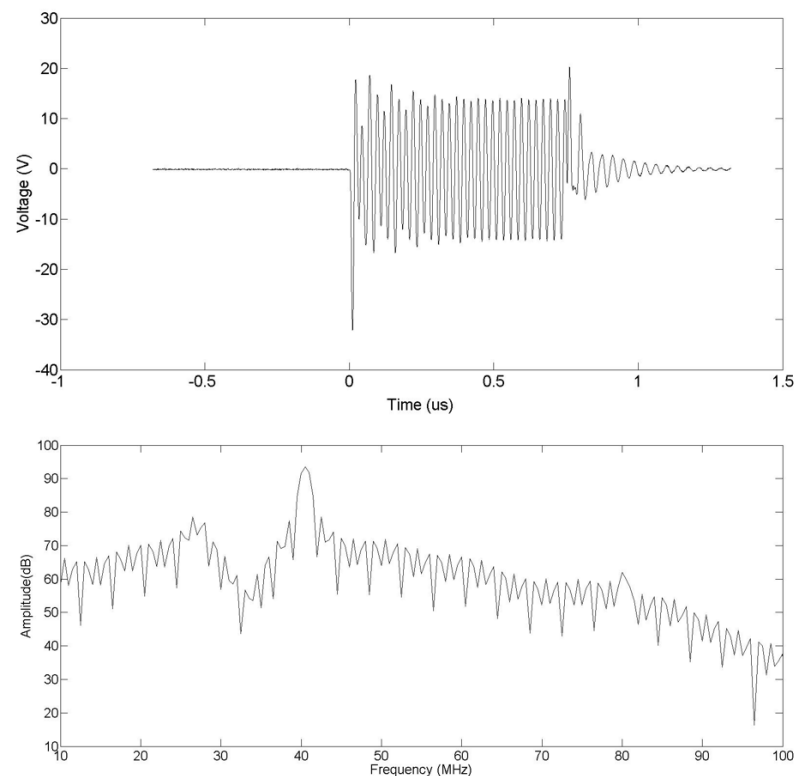


Figure 3.3-9 Verification signal from power amplifier. Gain=54dB, input: $V_p=200\text{mV}$, frequency=40MHz, cycle number=30, PRF=100Hz.

The whole system (containing function generator, power amplifier, transmit transducer, sampling cell including agar gel and water, receiving transducer and signal amplifier) was tested in a way replacing nanobubble by water and adjusting the voltage input to transducer to a level where the signal received in oscilloscope is at the same order of magnitude with nanobubble experiment. The system verification. The signal

in time domain and frequency domain is plotted in (Figure 3.3-10). The peak-peak voltage of received signal is 111 mV at the same order of magnitude to signal from nanobubble which is about 200 mV. Frequency component of harmonic wave (80MHz) was suppressed under background noise level. The whole system together with each instruments were demonstrated to be valid for non-linear property test.

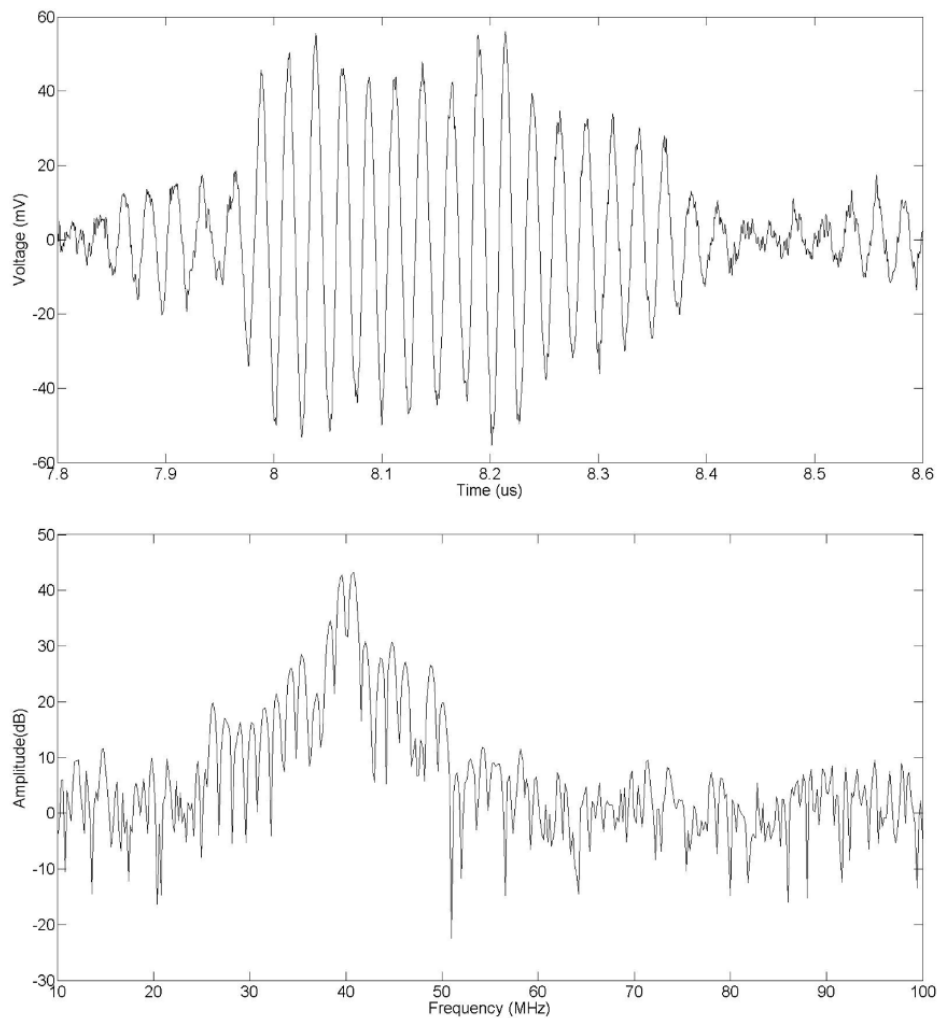


Figure 3.3-10 System verification signal in time domain (upper) and frequency domain (bottom). Frequency=40 MHz, cycle number=30, PRF=100 Hz.

3.3.5 Harmonic Property

Figure 3.3-11 shows a single successful backscatter pulse from water as reference and nanobubble. The signal amplitude of nanobubble is significantly larger than reference. This result verifies that the sampling window between 9.6 us to 11.6 us is suitable to test the harmonic property of nanobubble. Nanobubble can produce significant backscatter echo. From frequency domain plot, there is a significant second harmonic signal (80MHz) in the backscatter from nanobubble which does not exist in reference group.

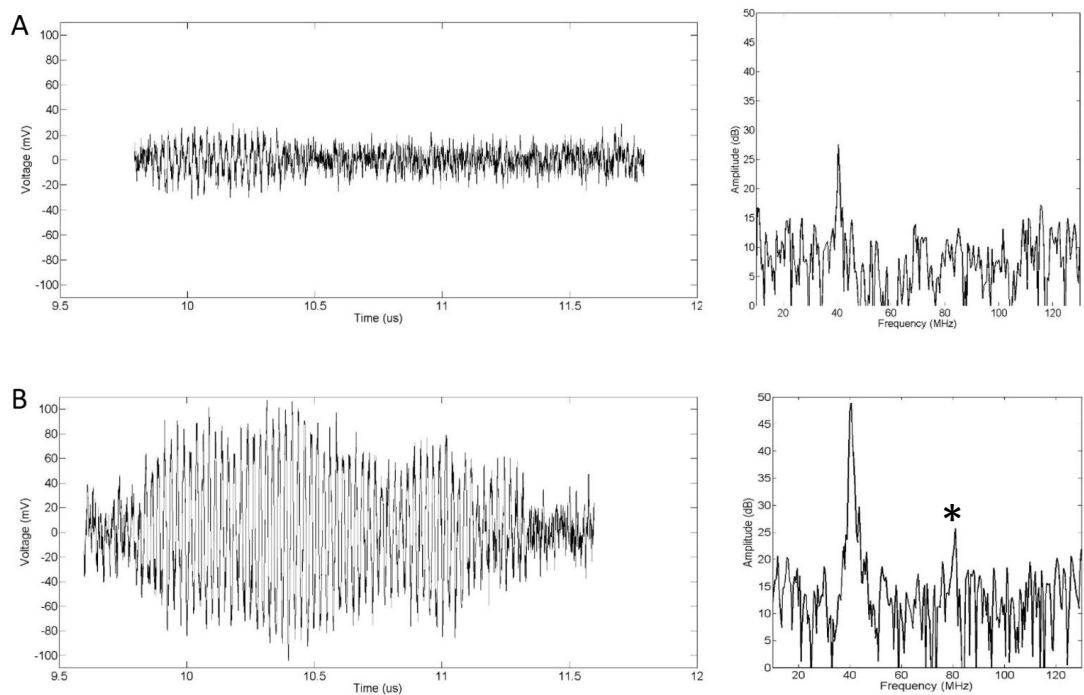


Figure 3.3-11 Backscatter signal from sample cell with (B) and without (A) nanobubble. Input voltage (p-p) =30 V, frequency=40 MHz, cycle number=30, PRF=100 Hz, OD500=3.0 time<1 min. *:80 MHz.

Over 200 successful pulse was averaged after Fourier Transformation and plotted in (Figure 3.3-12). In the reference signal, only one frequency component can be observed at 40MHz as transmitted. However there are two major frequency components in the signal from nanobubble. 40MHz is the fundamental frequency the same as transmit one and 80MHz is the second harmonic frequency double the transmit one which is generated by nanobubble non-linear oscillation. The second harmonic frequency is about 10dB larger than background signal. However in the 120MHz which is the third harmonic region, there is no significant difference from background frequency. This may be caused by the limitation of transducer bandwidth. There is also no significant sub- and ultra- harmonic frequency (half and $3/2$ of fundamental frequency).

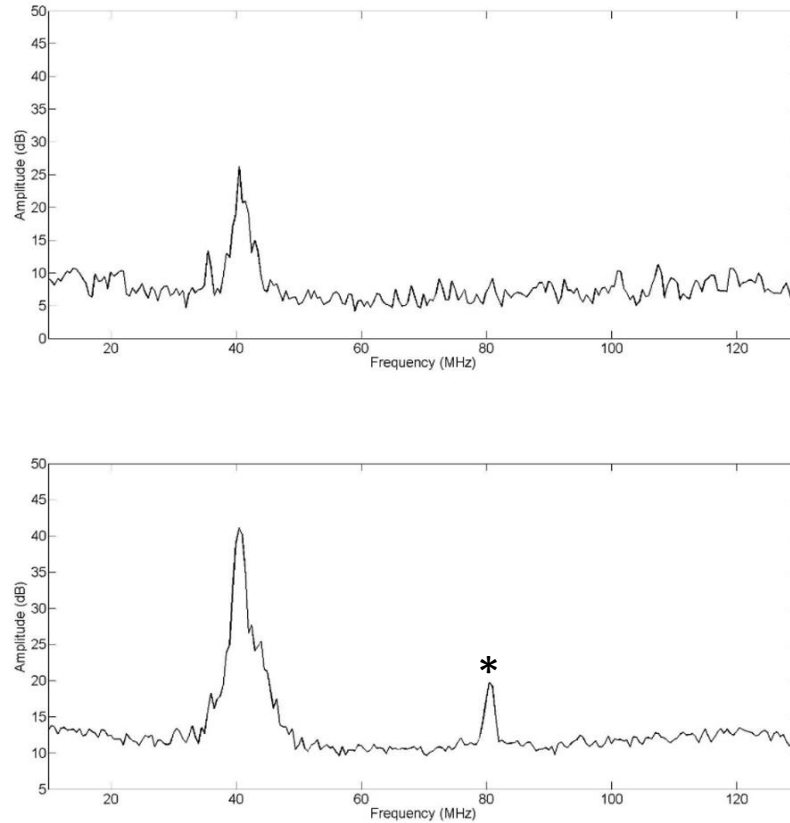


Figure 3.3-12 Frequency components from reference (up) and nanobubble (bottom) after 200 average. Input voltage (p-p) =30 V, frequency=40 MHz, cycle number=30, PRF=100 Hz, OD500=3.0, time<1 min. *:80 MHz.

Because it is hard to measure the acoustic pressure of frequency as high as 40 MHz. The pressure is alternatively presented by the normalized value. The reference of normalization is the critical pressure that starts to cause the rupture of nanobubble which can be observed by x10 stereomicroscope where bubble turns from white color to transparent when rupture. To calibrate the relation of voltage and acoustic pressure, transducer #1 made by the same material (LiNbO_3) was test at the frequency of 20 MHz. The result (Figure 3.3-13) shows good linearity of the input voltage and peak negative pressure. The maximum acoustic pressure tested up to 1.6MPa which is

greater than the critical hydrostatic pressure (1MPa) resulting in nanobubble rupture.

The acoustic pressure result from transducer #1 can be used as the reference for transducer #2 and #3 made by the same piezoelectric material.

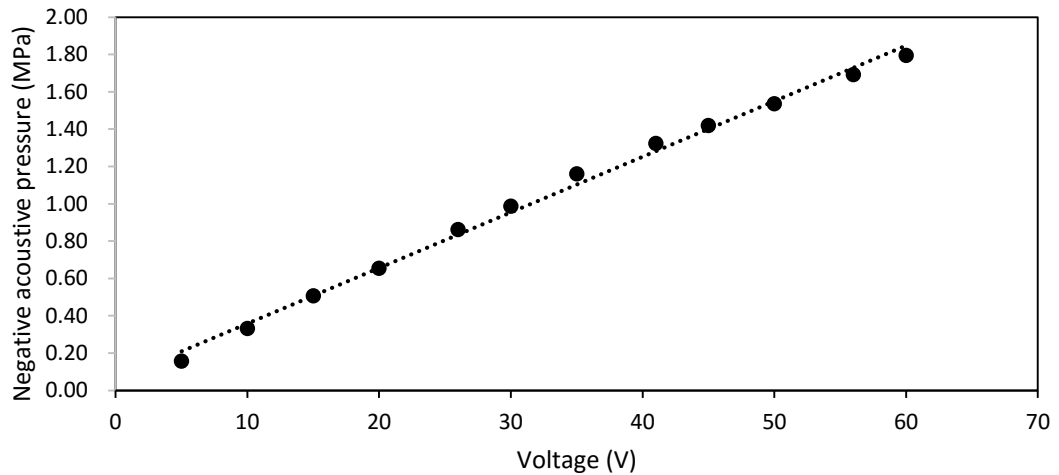


Figure 3.3-13 Peak negative acoustic pressure as the relation with input voltage ($r^2=0.995$). Transducer #1, frequency=20 MHz, sine wave, cycle number=30, PRF=100 Hz.

Harmonic property changes as the function of acoustic pressure was measured using 5 normalized pressure gradients (Figure 3.3-14). There is a threshold of second harmonic component in frequency domain. When the relative acoustic pressure smaller than 0.6, there is no second harmonic response. In the acoustic pressure larger than 0.6, the second harmonic increases with acoustic pressure.

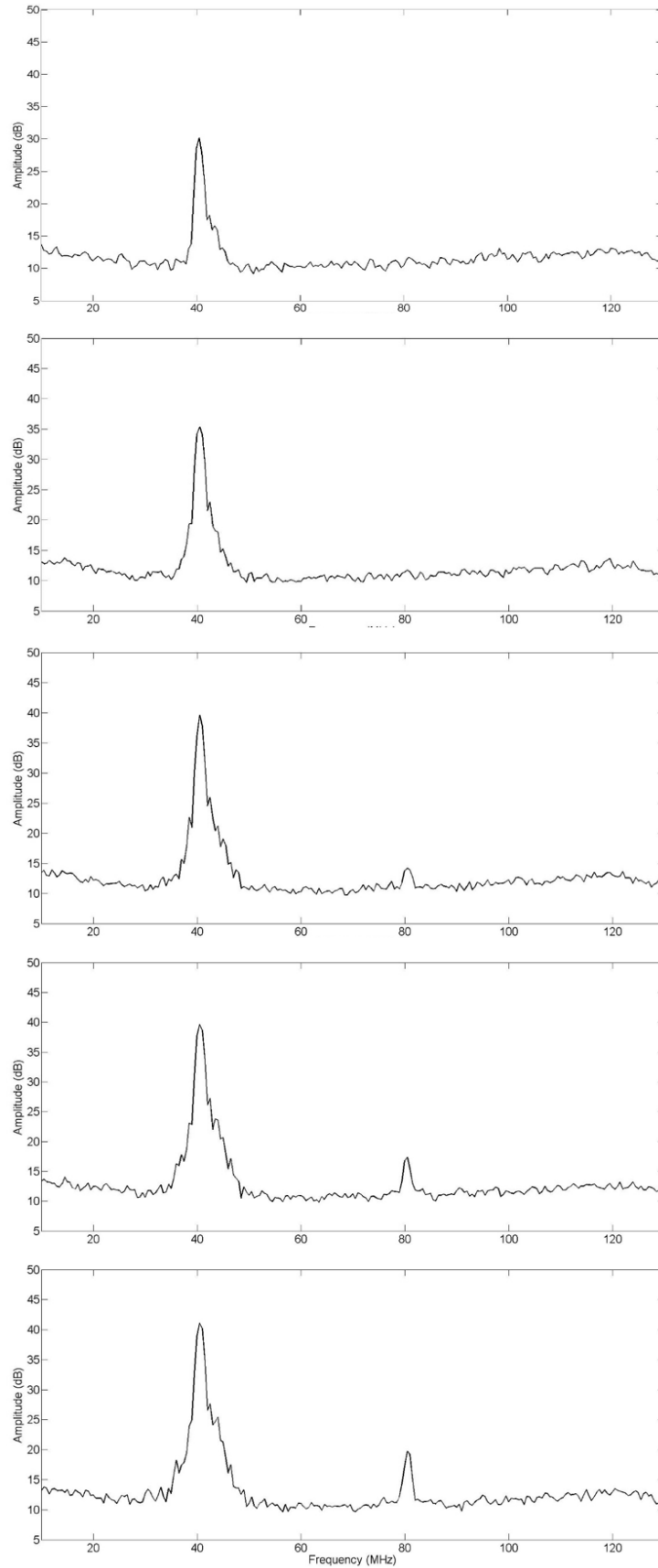


Figure 3.3-14 Nanobubble backscatter signal in frequency domain from up to bottom is related to normalized pressure 0.5, 0.6, 0.7, 0.8 and 0.9. Transmit signal:

transducer #2, frequency=40 MHz, sine burst, cycle number=30, PRF=100 Hz,
OD500=3.0, t<1 min.

Quantitative analysis of the relation of 2nd harmonic frequency Amplitude and acoustic pressure (Figure 3.3-15) was calculated.

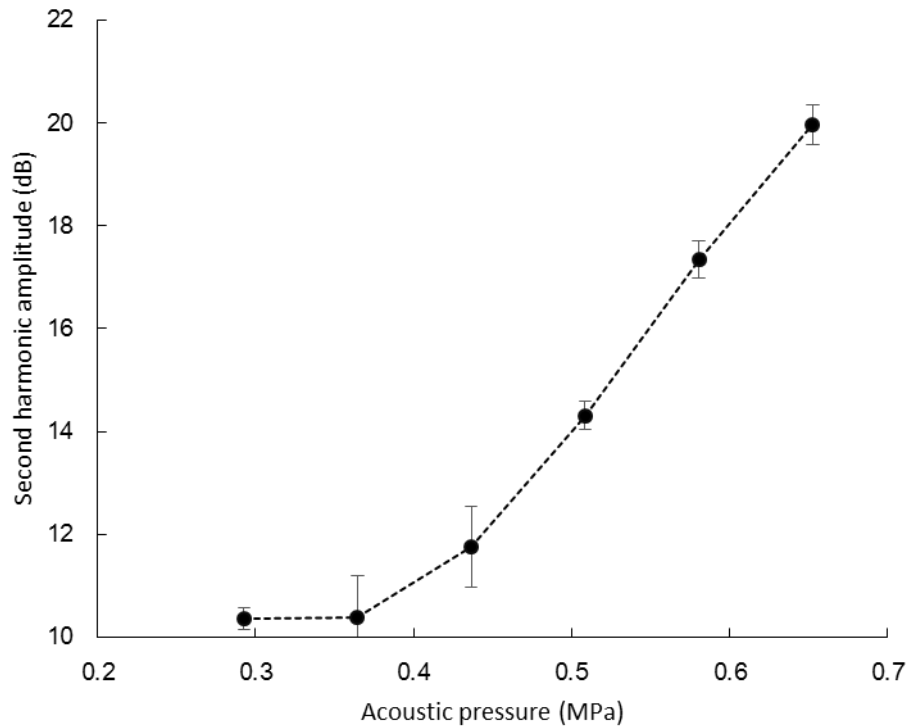


Figure 3.3-15 Amplitude 2nd harmonic frequency as the function of acoustic pressure. Transmit signal: transducer #2, frequency=40MHz, sine burst, cycle number=30, PRF=100Hz, OD500=3.0, t<1min.

The fundamental and second harmonic frequency dependence on time is also calculated every 0.5 mins under continuous stimulation at the relative acoustic pressure of 0.9. The result is plotted in (Figure 3.3-16). There is no significant

variations of both fundamental and 2nd harmonic frequency caused by continuous stimulation.

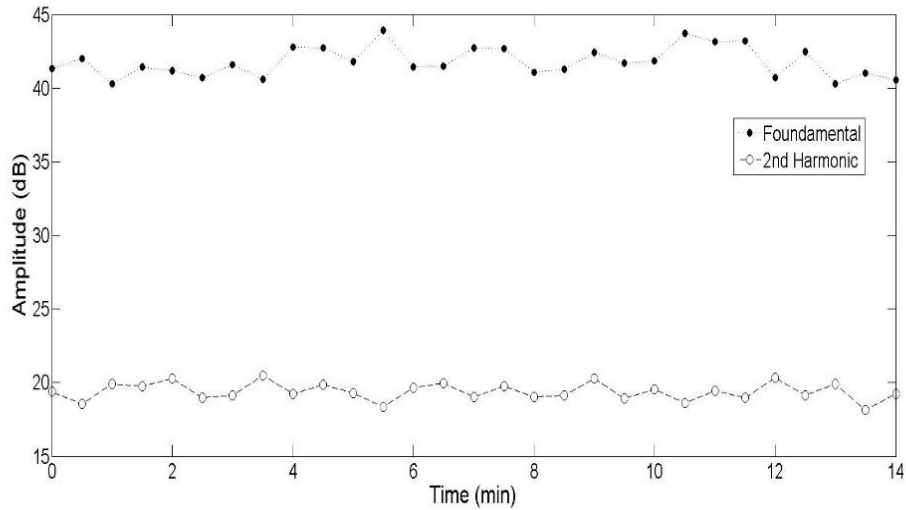


Figure 3.3-16 fundamental and second harmonic frequency amplitude in relation with time. Transmit signal: transducer #2, frequency=40MHz, sine burst, cycle number=30, PRF=100Hz, OD500=3.0.

3.3.6 B-mode Image Characterization

From (Figure 3.3-17), the biogenic nanobubble can provide strong contrast in B-mode image. Qualitatively, the signal intensity is increased with concentration. The threshold concentration of the nanobubble contrast can be as low as OD500=0.125 equal to about 0.05 nM. Nanobubbles can be broken by high intensity ultrasound pulse and signal before and after breaking have significant difference (Figure 3.3-18).

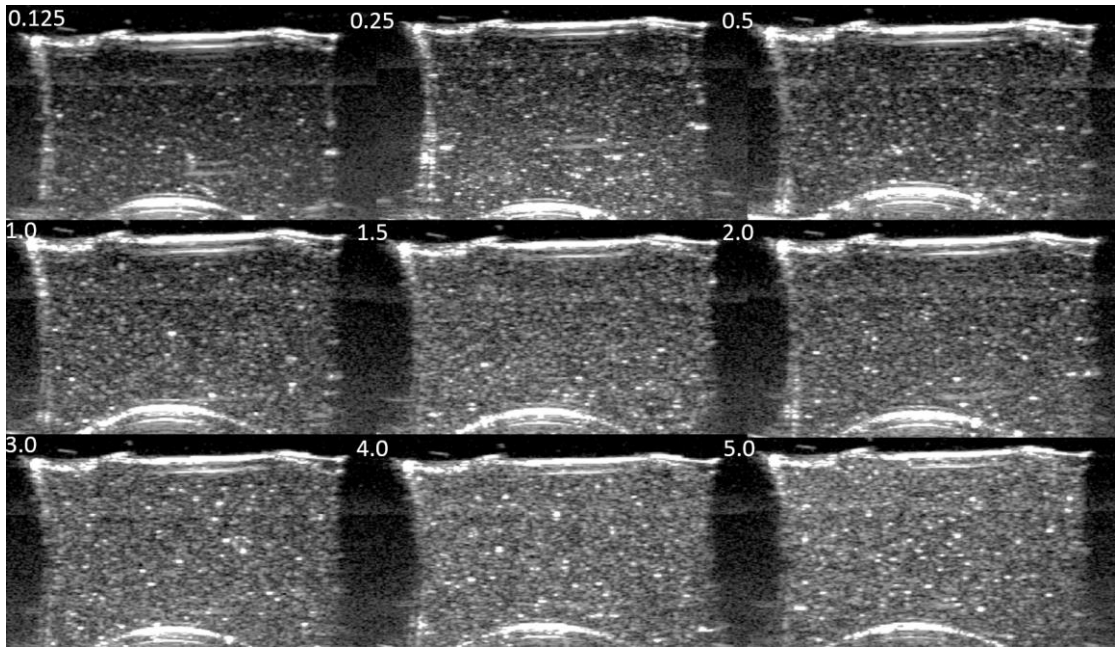


Figure 3.3-17 Ultrasound image of nanobubble as the function of concentration.
 (Frequency=40 MHz, n=3, number represent the optical density OD500).

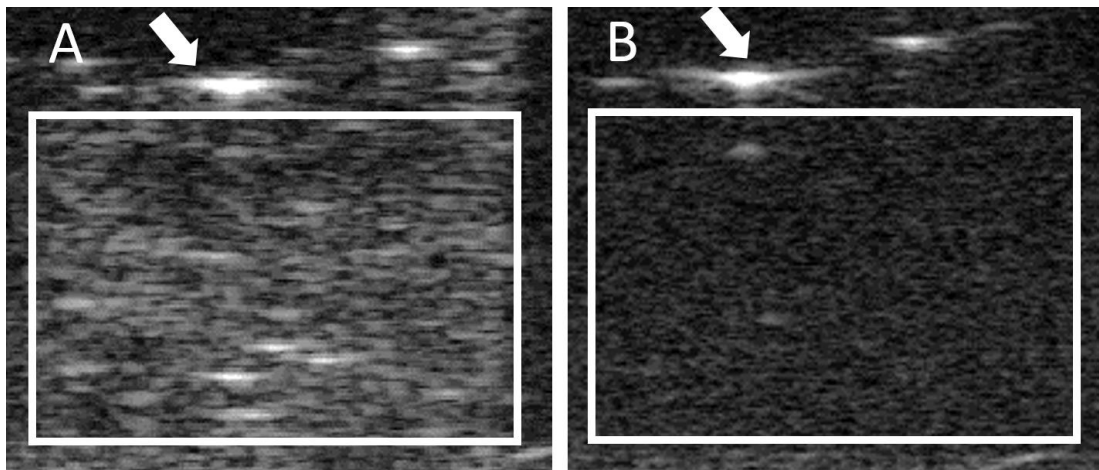


Figure 3.3-18 Ultrasound image of nanobubble before (A) and after (B) broken by high intensity ultrasound. (OD500=1.0). Arrows point to marker which is not influenced by high intensity ultrasound. White frames represent nanobubble region terms from gray to dark after bubble broken.

3.3.7 Ultrasonic Stability Test

From (Figure 3.3-19) the steady state stability test by ultrasound intensity is consistent with the result from concentration test by spectrophotometer. The three results all have no significant decrease compared to original one.

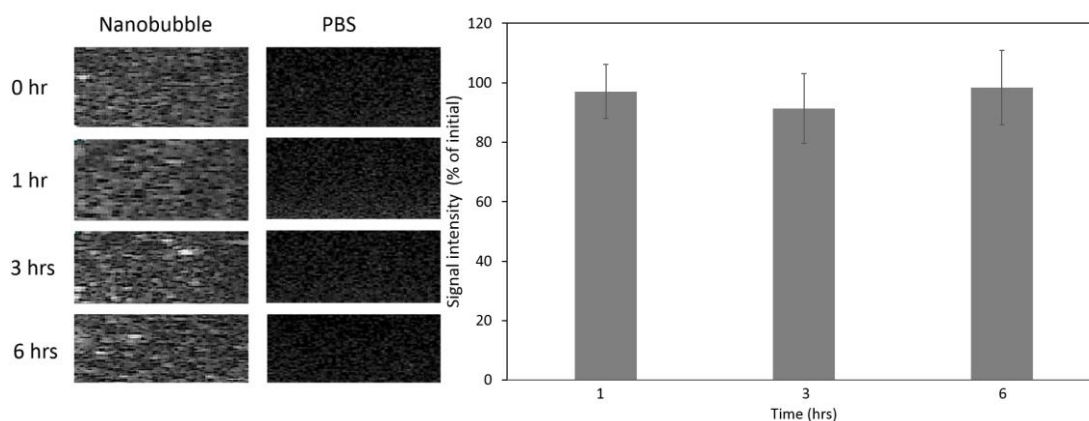


Figure 3.3-19 Ultrasonic image intensity compared to PBS in different time point. (n=3)

The result from stability test under sonicating is plotted in (Figure 3.3-20). Though there is continuously decrease of the ultrasound signal with time, no significant decrease is observed. The average signal intensity goes down to about 94% of the original one.

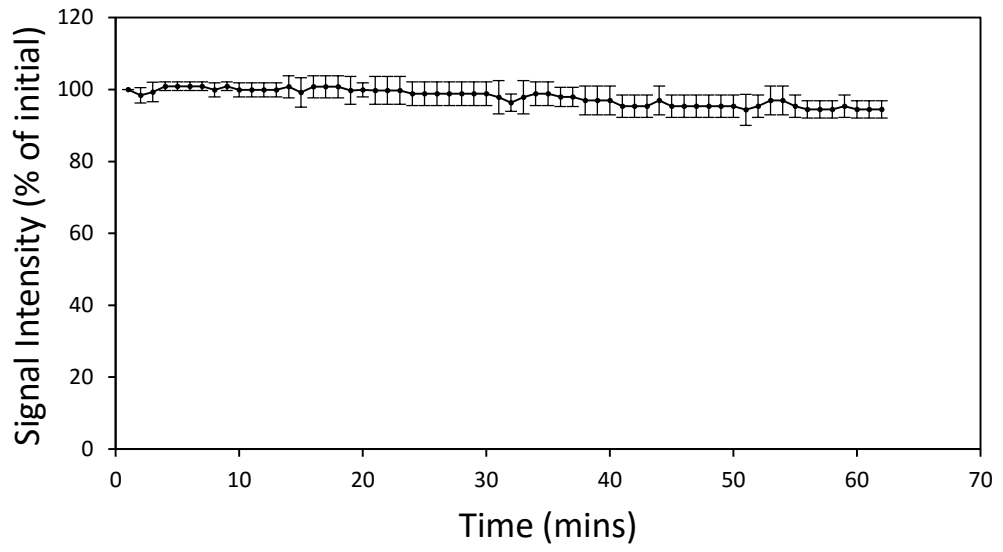


Figure 3.3-20 Signal intensity of ultrasound image from the sample stimulated by ultrasound pulse continuously for 60 mins. (n=3, frame rate=5Hz)

3.4 Discussion

In the attenuation measurement, the three transducers can cover broad range of frequency from 7MHz to 103MHz at the minimum amplitude of -20dB. In the two overlapping region, there is no significant difference between each transducers. This fact indicates that the measurement is not influenced by transducers.

The peak attenuation coefficient appears at 88MHz frequency within the region of 80MHz to 90MHz which is covered by the -20dB bandwidth of transducer #3. This region does not change in multiple measurement. According to the study conducted by other researchers, the peak region represent the harmonic frequency of bubble. Based on Feuillade's research⁷⁰, the cylinder shape bubble has only one resonance frequency independent of bubble/incident ultrasound angle provided that the ultrasound wavelength is much larger than size of bubble (>20 times). This theory confirms the discovery of our experiment. Besides, the cylinder shape bubble can also be treated as the spherical bubble with the same volume when its resonance frequency was calculated. The resonance frequency of cylinder bubble should be 1.1163 times that of same volume spherical bubble when the aspect ratio is 4. Based on the TEM result, the diameter of equal volume spherical bubble is 192nm which can represent the biogenic nanobubble. Using the Rayleigh-Plesset model, the resonance frequency of spherical bubble with diameter of 192nm is calculated to be 76MHz if shell parameter is the same as Sonovue. The corresponding resonance frequency of equal volume cylinder bubble (aspect ratio=4) should be 84.8MHz which is similar to our

find. The resonance frequency is meaningful for harmonic imaging because the second harmonic frequency should be the maximum when incident ultrasound frequency is half of the resonance frequency. To this nanobubble, 40MHz excitation ultrasound is most suitable for harmonic imaging.

The experiment system is demonstrated not to influence the nanobubble non-linear property test. From the nanobubble testing result, the second harmonic frequency component is significant. However there is no subharmonic, ultraharmonic and third harmonic frequency components in the non-linear response of nanobubble. The limited frequency bandwidth may partially attribute to this result. The second harmonic property is obvious at the acoustic pressure larger than certain level (0.6 relative pressure). When it appears, the amplitude of second harmonic component is almost linear to acoustic pressure. Both the first and second harmonic frequency is independent of time over 15 mins. The strong non-linear property of biogenic nanobubble indicates the ability to provide ultrasound contrast image.

The result of steady state stability by evaluating ultrasound intensity change is consistent with previous concentration test. Both the results support the conclusion that the biogenic nanobubble is much more stable than conventional nanobubble. The under-sonication stability of biogenic nanobubble is also proved to be as long as 1hr, which means it is suitable for long-term imaging.

4 BIOEFFECT CHARACTERIZATION

4.1 Introduction

Traditional microbubble have been widely used to carrying chemotherapy drug and can be controlled to rupture to release drug in target site by high intensity ultrasound stimulation.⁷² In addition to drug delivery, several groups have also investigated microbubbles and nanoparticles as vehicles for gene therapy.⁷³ Hosseinkhani *et al.* have shown efficient US-enhanced gene delivery using polyplexes of DNA and cationic-derivatized solid natural polymers in vitro.⁷⁵

One of the most important features of nanoparticle that can influence therapeutic effect is the endocytosis rate by tumor cells.⁷⁴ Researchers have found that tumor cell can internalize nanoparticles. However, the endocytosis rate is depended on nanoparticle size, shape, surface charge and material.⁷⁶ Whether the biogenic nanobubble can be engulfed by tumor cell deserves to be evaluated.

Nanobubble can be transferred to a molecular imaging probe by coating specific antibody ligand on surface. It can also be combined with other nanoparticles to perform multimodality imaging. Traditional nanobubble is unstable and hard to be surface modified. To extend the usage of biogenic nanobubble, surface modification ability should be tested.

4.2 Methods

4.2.1 Cell Culture

The HeLa cell was cultured in 25 cm² flask (Cell Culture Treated EasYFlasks, Thermo Scientific Company, Waltham, Massachusetts, USA) with Dulbecco's Modified Eagle Medium (DMEM) (Thermo Scientific Company, Waltham, Massachusetts, USA) in an incubator operated at 37 °C under a 5% CO₂ atmosphere. The subcultivation ratio is 1:2 ~ 1:6 for HeLa cell. The cell layer is rinsed by 0.25% Trysin-EDTA solution (Thermo Scientific Company, Waltham, Massachusetts, USA) by Centrifuge 1000rpm, 5min. The cells were stored with DMSO in - 85 °C Deep Freezer (VXE 490, Jouan) with -80 °C temperature.

4.2.2 PpIX Coating

To test the surface modification property of biogenic nanobubble and to track the nanobubble interacting with cells, the nanobubble surface was functionalized with fluorescence dye. In this experiment, Protoporphyrin IX (PpIX, C₃₄H₃₄N₄O₄) from Sigma Aldrich, a multifunctional fluorescence probe, was chosen to bond to the nanobubble surface. The formula and fluorescence absorption and emission wavelength was shown in (Figure 4.2-1). The nanobubble shell was composed of gas vesicle protein which contains amine group. The carboxyl group at the end of PpIX molecule was used to bind to amino group on the nanobubble surface using EDC/NHS (N-(3-dimethylaminopropyl)-N'-ethyl-carbodiimide/N-hydroxysulfosuccinimide).

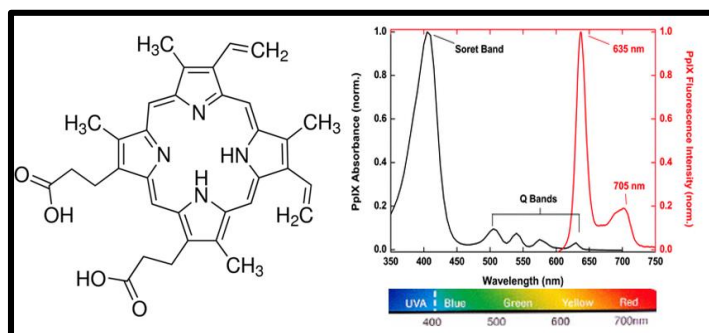


Figure 4.2-1 Molecule formula and fluorescence property of PpIX. (Information from Sigma Aldrich).

The First step is to link EDC (40 mM) to PpIX (4 mM) in the sulfo-NHS (100mM) activated intermediate in 0.1 M sodium phosphate, pH 7.4. After 15 mins reaction in room temperature, the reaction solution was added to nanobubble (1 nM, x10 volume) to the final concentration of (nanobubble: PpIX= 1 nM: 0.4mM). After 2 hours reaction in room temperature, the additional PpIX and EDC/NHS was washed out by centrifugation and PBS buffer. Centrifuge at 1100 rcf can bring the PpIX-nanobubble to the surface in 25 mins providing the depth of solution is 18 mm in 2 ml centrifuge tube. Each wash step can wash away 90% residual dyes.

4.2.3 PpIX-nanobubble Characterization

The zeta potential of purified PpIX-nanobubble was measured 3 times by zetasizer. The result was compared with nanobubble before PpIX coating to examine the surface charge changing caused by PpIX coating. The significant surface charge changing can indirectly prove that PpIX was successfully attached to nanobubble surface. Stability of PpIX-nanobubble was tested by measuring size distribution to examine whether

aggregation was happened caused by PpIX coating process. This test was done twice; one is the comparison between nanobubble before PpIX coating and after coating; another is to compare the PpIX-nanobubble in serum solution after 8 days to the original one. In all of the above test, the testing solution was diluted to the concentration in range of 0.1nM – 0.5nM.

Before the cell attachment test, the fluorescence property of PpIX-nanobubble was examined in vitro. PpIX-nanobubble was diluted to 0.5nM in PBS and fixed on glass slide to be observed under fluorescence microscope (Eclipse TS100, Nikon Corporation, Chiyoda, Tokyo, Japan). Two excitation light wavelength was tested, one the blue (405nm) and green (488nm) falling within the two absorbance peak region of PpIX. Bright field microscope (Eclipse TS100, Nikon Corporation, Chiyoda, Tokyo, Japan) and phase contrast microscope (Eclipse TS100, Nikon Corporation, Chiyoda, Tokyo, Japan) were used to observe the morphology and color change when compared with pure nanobubble.

4.2.4 Cell Attachment Experiment

The HeLa cell was cultured in a flask in DMEM with 10% FBS and 1% antibiotics to the final concentration of 10^6 cells covering the bottom of flask. Then the culture medium was removed and cells was washed twice by PBS. After that, the cells were digested from flask by 0.25% Trypsin-EDTA (Thermo Scientific Company, Waltham,

Massachusetts, USA) and collected by centrifuge with 1000 rpm and 5mins. All cells were dispersed equally in centrifuge tube and separated to be seeded confocal dishes (3×10^4 cells/dish) (200350, SPL life Science company, Hong Kong, China). The nanobubble or PpIX-nanobubble was prepared by diluted in DMEM solution to the concentration of 0.5nM. 200ul prepared nanobubble solution was added into cell culture in confocal dish and incubated overnight. For the control group, the same volume of DMEM was added and incubated overnight.

After one-night incubation, the additional medium in the dish was removed first. Then the cell attached on the dish bottom was washed by PBS 3 times. The cells were observed by phase contrast microscope, fluorescence microscope and confocal microscope. The excitation light wavelength was selected to be 405nm and 488nm. The explosion time was fixed for each observation.

In the experiment examining the influence of incubation way, the different incubation way was evaluated. In previous study, the nanobubble was added into cell culture when the cells were suspended in culture medium. However, in conventional cell culture method, the HeLa cell was cultured attached to the culture dish. Because the nanobubble is floats in the superficial of the solution, the cells attached on the bottom of dish is hard to contact with superficial nanobubble. Therefore we hypothesized that the incubation way could influence the nanobubble cell attachment. In the experiment

group, the cell was seeded to confocal dish one day before incubation. When the cells were attached on the bottom of dishes, nanobubble or PpIX-nanobubble was added to the cell culture and incubated overnight. In control group, nanobubble and cells all suspended in medium.

4.2.5 Image Analysis

Optical density of the fluorescence images was analyzed by ImageJ™. First, the image was transforms to 8-bit gray-scale picture. Color invert was done to recover the original optical density and then be calibrated. After that, the integrated optical density was calculated automatically representing the total fluorescence intensity from cells in the picture. The bright field image corresponding to the fluorescence image was analyzed by ImageJ to calculate the total cell area (pixel). The integrated optical density divided by total cell area was calculated for each pair of image to compare the difference of fluorescence intensity per cell area between experiment group and control group. This value represent the amount of nanobubble attached to or endocytosis by the cell.

4.3 Results

4.3.1 Nanobubble Endocytosis

Purified nanobubble diluted in PBS was observed using phase contrast microscope.

Nanobubble can be observed by phase contrast microscope (Figure 4.3-1). It is a white

dot under microscope, the diameter is calculated to be about 600nm which is close to

400nm longitudinal diameter of TEM result. The reason why it shows bright dot shape

in phase contrast microscope is because of the great diffraction index difference

between air inside nanobubble and surrounding water. However, the cylindrical shape

cannot be observed in microscope image caused by the limited resolution of optical

microscope. Why the diameter in microscope image is larger than the real size is

because of the light diffraction.

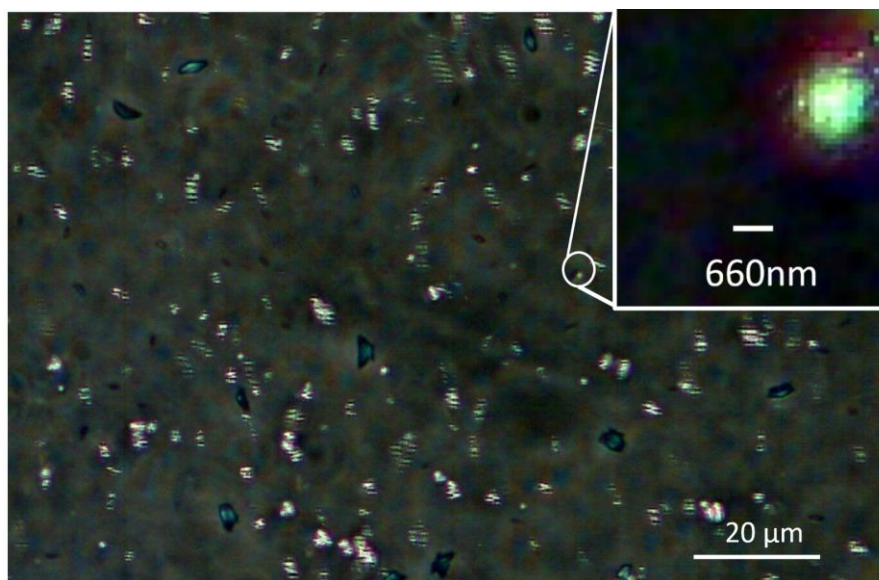


Figure 4.3-1 Image of purified nanobubble solution in PBS by phase contrast microscope. Concentration=0.5nM

This special property under phase contrast microscope may be helpful to observe the nanobubble endocytosis by tumor cell. After the HeLa cell and 0.5nM nanobubble was incubated overnight and washed 3 times, the sample was observed in phase contrast microscope (Figure 4.3-2). Some bright dot can be observed inside cell region. These bright dots are possible to be the nanobubble. However the difference is not significant, because in the control group without nanobubble shows some bright dot as well. These bright dot in control group may be the noise from intracellular organelle. For this reason, the bright field phase contrast microscope is not a valid method to investigate nanobubble endocytosis property.

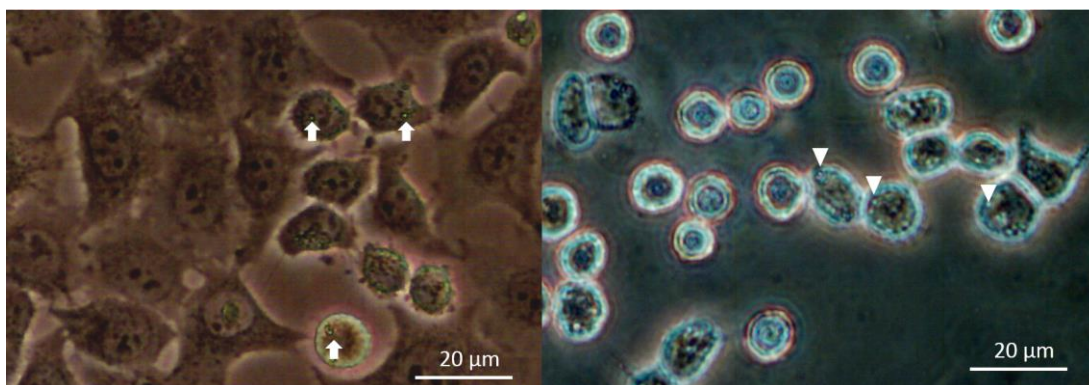


Figure 4.3-2 Control group without nanobubble (left) and HeLa cell incubated with nanobubble (right). Arrows and arrowheads point to suspicious nanobubbles.

4.3.2 PpIX Coating

PpIX was coated to nanobubble surface successfully using EDC/NHS. The result is shown in (Figure 4.3-3). The pure nanobubble is white color floating in the upper part of the solution because of the buoyance of air inside bubble. While when it is coated

by PpIX, the flowing layer turns to pink color which is the color of PpIX. This phenomenon indicates that PpIX is successfully bonding to nanobubble surface. Another direct evidence to prove the success of coating is the zeta potential change. Average zeta potential of nanobubble before PpIX coating is -41.7 mV and shifted to -55 mV after PpIX coating.

The stability was tested by analyzing the size distribution. When comparing the size distribution before and after PpIX coating, there is no significant difference (Figure 4.3-4). The average size of nanobubble before PpIX coating is 274.2 nm (PDI=0.077) and stay in 292.7 nm (PDI=0.229) after PpIX coating. This result indicates no aggregation happened after PpIX coating. The same test was done when diluted the PpIX-coated nanobubble into serum for 8 days (Figure 4.3-4). Before dilution to serum, the average size is about 292.7 nm (PDI=0.229) versus 315.8nm (PDI=0.373) 8 days after diluted in serum. This result indicates that the PpIX coated nanobubble stays stable without aggregation in serum solution. The stability can keep over 8 days.

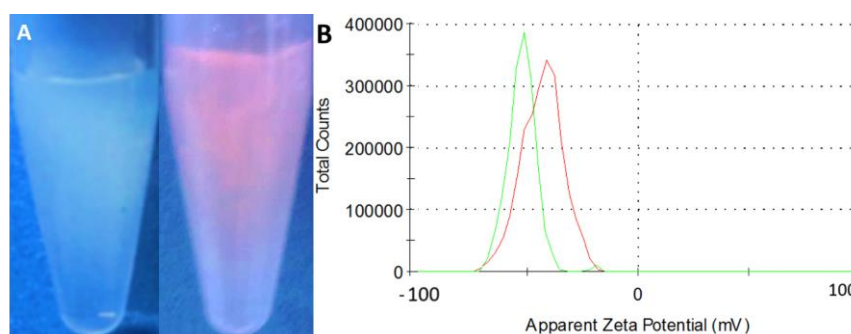


Figure 4.3-3 Comparison with pure nanobubble and nanobubble coated with PpIX. A, photo of nanobubble before (left) and after PpIX coating kept steady for 2 hrs. B, zeta potential of nanobubble before (red) and after (green) PpIX coating.

The fluorescence property of PpIX-nanobubble was characterized by fluorescence microscope. The PpIX-nanobubble is red dot when excited by 488 nm wavelength light, for the fluorescence peak of PpIX is 635 nm. The red dot corresponds to the bright dot in phase contrast microscope and dark dot in bright field microscope. The slight position shift is caused by Brown motion and buoyance flowing during the time two photo taken.

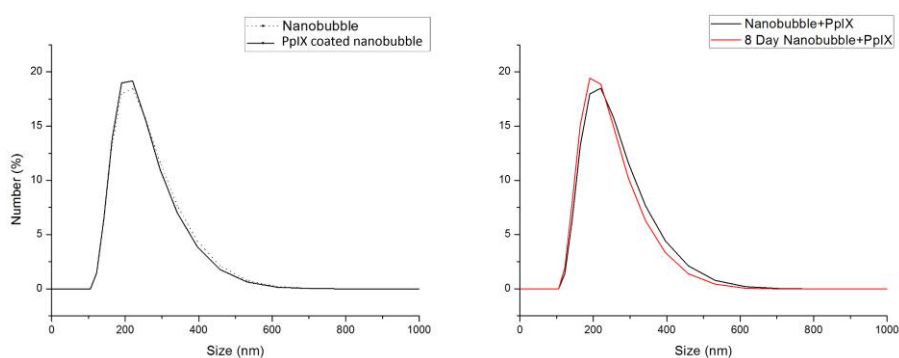


Figure 4.3-4 PpIX-nanobubble stability test by size distribution.

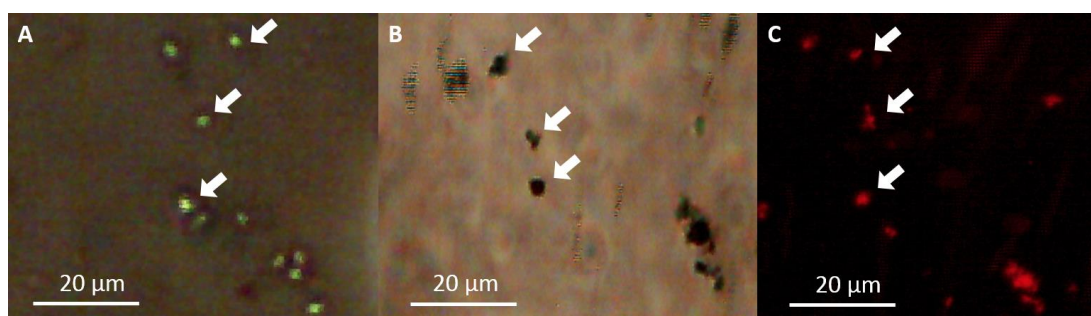


Figure 4.3-5 Microscope image of PpIX-nanobubble from phase contrast, bright field and fluorescence. Excitation light wavelength is 405 nm.

4.3.3 PpIX-nanobubble Endocytosis Property

The HeLa cell, after overnight incubation with PpIX-nanobubble was imaged using fluorescence microscope. The control group is the HeLa cell with same cell density

but incubated with PBS solution. From the result (Figure 4.3-6), the cells present green color in fluorescence image excited by 405 nm wavelength light because of cell autofluorescence property. The red dot represents the PpIX-nanobubble as characterized before. There is great density of red dots inside cell, whereas, they almost absent in the control group. The fluorescence result also has high correlation with the result from bright field microscope.

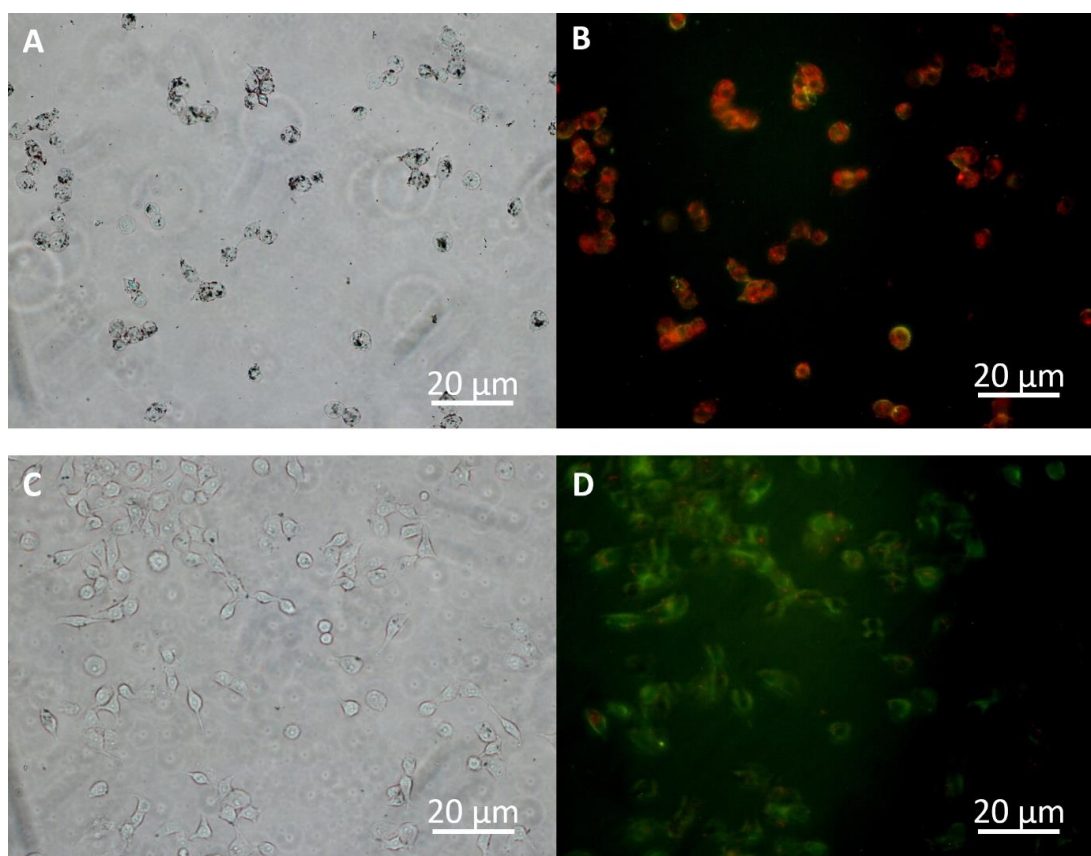


Figure 4.3-6 HeLa cell incubated with (A and B) and without (C and D) PpIX-nanobubble. A and C, bright field; B and D fluorescence microscope (Incubation overnight, nanobubble concentration= 0.5 nM, cell density= 3×10^4 cells/dish, excitation wavelength= 405 nm.)

The result (Figure 4.3-7) by large magnification discovers more detail information. The location of red dots in fluorescence microscope has high correlation with the dark dot in phase contrast microscope image. Besides, the brighter the red region in fluorescence image, the more dark dots can be found in the same region. This indicated that the fluorescence intensity can represent the PpIX-nanobubble concentration.

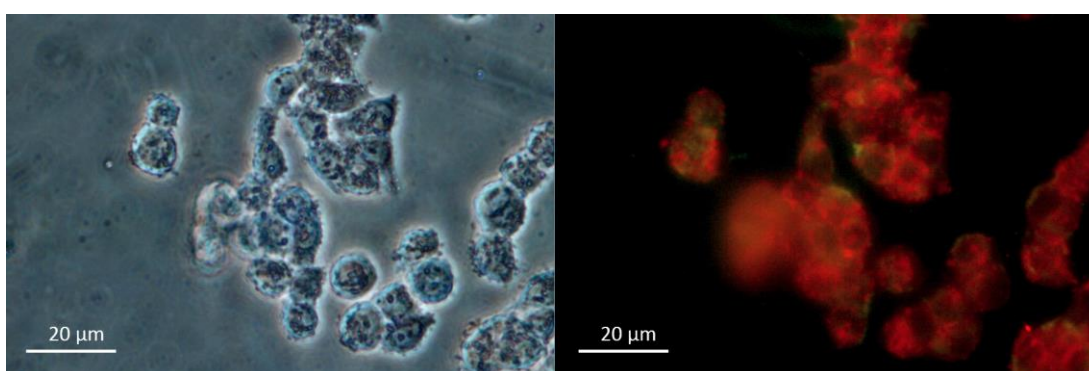


Figure 4.3-7 HeLa cell incubated with PpIX-nanobubble overnight. Left, phase contrast image; right, fluorescence image. Excitation light wavelength = 405 nm, nanobubble concentration = 0.5 nM, cell density = 3×10^4 cells/dish.

Quantitative analysis was conducted base on fluorescence image (Figure 4.3-8). There is significant difference of fluorescence intensity between PpIX-nanobubble incubated cell and control group. The red fluorescence intensity in experiment group is about 4 times larger than the one of control group.

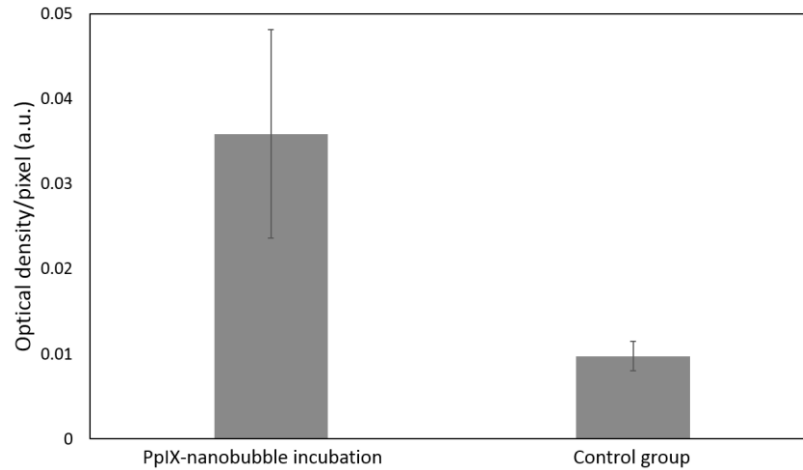


Figure 4.3-8 Optical density/pixel of PpIX incubation cells and control group. (n=8)

To further confirm that whether the nanobubble is internalized by HeLa cells or attached on cell membrane, result from confocal is analyzed. From (Figure 4.3-9), red dots can be found inside cells in the PpIX-nanobubble incubation group and disappears in control group. The red dots signal is from PpIX fluorescence on nanobubble surface. The fact that position of the signal is far from the edge of cell border indicates that the PpIX-nanobubble is internalized into cytoplasm, because the focal slice is in the middle layer of cells. This is also the reason that why black dots in bright field mode is more than fluorescence mode, because the signal is integrated in depth direction in bright field microscopy.

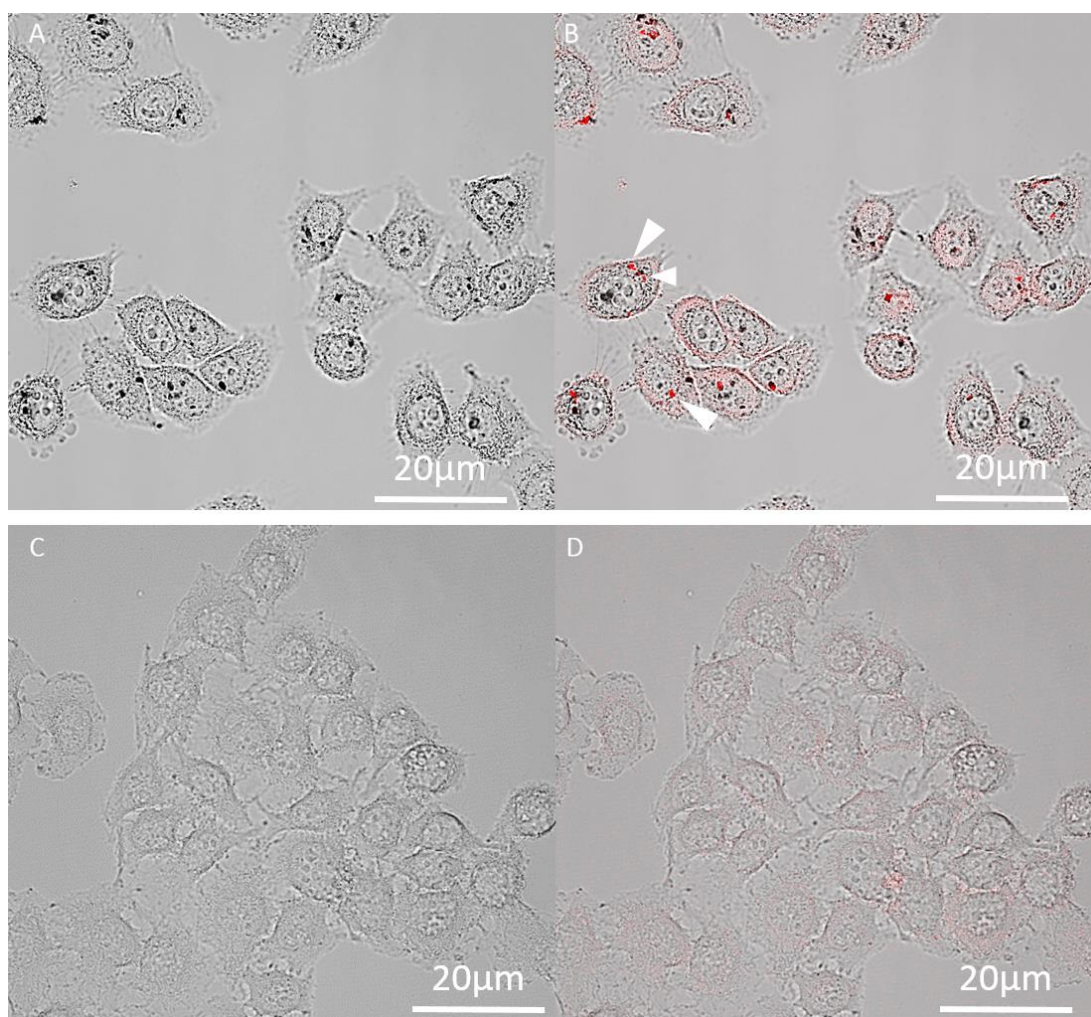


Figure 4.3-9 HeLa cells incubated with (A, B) and without (C, D) PpIX-nanobubble overnight imaged by confocal microscopy. A and C, bright field; B and D, bright field image merged with fluorescence image. Arrowheads point to PpIX-nanobubble.

Excitation light wavelength = 488nm, nanobubble concentration = 0.5nM, cell density= 3×10^4 cells/dish.

4.3.4 Incubation Way Influence on Cell Attachment

The conventional cell and nanobubble incubation way is different from the real in vivo situation. The cell attached to the dish will reduce the chance of nanobubble to attach to the cell. Meanwhile, the buoyance of nanobubble makes it flowing on surface of

culture medium, therefore the cell attaching to the bottom of culture dish cannot contact nanobubble. Two incubation way were tested and the result is plotted in (Figure 4.3-10). Corresponding with the cells in bright field image, more cells present red region (PpIX-nanobubble) in suspension cell incubation group than in dish-attached cell incubation. The quantitative analysis also confirm the result (Figure 4.3-11). But the difference is not significant.

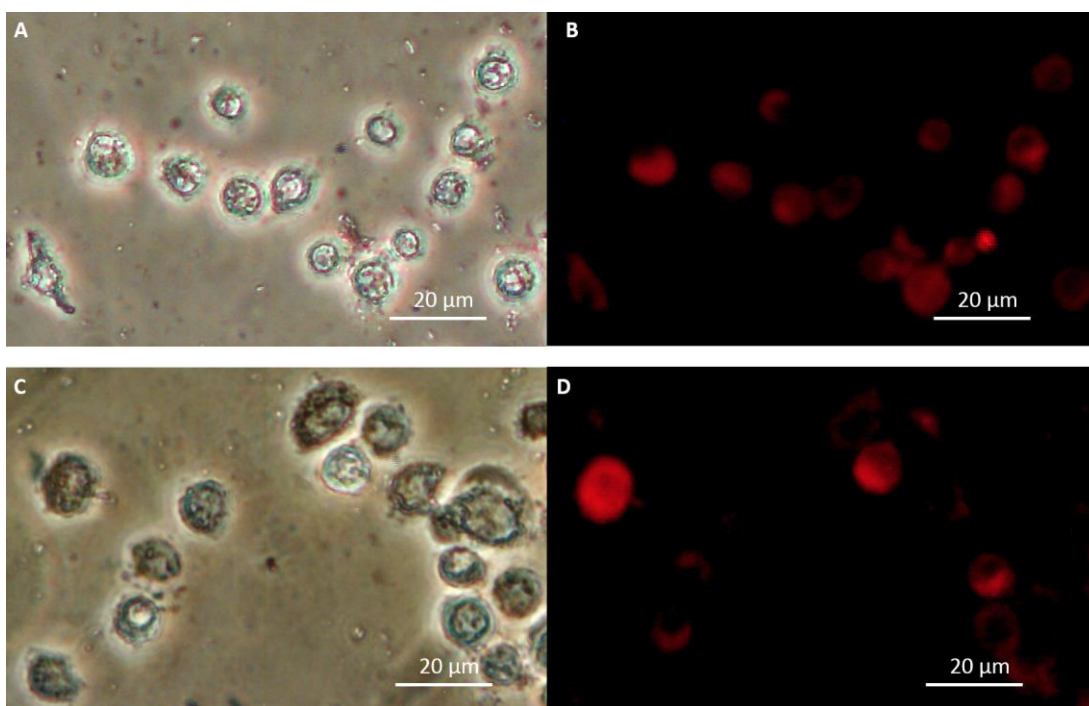


Figure 4.3-10 Cell endocytosis with different incubation way, suspension cell incubation (A and B) and dish-adherent cell (C and D). A and C, phase contrast microscope image; B and D, fluorescence microscope image. Excitation light wavelength = 488 nm, nanobubble concentration = 0.5 nM, cell density = 3×10^4 cells/dish.

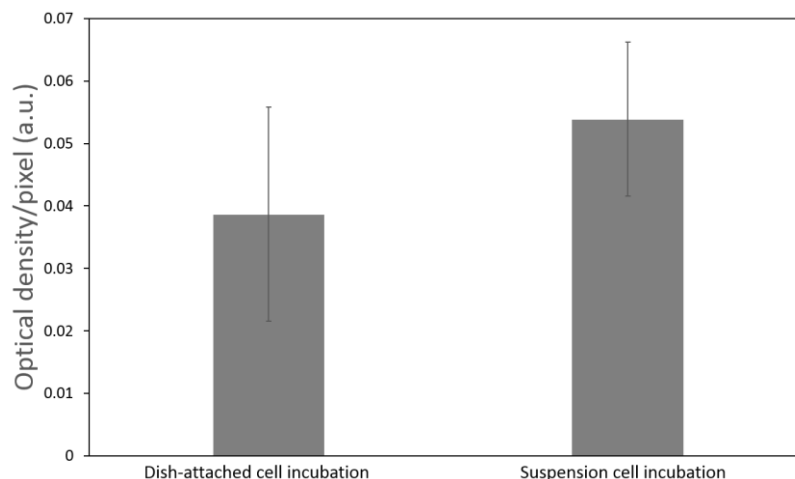


Figure 4.3-11 Optical density/pixel analysis based on fluorescence image between two incubation way. (n=4)

4.4 Discussion

Biogenic nanobubble can be observed as a bright dot using phase contrast microscopy. This may provide an easy way to count bubble concentration or study bubble reaction to ultrasound stimulation. However, because the cytoplasm is a complex environment where the attached or internalized nanobubble is hard to be delineated.

Nanobubble surface modification ability is tested by coating PpIX onto the nanobubble surface using EDC/NHS instead of avidin-biotin conjugation. Unlike lipid based nanobubble, the process in biogenic nanobubble is found to be extremely easy to operate without worrying about bubble breaking or aggregation during process. PpIX was succeeded to be attached on nanobubble surface. Easily surface modification property make the biogenic nanobubble easy to be attached with antibody ligand to become a smart probe for specific molecule or cell detection.

The PpIX providing nanobubble with fluorescence ability, make it be detectable under fluorescence microscopy. Both fluorescence microscopy and confocal microscopy have demonstrated that the nanobubble in this particle size can be internalized by tumor cell (HeLa). It means that the biogenic nanobubble can enter into tumor cytoplasm to deliver drug and gene and also can be controlled to release by ultrasound stimulation.

The cellular internalization property is governed by particle size, surface feature and shape. Pervious researches based on gold nanoparticle has demonstrated that the similar size and shape nanorod (200nm length 100nm diameter) can be efficiently took up by cells.⁷⁷ Besides, the carbon nanotube with length as long as 1000nm can be internalized by HeLa cells as well.⁷⁸ Our result is consist with these researches that up to 400nm length of NGV can be internalized by HeLa cell. In addition to the size, that the rod shape structure can facilitate the cell internalization has also been widely reported based on other nanoparticles. The surface of NGV is negatively charged and may cause repulsive interaction with positively charged cell membrane. However the real situation is more complex than theoretical prediction. The charge can also bond extracellular protein in serum-containing culture medium forming corona facilitating the non-specific adhesion to cell membrane.⁷⁷ The intrinsic protein shell and PpIX-coating also have unpredictable effect on cellular internalization.

5 CONCLUSION AND FUTURE STUDY

5.1 Conclusion

Biogenic nanobubble was successfully isolated from *Anabaena* Cyanobacteria. The size distribution consistency of the isolated nanobubble was studied and found to be almost constant comparing each batches. The morphology study reveals that the nanobubble is cylinder shape with average length of 395 nm and width of 97 nm, the value is closed to other researchers' results.

The acoustic characterization is focused on the nanobubble stability, resonance frequency and non-linear property. The biogenic nanobubble is found to be more stable compared with the results from ever reported nanobubble synthesized in laboratory way. The stability is evaluated in three aspects. Firstly, the biogenic nanobubble diluted in PBS can keep stable without breaking for over 6 hrs. This result is promising when compared with lipid based nanobubble of less than 30 mins existing time. Secondly, the size is also constant independent of time. Third, the stability under sonication is also long enough to be imaged continuously for over 1 hr. The strong stability can facilitate nanobubble long circulation time to accumulate in extravascular focused site providing that it can penetrate out of vessel wall.

The increased stability does not reduce the non-linear property of biogenic nanobubble. Biogenic nanobubble shows strong harmonic property especially second harmonic

frequency in relative low mechanical index. The special naturally formed structure make the nanobubble share both the strong stability and bubble nonlinear oscillation. The resonance frequency was found to be in 80MHz to 90MHz region. The frequency is relatively high compared to microbubble. Non-linear property together with enhanced stability enable biogenic nanobubble to accumulate in extravascular focused site and imaged by ultrasound non-linear imaging.

The biogenic nanobubble was also found to be suitable and easy for surface modification because of the enhanced stability and protein based shell structure. In our experiment, PpIX was successfully coated onto nanobubble surface using EDC/NHS method. The coating process is very complex for traditional nanobubble for its poor stability and surface tension interference caused by PpIX. Biogenic nanobubble at 100-400 nm size was demonstrated to be internalized by tumor cell. The conclusion was evaluated in four methods: bright field microscopy, phase contrast microscopy, fluorescence microscopy and confocal microscopy. Endocytosis property indicates the ability to perform therapeutic effect like drug delivery and gene delivery intracellular. Easily surface modification property make the biogenic nanobubble easy to be attached with antibody ligand to become a smart probe for specific molecule or cell detection. This property together with enhanced stability, non-linear property and endocytosis property facilitate it with great potential to perform extravascular or intracellular molecular imaging and therapy.

5.2 Future Study

To understand the biogenic nanobubble more comprehensively, more physical properties should be studied. Radiation force is an important property of bubble, by which the nanobubble can be pushed by ultrasound wave to accumulate in tumor region more efficiently than passive diffusion. With this property, nanobubble can act as the drug carrier for chemotherapy.

Another properties deserved to be studied is the cavitation property. Nanobubbles can oscillate stably or be broken in certain ultrasound intensity. In the former condition, the oscillated bubble can produce microstream and interface the surrounding biological structures like cell membranes. In the late conditions, the broken nanobubble can produce microjet and damage cell membrane or cytoskeleton. These properties have the potential to increase drug and gene delivery efficiency.

In future study, the gas vesicle will be used in vivo to further demonstrate its ability to perform molecular imaging in animal modal. Two major possible problems can be forecasted according to previous researches on other contrast agent and nanoparticle. The first one is bio-distribution. In real animal biological environment, the distribution of nano particle will be influenced by the effects like renal clearance, reticuloendothelial system and EPR effect. And bio-distribution of gas vesicle directly

determines the imaging performance and safety effect. Another important problem is signal to noise ratio. Because in real situation, the biological tissue will be a strong background noise. To differentiate the gas vesicle signal from biological tissue will be a great challenge. However, thanks to the strong second harmonic effect, the gas vesicle may be can identified by non-linear mode.

Our experiment demonstrated its ability of surface modification and indicates its potential for multimodality imaging, theranostic ability and cellular/molecule targeting ability. Further studies should be done to evaluate the multifunctional performance of the biogenic nanobubble.

REFERENCE

1. Gramiak R, Shah P M. Echocardiography of the aortic root. *Investigative radiology*, 1968, 3(5): 356-366.
2. Feinstein S B, Ten Cate F J, Zwehl W, et al. Two-dimensional contrast echocardiography. I. In vitro development and quantitative analysis of echo contrast agents. *Journal of the American College of Cardiology*, 1984, 3(1): 14-20.
3. Henze B A D. Validating of a transoeso-phageal ultrasonic-Doppler-probe to the detection of air in the venous blood. *Der Anaesthesist*, 1984, 1(99): 36.
4. Keller M W, Glasheen W, Kaul S. Albunex: a safe and effective commercially produced agent for myocardial contrast echocardiography. *Journal of the American Society of Echocardiography*, 1989, 2(1): 48-52.
5. Tanaka S, Kitamura T, Fujita M, et al. Color Doppler flow imaging of liver tumors. *AJR. American journal of roentgenology*, 1990, 154(3): 509-514.
6. Levene H B, Villapando E, Barnhart J L, et al. Aqueous dispersion of insoluble fibrous vegetable, mineral or hydrocolloid particles to enhance contrast: U.S. Patent 5,107,842. 1992-4-28.
7. Quay S C. Gaseous ultrasound contrast media: U.S. Patent 5,409,688. 1995-4-25.
8. Wu H. Custom-formulated phospholipid microbubbles and methods and uses thereof: U.S. Patent 8,974,818. 2015-3-10.
9. Grayburn P. Perflenapent Emulsion (EchoGen (R)): A New Long-Acting Phase-Shift Agent for Contrast Echocardiography. *Clinical cardiology*, 1997, 20(10): 12-18.
10. Weiss R J, Ahmad M, Villanueva F, et al. CaRES (Contrast Echocardiography Registry for Safety Surveillance): a prospective multicenter study to evaluate the safety of the ultrasound contrast agent Definity in clinical practice. *Journal of the American Society of Echocardiography*, 2012, 25(7): 790-795.

11. Wilson S R, Greenbaum L D, Goldberg B B. Contrast-enhanced ultrasound: what is the evidence and what are the obstacles. *American Journal of Roentgenology*, 2009, 193(1): 55-60.
12. Claudon M, Plouin P F, Baxter G M, et al. Renal Arteries in Patients at Risk of Renal Arterial Stenosis: Multicenter Evaluation of the Echo-enhancer SH U 508A at Color and Spectral Doppler US 1. *Radiology*, 2000, 214(3): 739-746.
13. Bhatia V K, Senior R. Contrast echocardiography: evidence for clinical use. *Journal of the American Society of Echocardiography*, 2008, 21(5): 409-416.
14. Celli N, Gaiani S, Piscaglia F, et al. Characterization of liver lesions by real-time contrast-enhanced ultrasonography. *European journal of gastroenterology & hepatology*, 2007, 19(1): 3-14.
15. Ferrara K, Pollard R, Borden M. Ultrasound microbubble contrast agents: fundamentals and application to gene and drug delivery. *Annu. Rev. Biomed. Eng.*, 2007, 9: 415-447.
16. Pislaru S V, Pislaru C, Kinnick R R, et al. Optimization of ultrasound-mediated gene transfer: comparison of contrast agents and ultrasound modalities. *European heart journal*, 2003, 24(18): 1690-1698.
17. Miller D L, Averkiou M A, Brayman A A, et al. Bioeffects considerations for diagnostic ultrasound contrast agents. *Journal of Ultrasound in Medicine*, 2008, 27(4): 611-632.
18. Ng K, Liu Y. Therapeutic ultrasound: its application in drug delivery. *Medicinal research reviews*, 2002, 22(2): 204-223.
19. P. Dayton, J. Allen, K. Ferrara, The magnitude of radiation force on ultrasound contrast agents, *J. Acous. Soc. Am.* 112 (2002) 2183–2192.
20. Perera R H, Solorio L, Wu H, et al. Nanobubble ultrasound contrast agents for enhanced delivery of thermal sensitizer to tumors undergoing radiofrequency ablation. *Pharmaceutical research*, 2014, 31(6): 1407-1417.

21. Prencipe G, Tabakman S M, Welsher K, et al. PEG branched polymer for functionalization of nanomaterials with ultralong blood circulation. *Journal of the American Chemical Society*, 2009, 131(13): 4783-4787.
22. Jokerst J V, Lobovkina T, Zare R N, et al. Nanoparticle PEGylation for imaging and therapy. *Nanomedicine*, 2011, 6(4): 715-728.
23. *Contrast Media in Ultrasonography: Basic Principles and Clinical Applications*[M]. Springer, 2005.
24. Kabalnov A, Klein D, Pelura T, et al. Dissolution of multicomponent microbubbles in the bloodstream: 1. Theory. *Ultrasound in medicine & biology*, 1998, 24(5): 739-749.
25. De Jong N, Emmer M, Van Wamel A, et al. Ultrasonic characterization of ultrasound contrast agents. *Medical & biological engineering & computing*, 2009, 47(8): 861-873.
26. Klonisch T, Wiechec E, Hombach-Klonisch S, et al. Cancer stem cell markers in common cancers—therapeutic implications. *Trends in molecular medicine*, 2008, 14(10): 450-460.
27. Ferrara K, Pollard R, Borden M. Ultrasound microbubble contrast agents: fundamentals and application to gene and drug delivery. *Annu. Rev. Biomed. Eng.*, 2007, 9: 415-447.
28. Klivanov A L. Ligand-carrying gas-filled microbubbles: ultrasound contrast agents for targeted molecular imaging. *Bioconjugate chemistry*, 2005, 16(1): 9-17.
29. Kwan J J, Borden M A. Lipid monolayer collapse and microbubble stability. *Advances in colloid and interface science*, 2012, 183: 82-99.
30. Wang C H, Huang Y F, Yeh C K. Aptamer-conjugated nanobubbles for targeted ultrasound molecular imaging. *Langmuir*, 2011, 27(11): 6971-6976.
31. Wheatley M A, Forsberg F, Dube N, et al. Surfactant-stabilized contrast agent on the nanoscale for diagnostic ultrasound imaging. *Ultrasound in medicine & biology*, 2006, 32(1): 83-93.

32. Tong H P, Wang L F, Guo Y L, et al. Preparation of protamine cationic nanobubbles and experimental study of their physical properties and in vivo contrast enhancement. *Ultrasound in medicine & biology*, 2013, 39(11): 2147-2157.
33. Yin T, Wang P, Zheng R, et al. Nanobubbles for enhanced ultrasound imaging of tumors. *International journal of nanomedicine*, 2012, 7: 895.
34. Fan X, Wang L, Guo Y, et al. Experimental investigation of the penetration of ultrasound nanobubbles in a gastric cancer xenograft. *Nanotechnology*, 2013, 24(32): 325102.
35. Yang H, Cai W, Xu L, et al. Nanobubble–Affibody: Novel ultrasound contrast agents for targeted molecular ultrasound imaging of tumor. *Biomaterials*, 2015, 37: 279-288.
36. Mai L, Yao A, Li J, et al. Cyanine 5.5 conjugated nanobubbles as a tumor selective contrast agent for dual ultrasound-fluorescence imaging in a mouse model. *PloS one*, 2013, 8(4).
37. Rapoport N, Gao Z, Kennedy A. Multifunctional nanoparticles for combining ultrasonic tumor imaging and targeted chemotherapy. *Journal of the National Cancer Institute*, 2007, 99(14): 1095-1106.
38. Milgroom A, Intrator M, Madhavan K, et al. Mesoporous silica nanoparticles as a breast-cancer targeting ultrasound contrast agent. *Colloids and Surfaces B: Biointerfaces*, 2014, 116: 652-657.
39. Casciaro S, Conversano F, Ragusa A, et al. Optimal enhancement configuration of silica nanoparticles for ultrasound imaging and automatic detection at conventional diagnostic frequencies. *Investigative radiology*, 2010, 45(11): 715-724.
40. Xie M, Shi H, Ma K, et al. Hybrid nanoparticles for drug delivery and bioimaging: Mesoporous silica nanoparticles functionalized with carboxyl groups and a near-

- infrared fluorescent dye. *Journal of colloid and interface science*, 2013, 395: 306-314.
41. Chen A M, Zhang M, Wei D, et al. Co - delivery of Doxorubicin and Bcl - 2 siRNA by Mesoporous Silica Nanoparticles Enhances the Efficacy of Chemotherapy in Multidrug - Resistant Cancer Cells. *Small*, 2009, 5(23): 2673-2677.
 42. Perera R H, Hernandez C, Zhou H, et al. Ultrasound imaging beyond the vasculature with new generation contrast agents. *Wiley Interdisciplinary Reviews: Nanomedicine and Nanobiotechnology*, 2015.
 43. Shapiro M G, Goodwill P W, Neogy A, et al. Biogenic gas nanostructures as ultrasonic molecular reporters. *Nature nanotechnology*, 2014, 9(4): 311-316.
 44. Minnaert M. XVI. On musical air-bubbles and the sounds of running water. *The London, Edinburgh, and Dublin Philosophical Magazine and Journal of Science*, 1933, 16(104): 235-248.
 45. Hoff L. Acoustic characterization of contrast agents for medical ultrasound imaging. *Springer Science & Business Media*, 2001.
 46. Ophir, J., & Parker, K. J. (1989). Contrast agents in diagnostic ultrasound. *Ultrasound in medicine & biology*, 15(4), 319-333.
 47. Shi W T, Forsberg F. Ultrasonic characterization of the nonlinear properties of contrast microbubbles. *Ultrasound in medicine & biology*, 2000, 26(1): 93-104.
 48. Cosgrove D. Ultrasound contrast agents: an overview. *European journal of radiology*, 2006, 60(3): 324-330.
 49. Phillips P, Gardner E. Contrast-agent detection and quantification. *European radiology*, 2004, 14: P4-P10.
 50. Walder D N, Evans A, Hempleman H V. Ultrasonic monitoring of decompression. *The Lancet*, 1968, 291(7548): 897-898.
 51. Miller D L. Ultrasonic detection of resonant cavitation bubbles in a flow tube by their second-harmonic emissions. *Ultrasonics*, 1981, 19(5): 217-224.

52. Vacher M, Gimenez G, Goutte R. Nonlinear Behaviour of Microbubbles: Application to their Ultrasonic Detection. *Acta Acustica united with Acustica*, 1984, 54(5): 274-283.
53. De Jong N, Cornet R, Lancee C T. Higher harmonics of vibrating gas-filled microspheres. Part one: simulations. *Ultrasonics*, 1994, 32(6): 447-453.
54. Chang P H, Shun K K, Wu S J, et al. Second harmonic imaging and harmonic Doppler measurements with Alburnex. *Ultrasonics, Ferroelectrics, and Frequency Control, IEEE Transactions on*, 1995, 42(6): 1020-1027.
55. Ahlborn F. Über die Wasserblüte *Bzssus flos aquae* und ihr Verhalten gegen Druck. 1894.
56. Strodtmann, S. 1895. Die Ursache des Schwebvermögens bei den Cyanophyceen. *Biol . Centralbl.* 15:113-115.
57. Klebahn, H. 1895. Gasvakuolen, ein Bestandteil der Zellen der Wasserblutebildenden *Phycchromaceen*. *Flora (Jena)* 80:241.
58. Walsby A E. Gas vesicles. *Microbiological reviews*, 1994, 58(1): 94.
59. Blaurock A E, Walsby A E. Crystalline structure of the gas vesicle wall from *Anabaena flos-aquae*. *Journal of molecular biology*, 1976, 105(2): 183-199.
60. Pfennig N, Cohen-Bazire G. Some properties of the green bacterium *Pelodictyon clathratiforme*. *Archiv für Mikrobiologie*, 1967, 59(1-3): 226-236.
61. Hayes P K, Walsby A E. The inverse correlation between width and strength of gas vesicles in cyanobacteria. *British phycological journal*, 1986, 21(2): 191-197.
62. Walsby A E, Bleything A. The dimensions of cyanobacterial gas vesicles in relation to their efficiency in providing buoyancy and withstanding pressure. *Journal of general microbiology*, 1988, 134(10): 2635-2645.
63. Walsby A E. The gas vesicle: a stable gas-filled structure in bacteria. A. O. Brubakk, BB Hemmingsen, and G. Sundnes (ed.), *Supersaturation and bubble formation in fluids and organisms*. Tapir Publishers, Trondheim, Norway, 1989: 69-103.

64. Jost M, Jones D D. Morphological parameters and macromolecular organization of gas vacuole membranes of *Microcystis aeruginosa* Kuetz. emend. Elenkin. Canadian journal of microbiology, 1970, 16(3): 159-164.
65. Walsby A E. Structure and function of gas vacuoles. Bacteriological reviews, 1972, 36(1): 1.
66. Walsby A E. The elastic compressibility of gas vesicles. Proceedings of the Royal Society of London B: Biological Sciences, 1982, 216(1204): 355-368.
67. Walsby A E. [70] The isolation of gas vesicles from blue-green algae. Methods in enzymology, 1974, 31: 678-686.
68. Buckland B, Walsby A E. A study of the strength and stability of gas vesicles isolated from a blue-green alga. Archiv für Mikrobiologie, 1971, 79(4): 327-337.
69. Cannata J M, Ritter T, Chen W H, et al. Design of efficient, broadband single-element (20-80 MHz) ultrasonic transducers for medical imaging applications. Ultrasonics, Ferroelectrics, and Frequency Control, IEEE Transactions on, 2003, 50(11): 1548-1557.
70. Feuillade C, Werby M F. Resonances of deformed gas bubbles in liquids. The Journal of the Acoustical Society of America, 1994, 96(6): 3684-3692.
71. Pfeifer F. Distribution, formation and regulation of gas vesicles. Nature Reviews Microbiology, 2012, 10(10): 705-715.
72. Ferrara, K., Pollard, R., & Borden, M. (2007). Ultrasound microbubble contrast agents: fundamentals and application to gene and drug delivery. Annu. Rev. Biomed. Eng., 9, 415-447.
73. UNGER E C, McCREERY T P, SWEITZER R H. Ultrasound enhances gene expression of liposomal transfection. Investigative radiology, 1997, 32(12): 723-727.
74. Raffa, V., Ciofani, G., Vittorio, O., Riggio, C., & Cuschieri, A. (2010). Physicochemical properties affecting cellular uptake of carbon nanotubes. Nanomedicine, 5(1), 89-97.

75. Hosseinkhani H, Aoyama T, Ogawa O, et al. Ultrasound enhancement of in vitro transfection of plasmid DNA by a cationized gelatin. *Journal of drug targeting*, 2002, 10(3): 193-204.
76. Kaneko O F, Willmann J K. Ultrasound for molecular imaging and therapy in cancer. *Quantitative imaging in medicine and surgery*, 2012, 2(2): 87-97.
77. Salem, A. K., Searson, P. C., & Leong, K. W. (2003). Multifunctional nanorods for gene delivery. *Nature materials*, 2(10), 668-671.
78. Raffa, V., Ciofani, G., Vittorio, O., Riggio, C., & Cuschieri, A. (2010). Physicochemical properties affecting cellular uptake of carbon nanotubes. *Nanomedicine*, 5(1), 89-97.